RADC-TR-90-168
Final Technical Report
May 1990

AD-A223 437

MAGNETOSTATIC WAVE TRANSDUCERS, RESONATORS AND DISPERSION CONTROL

University of Texas at Arlington

John M. Owens, Ronald L. Carter, W. Alan Davis, Younes Ataiiyan
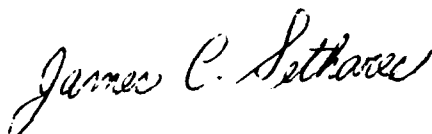
DTIC
ELECTE
JUN 2 8 1990
S E D

ROME AIR DEVELOPMENT CENTER
Air Force Systems Command
Griffiss Air Force Base, NY 13441-5700

90 06 28 015

This report has been reviewed by the RADC Public Affairs Division (PA) and is releasable to the National Technical Information Service (NTIS). At NTIS it will be releasable to the general public, including foreign nations.

RADC-TR-90-168 has been reviewed and is approved for publication.

APPROVED: *James C. Sethares*

JAMES C. SETHARES
Project Engineer

APPROVED: *John K. Schindler*

JOHN K. SCHINDLER
Acting Director
Directorate of Electromagnetics

FOR THE COMMANDER: *John A. Ritz*

JOHN A. RITZ
Directorate of Plans & Programs

REPORT DOCUMENTATION PAGE

Public reporting burden for this collection of information is estimated to average 1 hour per response, including the time for reviewing instructions, searching existing data sources gathering and maintaining the data needed, and reviewing the collection of information. Send comments regarding this burden estimate or any other aspect of this collection of information, including suggestions for reducing this burden, to Washington Headquarters Services, Directorate for Information Operations and Reports, 1215 Jefferson Davis Highway, Suite 1204, Arlington, VA 22202-4302, and to the Office of Information and Regulatory Affairs, Office of Management and Budget, Washington, DC 20503.

1. AGENCY USE ONLY (Leave Blank)	2. REPORT DATE	3. REPORT TYPE AND DATES COVERED
	May 1990	Final Oct 83 - Jun 87

4. TITLE AND SUBTITLE

MAGNETOSTATIC WAVE TRANSDUCERS, RESONATORS AND DISPERSION CONTROL

6. AUTHOR(S)

John M. Owens, Ronald L. Carter, W. Alan Davis
and Younes Ataiiyan

5. FUNDING NUMBERS

C - F19628-84-K-0029
PE - 61101F
PR - 2305
TA - J5
WU - 40

7. PERFORMING ORGANIZATION NAME(S) AND ADDRESS(ES)
University of Texas at Arlington
Electrical Engineering Department
P O Box 19016
Arlington TX 76019

8. PERFORMING ORGANIZATION REPORT NUMBER

N/A

9. SPONSORING/MONITORING AGENCY NAME(S) AND ADDRESS(ES)

Rome Air Development Center (EEAC)
Hanscom AFB MA 01731-5000

10. SPONSORING/MONITORING AGENCY REPORT NUMBER

RADC-TR-90-168

11. SUPPLEMENTARY NOTES

RADC Project Engineer: Peter J. Rainville/EEAC/(617) 377-4663

12a. DISTRIBUTION/AVAILABILITY STATEMENT

Approved for public release; distribution unlimited.

12b. DISTRIBUTION CODE

13. ABSTRACT (Maximum 200 words)
This report describes the design of magnetostatic surface waves (MSW) and transversal filters. First, a variable time delay device is described that uses a cascaded surface wave device and a backward volume wave device. Transducers composed of periodic arrays of shorted microstrip lines are described. Theoretical and experimental work has resulted in the first "true" synthesized magnetostatic wave transversal filter. Furthermore, sample delay lines showed less than 16 dB insertion loss and 16 Hz bandwidth at 26 - 40 GHz.

14. SUBJECT TERMS
Magnetostatic Surface Waves
Transversal Filter

15. NUMBER OF PAGES
160

16. PRICE CODE

17. SECURITY CLASSIFICATION OF REPORT	18. SECURITY CLASSIFICATION OF THIS PAGE	19. SECURITY CLASSIFICATION OF ABSTRACT	20. LIMITATION OF ABSTRACT
UNCLASSIFIED	UNCLASSIFIED	UNCLASSIFIED	UL

NSN 7540-01-280-5500

TABLE OF CONTENTS

1. INTRODUCTION AND SUMMARY

A military need exists for microwave solid state device technology with complementary analog signal processing capabilities which has been developed over the past ten years in surface acoustic waves (SAW) technology. In this technology, non-recursive transversal filters have been realized through either interdigital transducers and/or periodic reflective arrays defined on the piezoelectric substrates in which the surface acoustic waves are propagated. Utilizing this technology simple delay lines, complex matched filters, high Q resonators and chirp filters, have been realized in the VHF, UHF, frequency range. Unfortunately, extension of this technology to the microwave region ($f > 1GHz$) has been difficult. At these frequencies, the surface acoustic wavelength is less than $1\mu m$ making fabrication difficult and the propagation loss becomes excessive (>100 db/μsec at 10 GHz).

Final report contract AFOSR 80-8264 summarizes the results of a viable technological realization of this goal through magnetostatic waves (MSW) propagating at microwave frequencies in magnetically biased, liquid phase epitaxial films of Yttrium Iron Garnet (YIG) grown on Gadolinium Gallium Garnet (GGG). This technology has a number of advantages; low loss (<30 db/μsec at 10 GHz), tunable by bias field to any center frequency (1-40 GHz), and finally a well understood and characterized wave phenomena (MSW). The necessary non-recursive transducer filtering is achieved through a multi-element transducer and/or the interaction of the MSW with periodic structures in or on the YIG film.

This report summarizes the work accomplished toward achieving

1

MSW transversal filtering. First, studies of a variable time delay device based on a cascaded MSSW forward wave delay line and an MSBVW backward wave delay line, are presented. Next, studies of MSSW (Magnetostatic Surface Wave) transducers composed of periodic arrays of narrow shorted microstrips are summarized. A 3 port model for this type of transducer and experimental measurements of test devices were carried out to verify the model. A synthesis procedure has been developed to allow synthesis of the desired response function. Experimental studies of synthesized filters has resulted in the first "true" synthesized MSW transversal filter. Finally, studies of MSSW and MSFVW delay lines at Ku Band (26-40GHz) were carried out resulting in sample delay lines with less than 16db insertion loss and 1 GHz bandwidths.

Pulse compression systems utilizing surface acoustic wave (SAW) dispersive delay lines have been under intensive investigation for the past 14 years. These studies have concentrated primarily on using the SAW linear dispersive delay line for downchirp phase coding with quadratic phase error less that one degree in the expander section of the SAW pulse compression system. The low time-sidelobes is achieved by appropriate amplitude weighting in the compressor section. Time-bandwith products of over 1000 with greater than 40 dB sidelobe suppression have been obtained for the SAW pulse compression system. The typical operating center frequency for a SAW device is less than 1 GHz (due to the physical limit of technology). For radar systems of higher operating frequencies (in the GHz region), mixing is required to convert the radar carrier frequencies to the operating frequencies of the SAW pulse compression subsystem.

A new technology based on "slow" magnetostatic wave (MSW) propagation in a magnetically biased epitaxial Yttrium Iron Garnet (YIG) is emerging as a complementary signal processing technology to SAW at microwave frequencies (1-20 GHz). Three major propagating modes with the propagation direction in the film plane have been used in device applications. These three modes are magnetostatic surface wave (MSSW) mode in which the bias field is perpendicular to the direction of the wave propagation and in the plane of the film, magnetostatic forward volume wave (MSFVW) mode in which the bias field is perpendicular to the film and the propagation direction, and magnetostatic backward volume wave (MSBVW) mode in which the direction of the bias field is the same as the propagation direction. These modes are dispersive and characterized by a limited propagation passband width (.5 to 2.2 GHz) with the center frequency electronically tunable between 1 to 20 GHz by adjusting the bias field. The 1-20 GHz center frequency range of this MSW modes makes signal processing possible directly at radar carrier frequency and the typical group delays of the modes are between 50 nsec/cm to 1000nsec/cm, depending on the YIG film thickness and the bias magnetic field used. This dispersive slow wave structure of magnetostatic wave makes the investigation of MSW devices in pulse compression logical.

2. MAGNETOSTATIC WAVE DISPERSION CONTROL

2.1 Linearly Dispersive Time-Delay Control of Magnetostatic Surface Wave by Variable Ground Plane Spacing

2.1.1 Introduction

The propagation characteristics of magnetostatic waves in epitaxial Yttrium Iron Garnet (YIG) films have been extensively investigated both experimentally and theoretically for a number of years (1-4). These studies have shown that the delay versus frequency characteristics of MSSW delay lines of a YIG film spaced from a ground plane are functions of the saturation magnetization, bias field, YIG film thickness, and ground plane spacing. A study of how different parameters affect the delay characteristics of surface waves indicated that dispersion control by ground plane spacing is most effective (4). This chapter described the theoretical and experimental results on the theoretical simulation and experimental evaluation of a magnetostatic surface wave variable ground plane spacing delay line with linear group delay.

2.1.2 Theoretical Simulation

Figure 2.1.1 shows the variation of the group delay with frequency for MSSW delay lines with ground plane spacing (Ti) and propagation length (Li) as adjusting parameters. The YIG film thickness used in these calculations is 30 um. Examination of this figure indicates that it is possible to achieve a linear variation of delay by adjusting the length of the short section (Li) of the step ground plane as shown in Figure 2.1.2. A nine step ground plane

structure is selected, with an eight step ground plane in the middle of this MSSW stepped ground plane delay line. The separation of this eight step ground to the YIG film can be adjusted by a pair of set screws. The ninth step in this MSSW delay is fixed by the substrate thickness which is 250 μm. The propagation length can be adjusted by photographically changing the single bar transducer separation between it and this edge of the substrate. The length of each section is then optimized to provide a minimum deviation from quadratic phase over the linearized delay bandwidth. The linear time delay characteristic which is obtained by summing the individual time delay corresponding to each section of the MSSW 9 stepped ground plane structure, is shown in Figure 2.1.3. A linear regression fit is also shown in this figure which indicates a linear delay region between 2.89 to 3.33 GHz (Figure 2.1.4.). The R.M.S. deviation from quadratic phase over this 440MHz bandwidth is 8 degrees. The corresponding time bandwidth product (TBP) is near 120 for this nine stepped ground plane MSSW theoretical simulated linear delay line.

2.1.3 Experimental Evaluation

Due to the difficulty and long waiting period for fabrication of the eight stepped center ground plane, a continuously variable ground plane is used to provide the variation of ground plane spacing to the YIG film along the propagation direction of the MSSW delay line. The separation of this continuously variable ground plane to the YIG film can be adjusted by changing structure of the ground plane and varying the distance of this ground to the film by a pair of set screws.
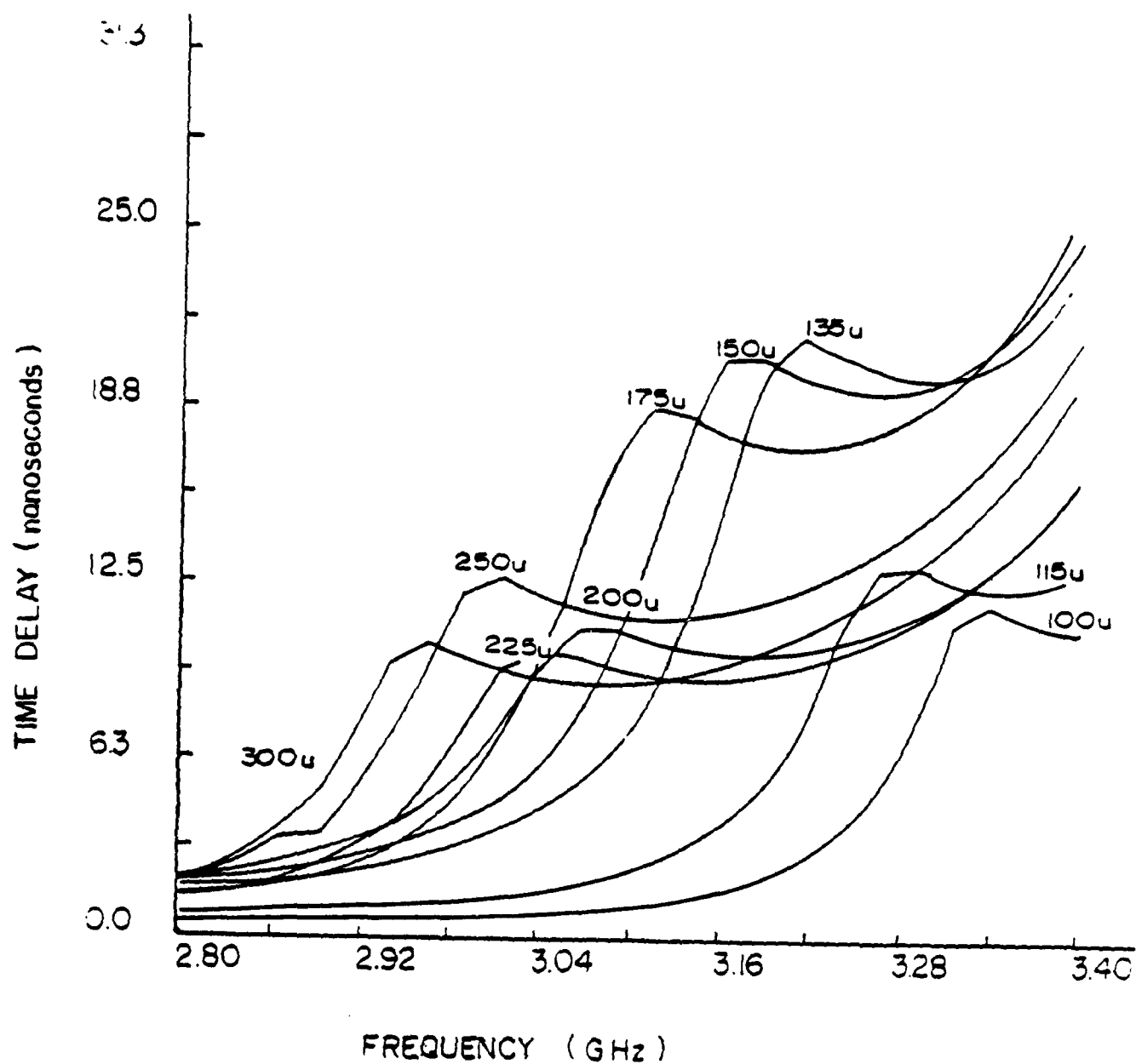
Figure 2.1.1   Variation of group delay with frequency
              for MSSW delay lines with ground plane
              spacing (Ti) and propagation distance
              (Li) as adjusting parameters.

6

Ti(uM)	Li(cm)
300	.18
250	.20
225	.15
200	.15
175	.23
150	.22
135	.20
115	.10
100	.07

Table 2.1.1   Ground plane spacings and lengths for a nine-
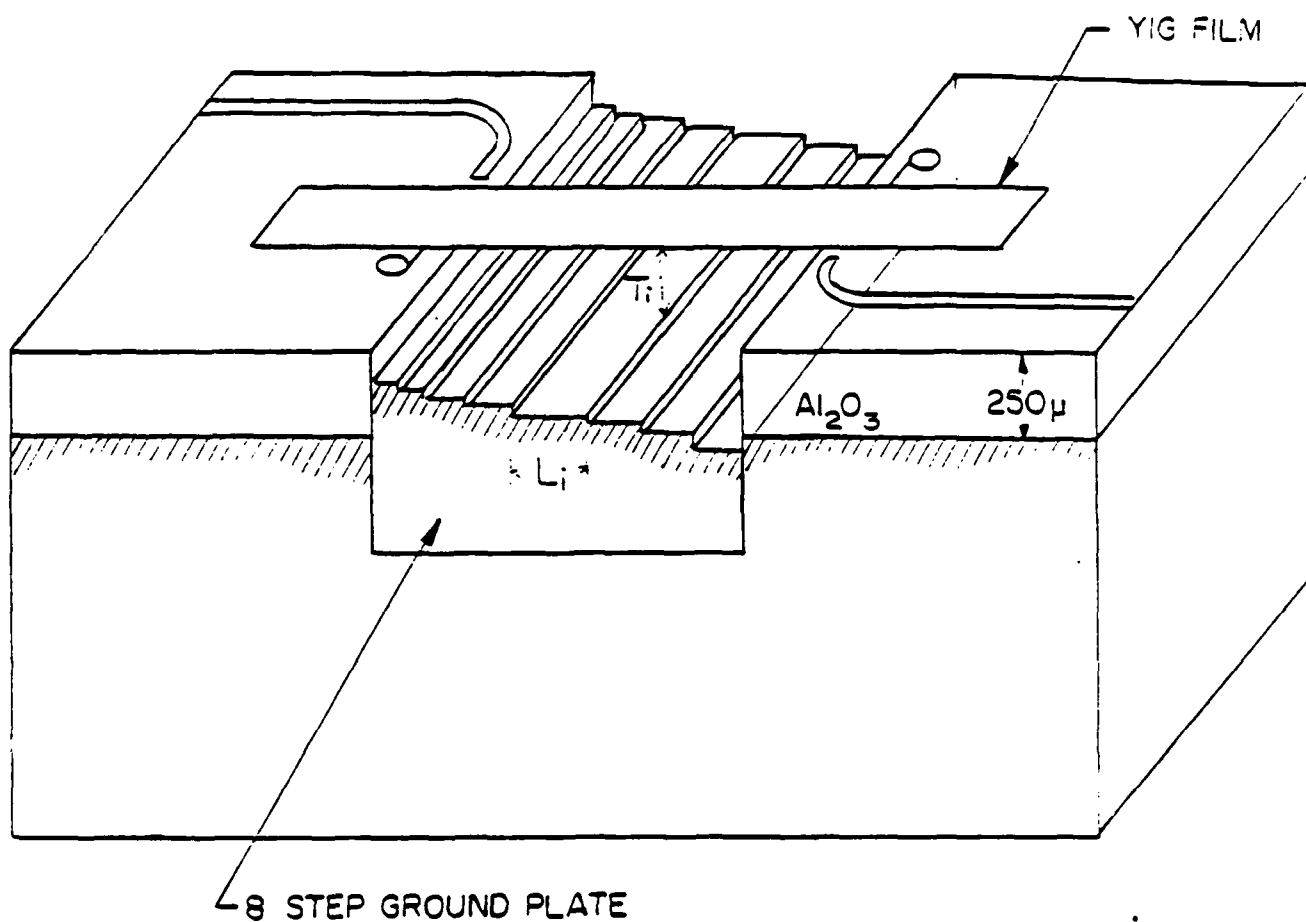section delay line

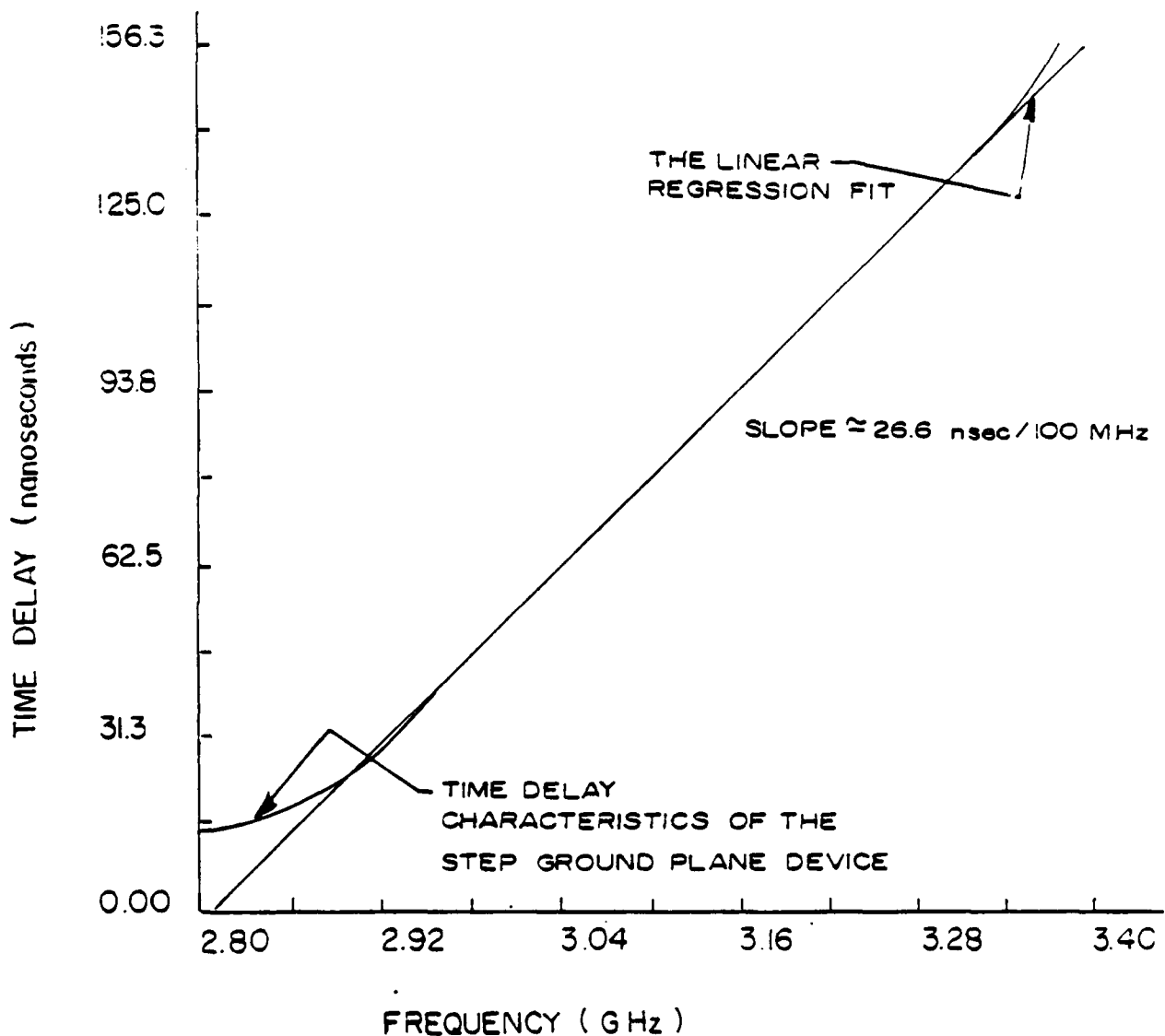Figure 2.1.2 MSSW Delay line with stepped ground plane

Figure 2.1.3   The summation of the individual time delay section in the 9-step ground plane structure, with dimension shown in table 2.1, results a linear time delay characteristic between 2.89 to 3.33 GHz. Thickness of YIG is 30 uM.
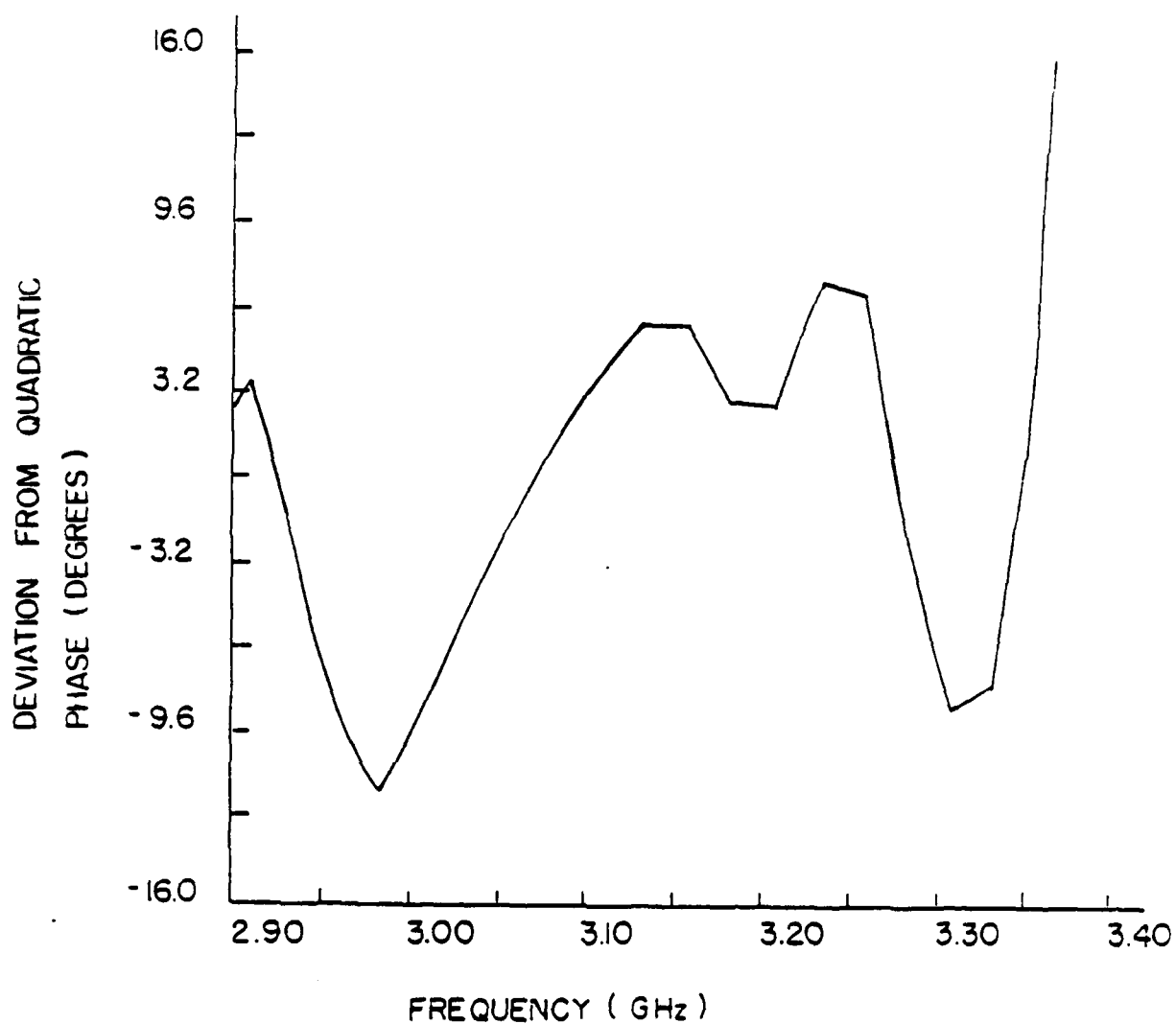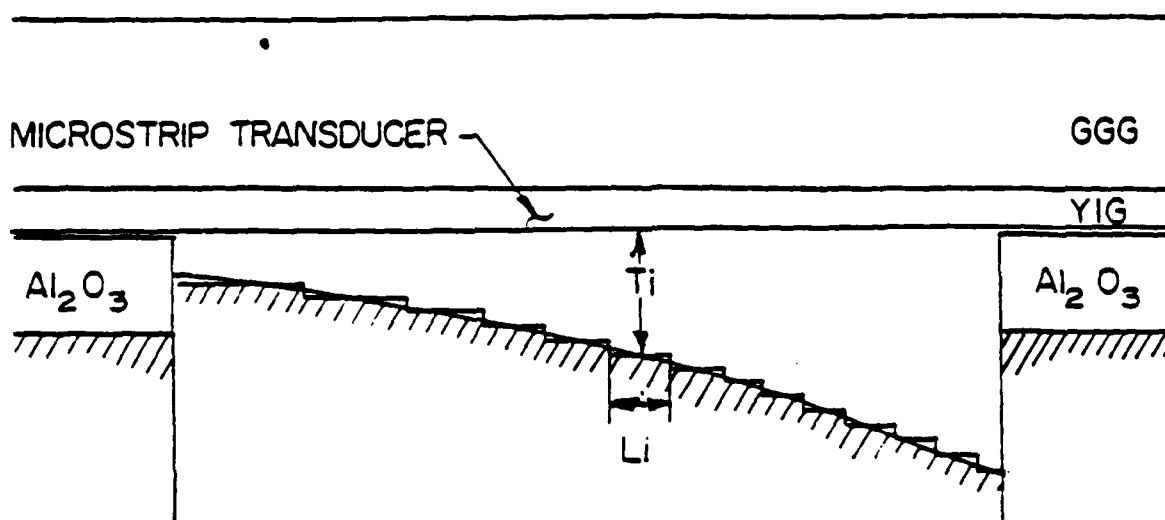
9

Figure 2.1.4 The quadratic phase error of the linear delay
region of the 9-step ground plane structure
The R.M.S. deviation from quadratic phase in this
bandwidth is 8 degrees.

10

Figure 2.1.5 shows a sketch of the MSSW variable ground plane delay line. The device is in a "flipped" configuration with the YIG film flipped over the single bar microstrip transducer. A pair of shorted-circuited 50 μm-wide, 3 mm-long, and 3 μm-thick microstrip couplers are used for the launching and receiving of the microwave energy for MSSW propagation along the YIG film. A 25 μm-thick 3mm-wide YIG film and 15 μm-thick Gadolinium Gallium Garnet (GGG) substrate was used for the delay measurement. The HP 8409B automatic network analyzer was used to measure the reflection and transmission parameters of the device under test.

The group delay was then obtained from the S_{12} phase data by calculation of phase slope. Since this is a differentiation process, the resolution is determined both by the frequency aperture (Δf) and the phase detector resolution of the network analyzer. By increasing the frequency aperture and the corresponding phase difference, an averaging effect is performed to reduce the time delay ripples. A 30 MHz frequency aperture is chosen in order to optimize the calculated time delay obtained from the automatic network analyzer phase measurement. A modification of the control program of the automatic network analyzer is performed to compute the absolute phase change as a function of frequency over the frequency bandwidth of interest. For a linear delay bandwidth, the corresponding absolute phase function is a quadratic function of frequency. (For a constant delay bandwidth, the corresponding absolute phase function is a linear function of frequency). A root mean square fit is then performed for this experimentally determined phase data. The deviation from quadratic phase defined as the experimental phase data is then used as the parameters to determine

11

MICROSTRIP TRANSDUCER —   GGG

                                                            YIG

Al$_2$O$_3$ Ti   Al$_2$O$_3$

                              Li

A 15 STEP GROUND PLANE MODEL IS USED TO
OBTAIN THE THEORETICAL CASCADED DELAY
CHARACTERISTIC

i	Ti (µm)	Li (cm)
1	800	.0516
2	750	.0253
3	700	.0303
4	650	.0303
5	600	.0357
6	550	.0506
7	500	.0648
8	450	.0901
9	400	.0972
10	350	.1245
11	300	.2000
12	250	.1708
13	200	.2260
14	150	.1190
15	140	.1300

Figure 2.1.5 Sketch of continuously variable ground-plane MSSW
            delay line

the deviation from linear delay (quadratic phase) over the bandwidth of interest of the device under test.

By carefully adjusting the separation of the continuously variable ground plane to the YIG film, linear delay of bandwidth up to 500 MHz can be experimentally obtained with phase error less than 20°. The slope of the linear region can also be adjusted by changing the structure of the continuously variable ground plane. Figure 2.1.6 shows the experimental delay measurement of one of the devices under test. A linear delay of 500 MHz bandwidth (between 2.62 to 3.12 GHz) with a slope of 15.3 nsec/100 MHz was observed. Figure 2.1.7 shows the quadratic phase error of this device in the linear delay region. The corresponding R.M.S. phase error is 13°. The insertion loss over the linear region is between 15 to 20 dB (unmatched). The separation of this continuously variable ground plane to the YIG is roughly determined by removing the "flipped" over YIG film and measuring the profile of the MSSW delay line along the direction of propagation. A 50μm air gap was added to the measured data to represent the air gap that is unavoidable in the flipped configuration. A 15-step ground plane structure, with dimensions given in Figure 2.1.5, was then used to approximate the continuously variable ground plane structure measured. The computed delay characteristic of this 15-step model is also in Figure 2.1.6. The difference between this computed delay characteristic and the experimental linear delay characteristic is quite large. This large discrepancy is due to the error associated with the measurement of the bias field strength, YIG thickness, and separation of the ground plane to the YIG film.
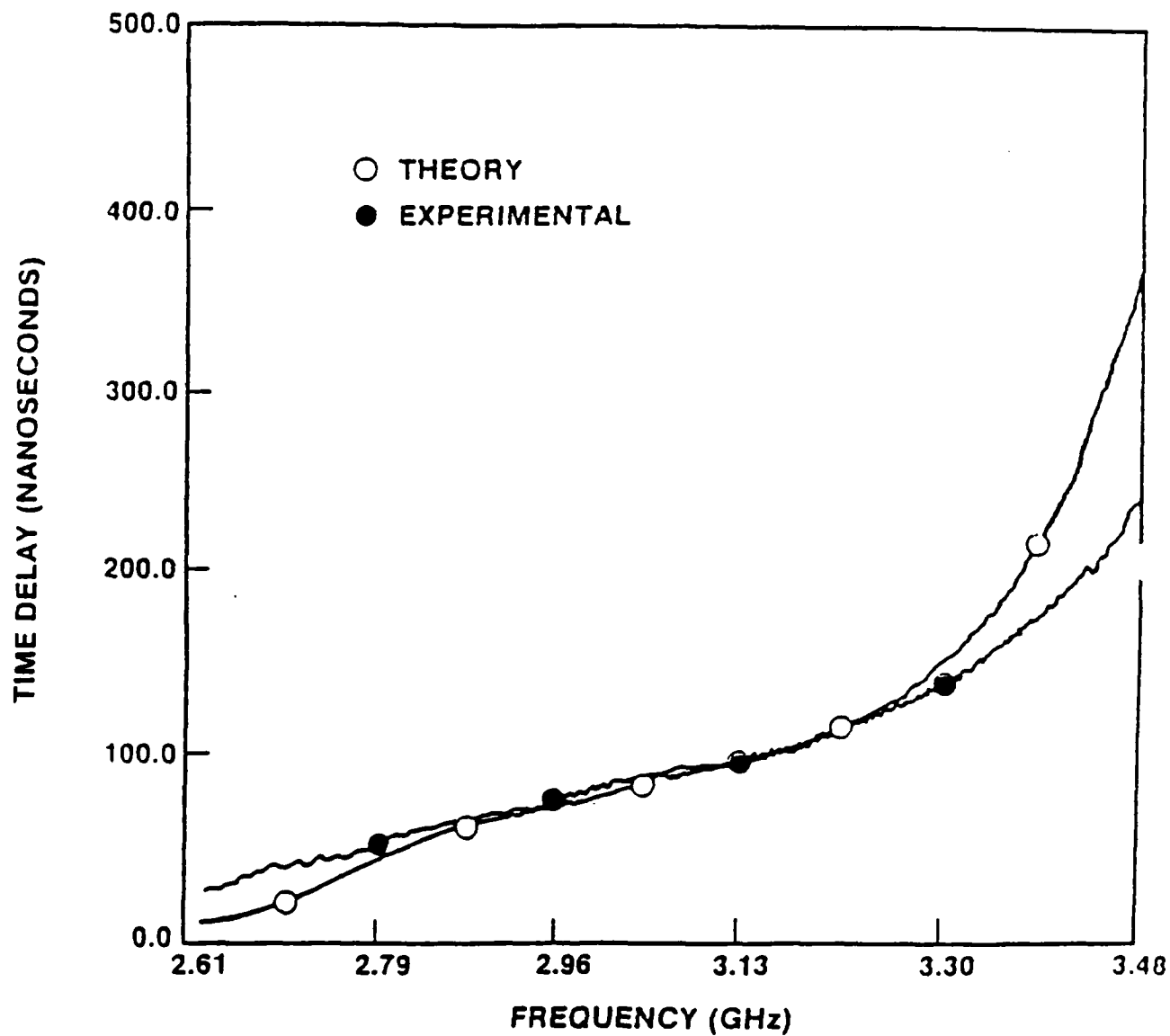
13

Figure 2.1.6 Experimental dispersion curve for a variable
ground plane MSSW delay line. The theoretical
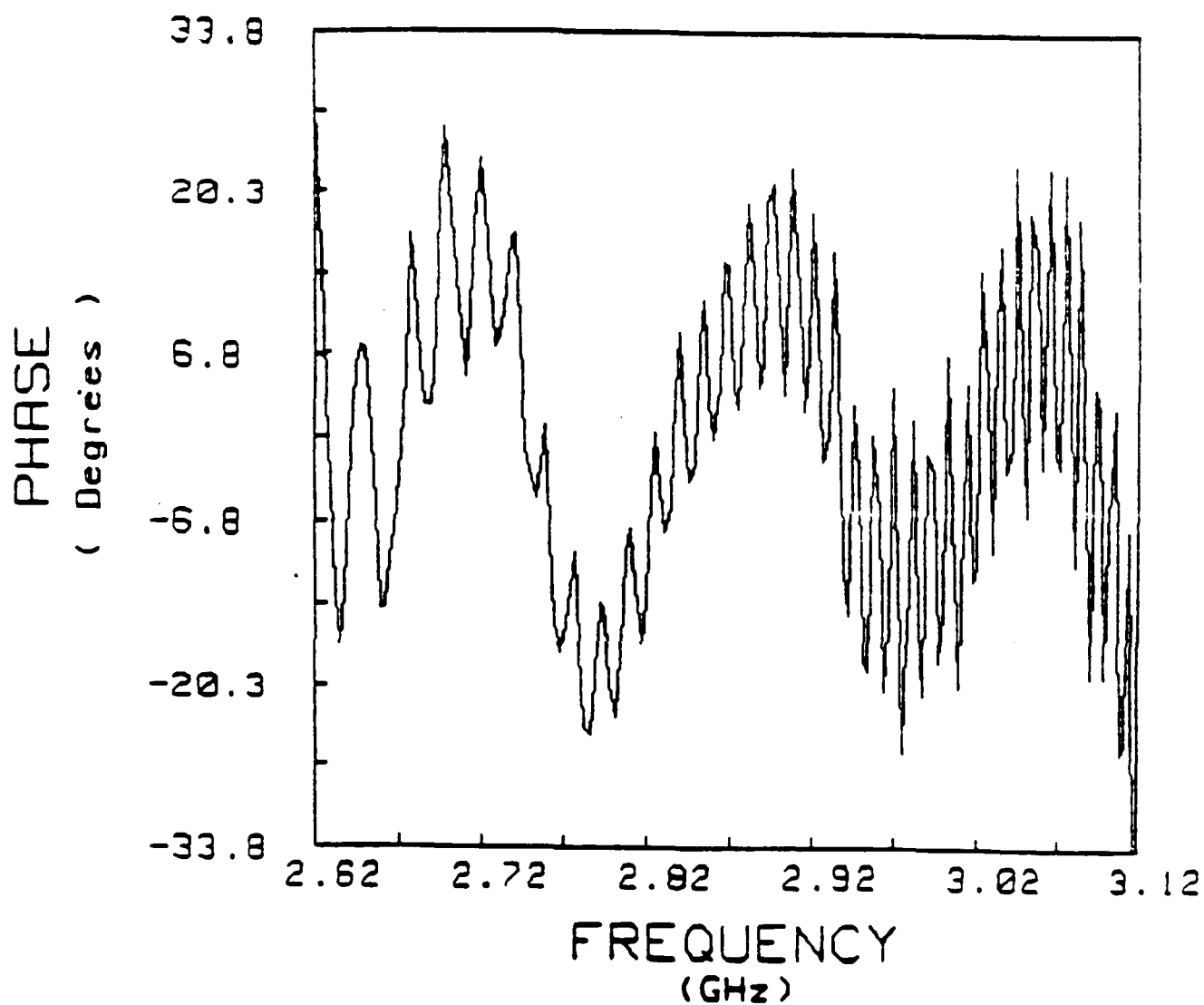curve was calculated for a 15 step model.

14

Figure 2.1.7 The quadratic phase error of the continuously
variable ground plane MSSW delay line
The R.M.S. phase error is 13 degrees over the
linear delay bandwidth.

15

Applications of these MSSW linear delay devices include pulse compression systems (5,6), compressive receivers and variable time delay devices utilizing a cascade configuration with a linearized backward volume wave device (7,8).

2.2 Electronically Variable Time Delay Using Cascaded Magnetostatic Wave Delay Lines

2.2.1 Introduction

Two features which make magnetostatic wave (MSW) devices attractive are (a) an operating frequency range above 1 GHz and (b) electronic tunability. Both of these features are required for electronically variable time delay components used in phase array radar and communication systems. The basic architecture for a variable time delay device based on MSW technology was described originally by Sethares, Owens and Smith (7). A Schematic of their approach is illustrated in Figure 2.2.1. Briefly, two MSW delay lines, one biased to operate in the backward volume wave (MSBVW) mode, and the other biased to operate in the surface wave (MSSW) mode, are cascaded together. The dispersion (i.e., the delay vs. frequency) of the MSSW device has a positive slope, while the slope of the MSBVW dispersion is negative. If the absolute magnitudes of these two slopes are identical, and if the dispersions are linear, then the net dispersion of the cascaded device will be zero over a common frequency band. If the frequency domain of one delay line is shifted by changing the strength of its applied biasing field, then the absolute delay of the cascaded device will also be shifted. Thus, different values of constant delay can be obtained by simply changing the strength of the bias by a small amount. One impediment to the realization of a device of this type with large bandwidth is that in general the dispersion of typical MSW devices is nonlinear. In the original experiments no attempt was made to linearize the individual dispersions. Even so the results were generally

17

encouraging. In this chapter an improved version of the original device in which care has been taken to linearize the dispersion for both the surface and backward modes is reported.

2.2.2 Theory

From the study of the dispersive characteristics for MSSW and MSBVW delay line, it is found that the shape of the dispersion curve is strongly dependent on the thickness of the film and the spacing above the ground plane. It has been demonstrated (9) that the linearity of the dispersion can be substantially improved by carefully adjusting the spacing between the ground plane and the YIG film. Thus, the ground spacing technique was incorporated into the design of the delay line components of the cascaded device.

A linear MSBVW dispersion curve can be obtained in a straight forward manner by using a 35 μm thick layer of YIG spaced 250 μm above the ground plane. This spacing is very close to the standard for MSW delay lines, and no special fabrication techniques are required, other than some polishing of the dielectric spacer. It requires a much closer ground plane spacing to achieve the same results with the MSSW mode and past experience has shown that ground current losses increase as the spacing decreases.

To circumvent this problem a variable ground plane structure of the type reported by Chang, Owens, and Carter (10) was selected for the MSSW device. The essence of this approach is that the YIG delay line is held above a ground plane whose distance from the YIG film is a function of the path length. A schematic of the technique is shown in Figure 2.2.1, with experimental results shown in Figure 2.2.2 and Table 2.2.1. The advantage of this approach is that in principle optimum dispersion control can be achieved and the minimum
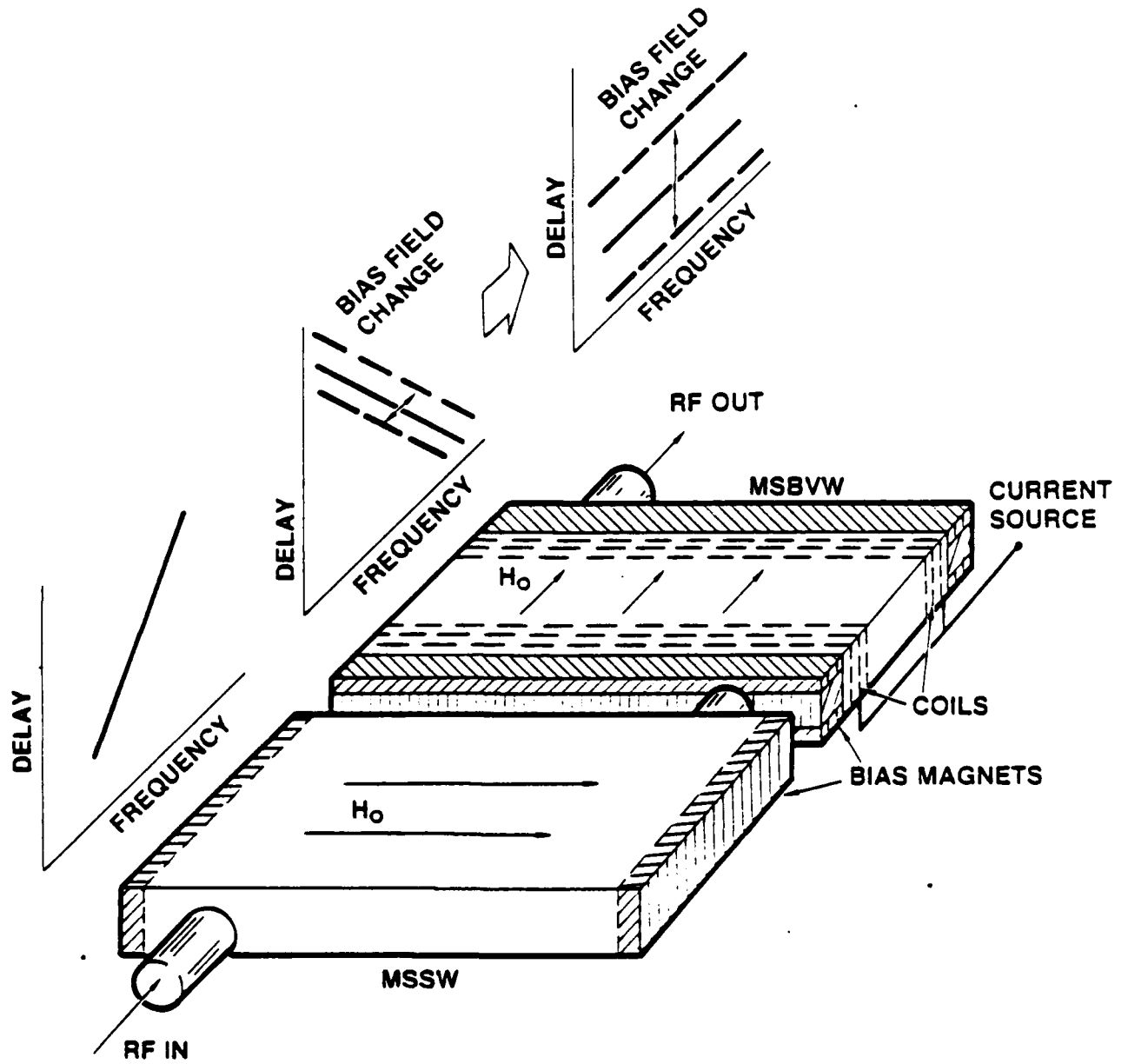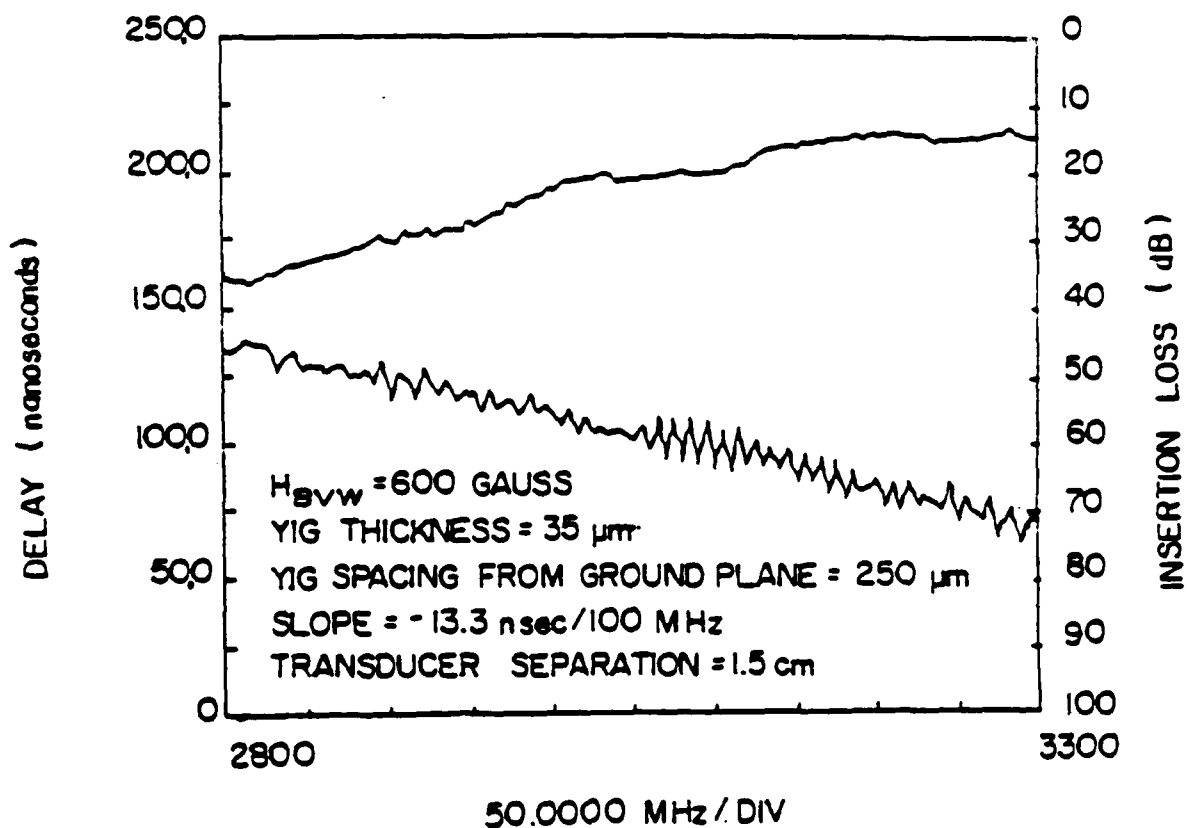
18

Figure 2.2.1   Schematic of the MSW variable time delay device

Upper curve: Transmission loss for the MSBVW delay line.

Lower curve: Delay versus frequency with arrows defining a band of linear delay.

Figure 2.2.2   The characteristic of the MSBVW delay line

20

H(BVW)	Slope(nsec/100MHz)	R.M.S. PH. ERROR
550	-14.0	8.9
575	-12.5	7.7
600	-12.6	7.3
625	-13.6	7.9
650	-14.1	11.0

Transducer separation: 1.5 cm
YIG Thickness: 35uM
Ground spacing: 250uM
Bandwidth: 2.9 to 3.15 GHz

Table 2.2.1 The effect on changing the slopes of the MSBVW linear delay line by adjusting the bias field

spacing required is greater than in the uniform spacing case.

For both modes of propagation the figure of merit is defined in terms of the phase deviation from the appropriate theoretical phase vs. frequency curve. If the delay time is a linear function of the frequency then the phase dependence on frequency is quadratic. On the other hand, if the delay time is constant over the frequency band, then the phase is a linear function of frequency. In principle, it is possible to achieve close to zero deviation from quadratic phase over a bandwidth of 500 MHz centered at 3 GHz using the ground plane spacing techniques described in Chapter 2.1

2.2.3 Experimental Results

A cascaded device was prepared using a MSSW delay line with a variable ground plane and a MSBVW delay line with a YIG film thickness of 35 μm and ground plane spacing of 254 μm. The ch racteristic of the MSBVW delay line is shown in Figure 2.2.2. The variable ground plane was prepared by polishing a ground plane into a smooth curve. The ground plane curve was optimized by alternating vs. frequency measurements with block sanding until the desired dispersion curve was obtained.

The delay line material was prepared by growing YIG films on the 1 inch diameter Gadolinium Gallium Garnet (GGG) wafers using the Liquic Phase Epitaxy (LPE) method. The YIG thickness for the MSSW delay line was 25 μm, while the thickness of the MSBVW delay line YIG was 35 μm. The wafers were cut into bars for delay line use, and the ends of these bars were beveled to reduce reflections.

The individual delay lines were experimentally evaluated with

an automatic network analyzer. Large laboratory electromagnets were used to supply the necessary d.c. bias. In the final configuration both the MSSW delay line and the MSBVW delay line exhibited R.M.S. phase deviation from quadratic of about 13° over approximately 500 MHz bandwidth centered at 3GHz. Experimental plots from the network analyzer of delay time vs. frequency for both MSSW and MSBVW devices are given in Figure 2.2.3. The slopes of these curves are 9.6 nsec/100 MHz and -9.7 nsec/100 MHz, respectively.

It is found that by adjusting the d.c. bias field of the variable ground plane MSSW delay line, the dispersion characteristic of the linear delay bandwidth becomes nonlinear. In fact, the deviation from quadratic phase over the frequency band of interest increases substantially by changing the bias field. For the backward volume wave delay line, the linear bandwidth can be changed by adjusting the bias field. The dispersion characteristic over the bandwidth of interest remains linear with a slight adjustment in the slope. Table 2.2.1 gives the effect of changing the d.c. bias of the MSBVW delay line on the slopes of the linearized frequency band. Because of these experimental results, the bias field for the MSSW linear delay line is fixed at the same value, whereas the bias field of the MSBVW linear delay line can be changed to provide adjustment for the time delay in the cascaded device. These two MSW delay lines are then cascaded together to provide the variable time delay experiments.

Delay vs. frequency curves experimentally obtained from the cascaded MSSW and MSBVW device are shown in Figure 2.2.4. To obtain these curves the bias on the MSSW delay line was held constant at 410 Gauss while the bias applied to the MSBVW delay line was varied
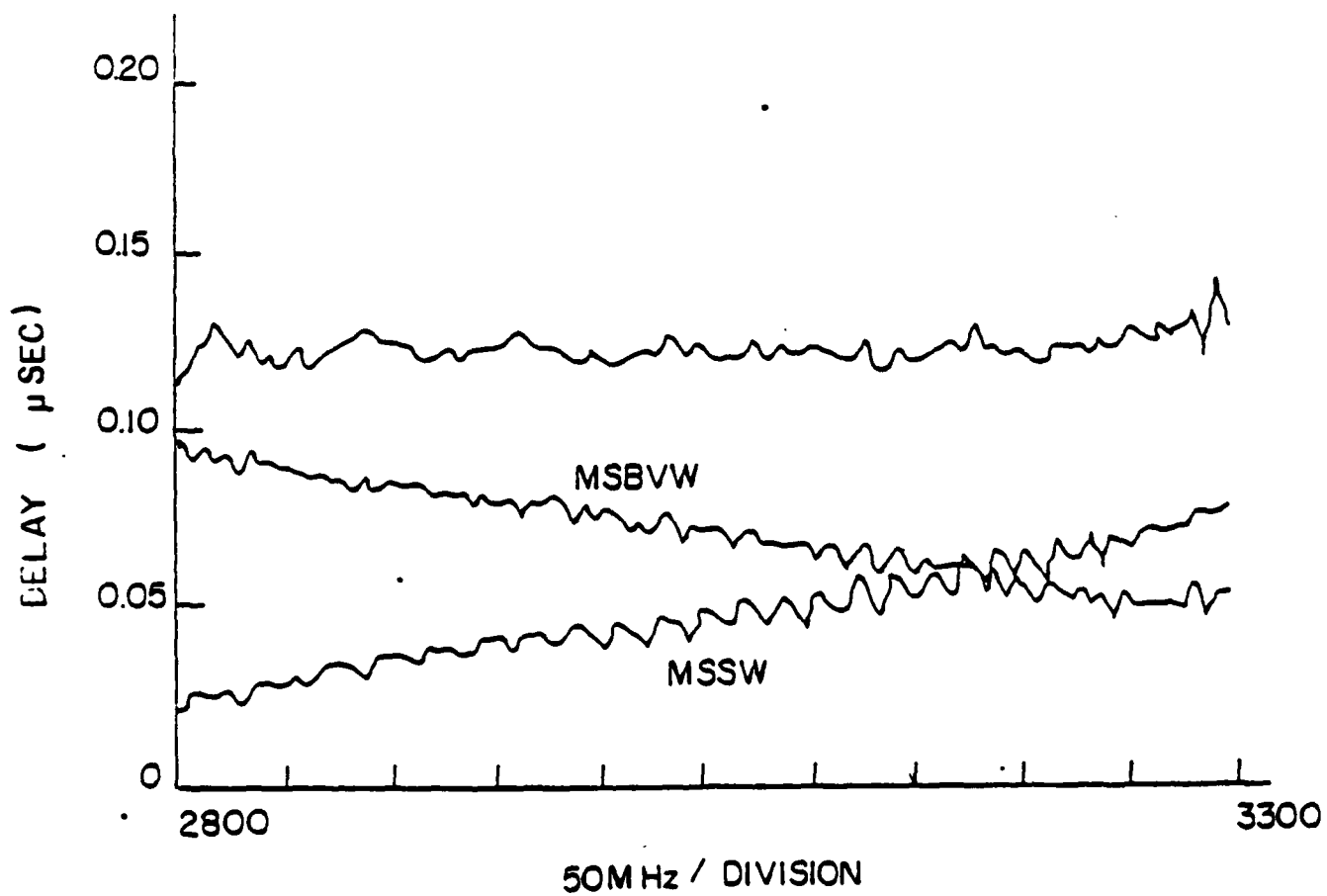
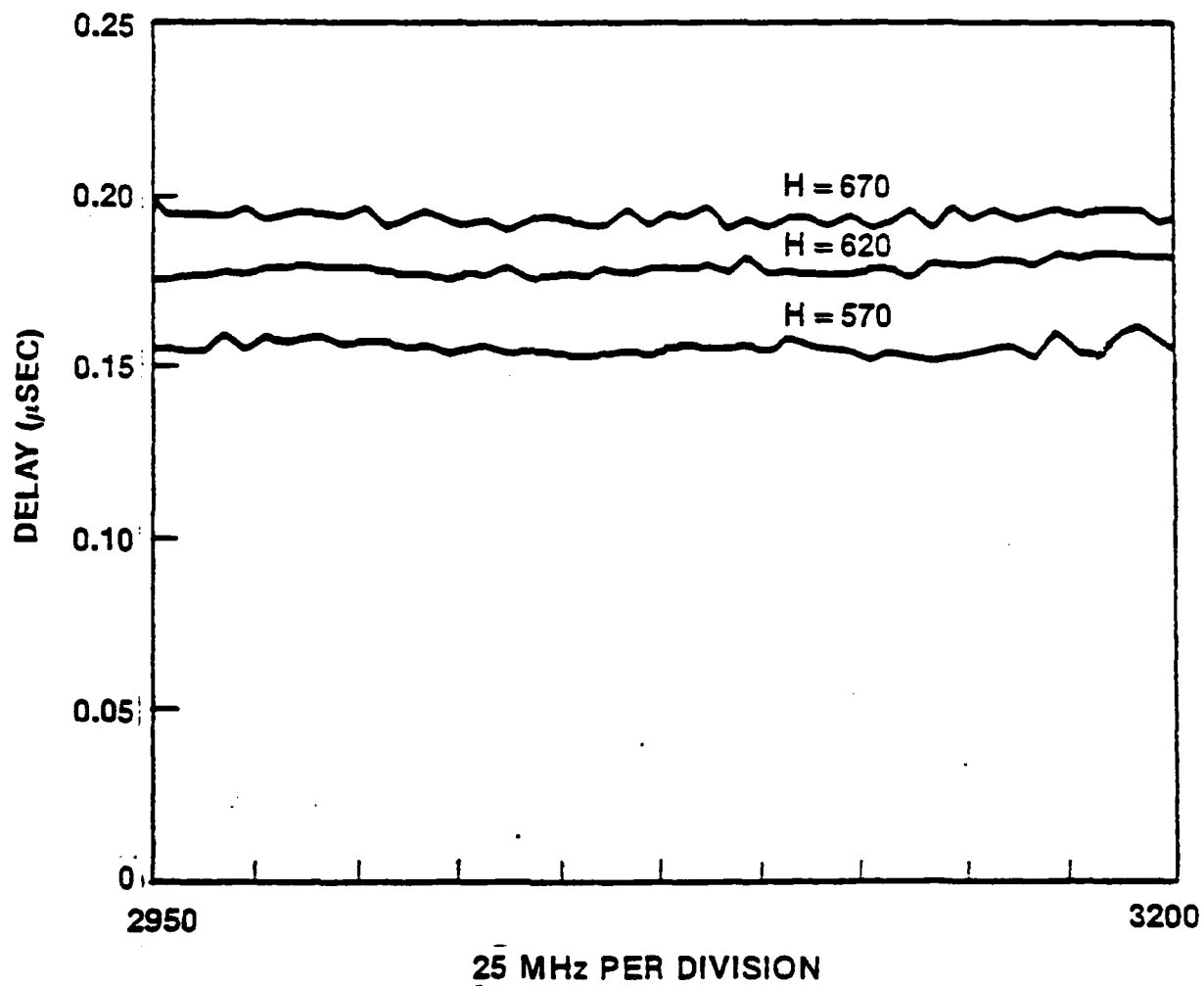Figure 2.2.3   MSSW and MSBVW dispersion curve and their sum

Figure 2.2.4   Dispersion curves for cascaded delay line as a

function of bias field

Current weighting in the form of $\dfrac{\sin (x)}{x}$ in a 16 element filter

from 540 to 650 Gauss. The data obtained are summerized in Table 2.2.2. The maximum delay differential obtained was 42nsec with an applied bias field of 110 Gauss. The bandwidth of this variable delay line is between 2.9 and 3.15 GHz, while the R.M.S. phase deviation from linearity ranged from 6.4° to 12.9°. These values are quite acceptable for a number of phased array radar/communications applications and represent a significant advancement in the state-of-the-art for MSW devices.

There is one problem with the cascaded device as it stands now. The insertion loss is high, approximately 35 dB across the band. This high value is a result of the device not being tuned. The loss could be reduced considerably with proper matching of the transducers.

2.2.4 Summary

An electronically variable time delay device comprised of two cascaded MSW delay lines has been fabricated and evaluated, and the operating characteristics are substantially better than previously reported embodiments of this device. The improvements are due mainly to the linearization of the two component dispersions. With a reduction in insertion loss and compact packaging, a device of this type will be ready for service in phased array systems.

Experimental results for the MSW Variable
Time delay lines

H$_{BVW}$(Gauss)	T(nsec)	R.M.S. (degrees)
540.0	149.6	9.75
550.0	154.7	12.90
562.5	159.7	11.10
575.0	164.7	10.60
587.5	169.3	9.50
600.0	173.8	9.10
612.5	178.0	6.40
625.0	182.4	6.80
637.5	186.7	6.40
650.0	191.4	12.20

Bandwidth: 2.9 TO 3.15 GHz

Table 2.2.2 Experimental results for the MSW Variable Time
delay lines

2.3 Passive Magnetostatic Wave Pulse Compression Loop

2.3.1 Introduction

A MSW pulse compression loop using active expended chirp signal generation and magnetostaic surface wave (MSSW) delay line with a nonlinear delay characteristic as the compression filter, was first demonstrated by K.W. Reed, et.al of this laboratory [11]. The "down chirp" signal was generated by a voltage controlled oscillator driven by a programmable sweep voltage with a matched nonlinear phase characteristic appropriate to the intrinsic non linearity of MSSW delay line. Phase predistortion techniques were used to achieve a 24 dB sidelobe ratio with a time-bandwidth product of 30.

In this study a matched pair of quadratic phase MSW delay lines with a center frequency of 3.2 GHz and 3 dB bandwidth of 320 MHz have been used as expander and compressor devices for pulse compression loop. A schematic diagram of the MSW pulse compression loop is shown in Figure 2.3.1. Appropriate amplitude weighting by using loop transducers in the MSSW device have provided 30 dB sidelobe suppression.
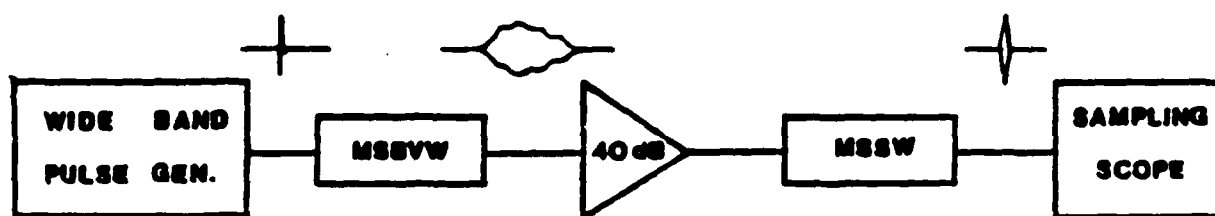
BLOCK DIAGRAM OF MSW PULSE COMPRESSION LOOP

Figure 2.3.1 Block diagram of MSW pulse Compression loop

2.3.2 Passive Generation Of The Down Chirp Coded Signal

A simple linear backward volume wave delay line, driven by a fast rise pulse generation, was used for the passive generation of the FM down chirp signal. The linear MSBVW dispersion characteristic was obtained in a straight forward manner by using a 50 um thick layer of YIG film spaced 250 μm above the ground plane. The linear dispersive curve of this delay line is shown in Figure 2.2.3. The slope of this linear delay line is -9.1 nsec/100 MHz. with deviation from quadratic phase less than 10 degrees over 500 MHz bandwidth at 3 GHz center frequency. The insertion loss of this delay line is 12-15 dB over the 500 MHz bandwidth.

2.3.3 MSSW Linear Matching Filter

The "matched" filter required in this pulse compression loop is a delay line with a time-inverted replica of the expanded signal as its impulse response. Since a linear MSBVW delay with a "down-chirp" quadratic phase characteristic is used to generate the down chirp signal, a linear delay with opposite constant delay slope over the same frequency band must be employed as the matched filter. The variable ground plane spacing technique described, in Chapter 2.1, has been used to achieve the required quadratic phase "up chirp" characteristics in a MSSW delay line. [10]. The slope of the dispersion characteristic, shown in Figure 2.2.3, is 9.7 nsec/100 MHz with a R.M.S. phase error less than 12 degrees over a 500 MHz bandwidth at 3 GHz center frequency.

2.3.4 Experimental Results

Initial experimental results, using single bar transducers in the MSSW delay line, showed only 20 dB of sidelobe suppression. This is a result of incorrect amplitude weighting and phase

30

distortion at the band edge. The 3 dB pulse width is approximately 5.5 nsec with a time bandwidth product of 24. An improved MSSW device was designed with a loop transducer to achieve a better weighting function characteristic for the MSSW pulse response envelope. The deviation from the Hamming weighting function was + or - 2.5 dB over the 320 MHz bandwidth at 3.2 GHz center frequency for a loop transducer of 250 μm loop spacing. The quadratic phase behavior was matched by adjusting the ground plane according to chapter 2. A 30 dB peak sidelobe ratio was obtained by using this loop transducer MSSW linear delay as the compressor in the MSW pulse compression loop with no phase predistortion. The characteristic of the MSBVW linear delay line down chirp filter, used as the impluse expander in the MSW compression loop, is summarized in Table 2.3.1. The characteristic of the MSSW linear delay line, used as the compressor in the MSW compression loop, is summarized in Table 2.3.2. The recompressed signal obtained by this pair of MSW matching

THE CHARACTERISTIC OF MSBVW LINEAR
DELAY LINE DOWN CHIRP FILTER

YIG THICKNESS: 50 μm
SPACING TO GROUND: 250 μm
BANDWIDTH:500 MHZ
CENTER FREQUENCY: 3.2 GHz
BIAS FIELD: 590 Gauss
TRANSDUCER SEPARATION: 1 cm
INSERTION LOSS: 12 TO 15 dB
DEVIATION FROM QUADRATIC PHASE: 10°
SLOPE OF LINEAR DELAY: -9.1 nsec/100 MHz

Table 2.3.1 The characteristic of the MSBVW linear down chirp
expansion filter

THE CHARACTERISTIC OF THE MSSW LINEAR
DELAY LINE COMPRESSION FILTER

VARIABLE GROUND PLANE SPACING
YIG THICKNESS: 25 µm
BANDWIDTH: 320 MHz
CENTER FREQUENCY: 3.2 GHz
BIAS FIELD: 410 Gauss
DEVIATION FROM QUADRATIC PHASE: 12°
SLOPE OF THE LINEAR DELAY: 9.7 nsec/100 MHz
WEIGHTING: loop transducer
            250 µM loop spacing

Table 2.3.2 The characteristic of the MSSW linear compression filter

filters is shown in Figure 2.3.2 with 8 nsec 3 dB pulse width and a time bandwidth product of 12.

2.3.5 Conclusion

A pulse compression loop using a pair of matched MSW delay lines with passive (impulse) generation has been demonstrated with -30 dB time sidelobes and a time bandwidth. Finally, a comparison of the SAW and MSW pulse compression loop is summarized in Table 2.3.3. As shown in this table the compression gain of MSW compression loop is modest by SAW standards. However, significant potential for increase in gain exists, as well as good potential for better sidelobe suppression.
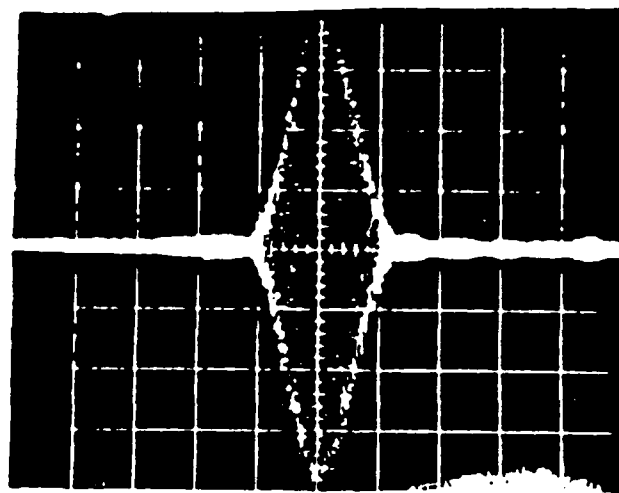
Figure 2.3.2 Experimentally recompressed pulse from loop transducer device

SAW	MSW
IF freq (<1 GHz)	RF freq (1-20 GHz)
-3 dB pulse width 8 to 1000 nsec	-3 dB pulse width 2 to 10 nsec
weighting using interdigital transducer	weighting approximate by loop transducer
TBP 50 to 1500	TBP 12 to 30 (experimental)
sidelobe levels 30 to 45 dB	sidelobe levels 24 to 30 dB

Table 2.3.3 A comparison of SAW and MSW pulse compression loop

2.4 Magnetostatic Surface Wave Matching Network

Impedance matching provides a method of maximum power transfer between the signal source and the load. Usually, a quarter wavelength microstrip line-section is required for impedance matching when the value of the source resistance is quite different from that of the load impedance. However, the quarter wavelength is bandwidth limited. From early work of microstrip transducer theory and experiments, it was known that the input impedance of a single bar transducer, used as a microwave energy coupler in the "flipped" configuration with the YIG film flipped over the single bar microstrip transducer, depends on the length and width of the single bar microstrip and the thickness of the YIG film [12]. Experimentally, the coupling between electromagnetic waves and MSW is strong, and the resultant input impedance of a single bar MSW microstrip transducer of length in the order of millimeters is in the range of 50 Ohms. Theoretically, by adjusting the length of the single bar transducer, the real (resistance) part of the input impedance can be selected, so that it is close to the source resistance of 50 Ohms. Therefore, by adjusting the length of the single bar transducer, input impedance matching can be performed. The length of the microstrip is then adjusted accordingly to obtain, to first order, the input matching circuit. Usually, the imaginary (reactance) part of this microstrip transducer is inductive; one way to compensate this inductive reactance is to introduce a series input capacitor. Another way is to use one short section of microstrip transmission line to rotate the input impedance to the real axis of the Smith chart and a

37

quarter wavelength line-section of appropriate characteristic impedance to match this inductive reactance to the source impedance that is usually 50 Ohms.

The objective of this study is to reduce the insertion loss associated with the mismatch in the continuously variable ground plane magnetostatic surface wave linear delay device. This device was 50 µm-wide by 3 mm-long, had a 3 µm thick microstrip transducer and had a 25 µm YIG flipped over on it. It was measured with the external bias field of 410 Gauss with the output short circuited in the MSSW mode. The HP 8409B automatic network analyzer was used to measure the reflection parameters of the device. The reference plane chosen in this measurement was in the end of the 50 Ohms cable with a SMA male connector. The rotation of the input impedance data due to the electronic length of the SMA connector and the 50 Ohm microstrip line is accomodated by using a NEG statement in the COMPACT analysis program. The corrected input impedance is shown in Figure 2.4.1. The bandwidth of interest in this case is from 2.9 to 3.15 GHz or only 250 MHz. The resistance of this set of data from 2.9 to 3.15 GHz is close to 50 Ohms. One can match the reactance of this set of data to 50 Ohms by a series capacitor of 1.9 pF or by using a 50 Ohm 30 degree microstrip line to rotate the parameters to the resistance axis on the Smith Chart and a 65 Ohm quarter wavelength transformer to match the parameters to 50 Ohms. Figure 2.4.2 shows the theoretical predicted reflection coefficients by COMPACT by using the 50 Ohm 30 degree microstrip line and the 65 Ohm 90 degree microstrip as the matching network. An experimental matching network using the

S11
B

f1:   2.80000

f2:   3.30000
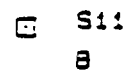
Figure 2.4.1 The reflection coefficients of the MSSW device with
            a shorted-circuited 50 μm-wide, 3 mm-long, and 3 μm-
            thick microstrip transducer in the "flipped"
            configuration
            Thickness of YIG is 25 μm

39
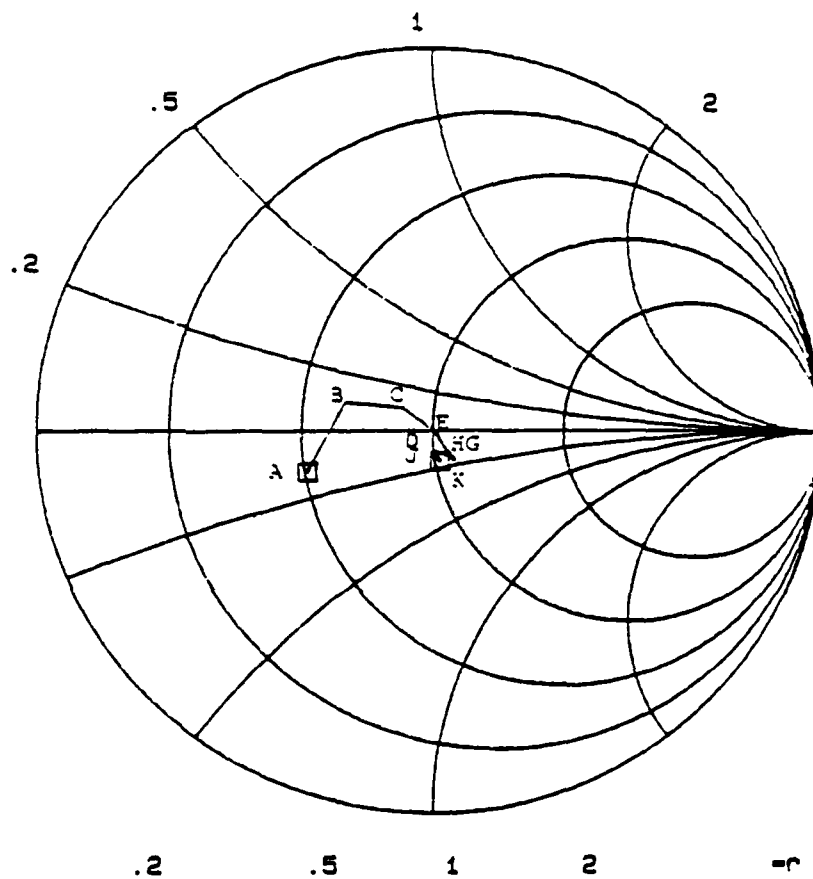
Figure 2.4.2 Theoretical predicted results by COMPACT on the
reflection coefficients by using a 50 Ohm 30 degrees
microstrip line and a 65 Ohm 90 degree microstrip
line as the matching network

50 Ohm 30 degree microstrip line and the 65 Ohm 90 degree microstrip transformer was built and tested. Figure 2.4.3 shows the measured data of this device. This is very close to the theoretical predicted data shown in Fig 2.4.2.

Experimentally, one finds that the reflection coefficients are the same for devices with or without the continuously variable plane structure, but the insertion loss for the device with a continuously variable ground plane is higher due to ground current loss. Therefore, the matching network should work for a device with or without a ground plane. By matching the input impedance, the loss due to reflections is minimized. Figure 2.4.4 shows the insertion loss of the MSSW delay line without the variable ground plane structure and without the matching network from 2.8 to 3.3 GHz; the maximum insertion loss from 2.9 to 3.15 GHz is about 15 dB whereas the minimum insertion loss in this frequency band is 11 dB. Figure 2.4.5 shows the improvement due to the matching network for the MSSW delay line without the center variable plane structure; the maximum insertion loss is 12 dB and the minimum value is 8 dB. The overall improvement is about 3 dB across the bandwidth of interest.
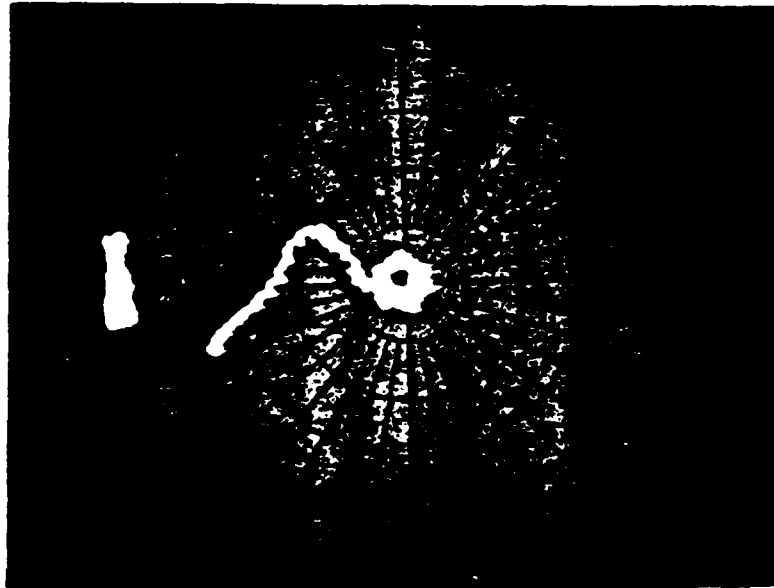
Figure 2.4.3 The experimental measured data on the reflection
coefficients of the matching network by using a
50 ohms 30 degrees microstrip line and a 65 ohms
quarter wavelength microstrip transformer
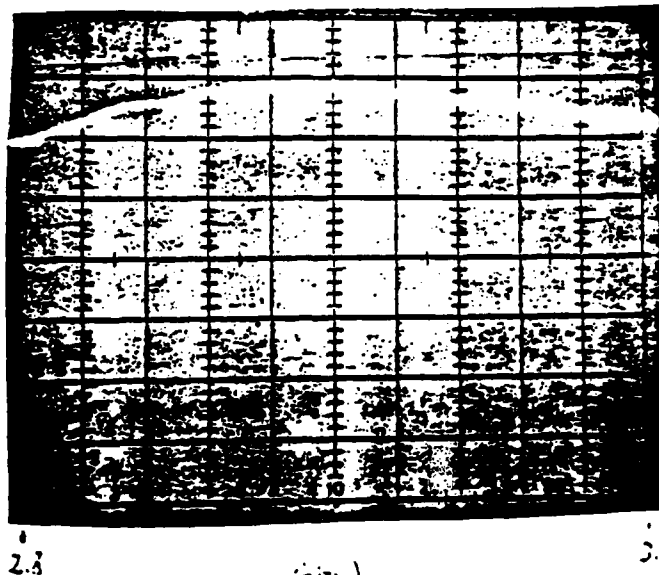
Figure 2.4.4 The insertion loss of the non-matched MSSW delay
line 2.8 to 3.3 GHz
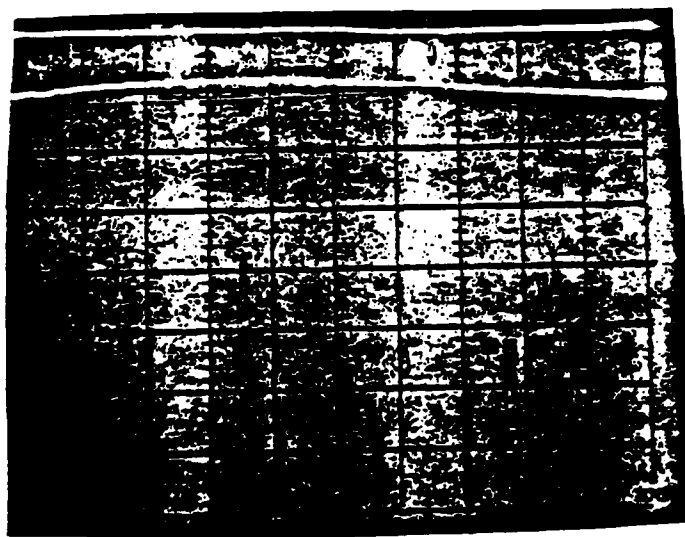
Figure 2.4.5   The insertion loss of the matched MSSW delay line
from 2.9 to 3.15 GHz

2.5 REFERENCES

1. R.W. Damon, and J.R. Eshbach, "Magnetostatic modes of a ferromagnet slab", J. Phys. Chem. Solids, 1961, 19, pp. 308-320.

2. W.L. Bongianni, "Magnetostatic propagation in a dielectric layered structure", J. Appl. Phys., 1972, 43, pp. 2541-2548.

3. J.M. Owens, and R.L. Carter, "Magnetostatic advance: the shape of wave to come", MSN, 1983, 13, pp. 103-111.

4. J.D. Adam, M.R. Daniel, P.R. Emtage, and R.W. Weinert, "MSW variable time-delay techniques", Rome Air Development Centre, Electronic Systems Division, Final Report, Contract F19628-80-C-0150, 1982.

5. K.W. Reed, J.M. Owens, C.V. Smith, Jr., and R.L. Carter, "Simple magnetostatic delay lines in microwave pulse compression loops", 1980 Int. Microwave Symp. Digest, 80 CH 1545-3 MTT, pp. 40-42.

6. Kok Wai Chang, Duccio Gerli, R.L. Carter, and J.M. Owens, "Passive Manetostatic Wave Pulse Compression Loop", Accepted for publication in 1984 Int. Microwave Symp. Digest.

7. J.C. Sethares, J.M. Owens, C.V. Smith, Jr., "MSW nondispersive, electronically-tunable time delay elements", Electron. Lett., 1980, 16, pp. 825-826.

8. L.R. Adkins, R.L. Carter, Kok Wai Chang, H.L. Glass, J.M. Owens, and F.S. Sterns, "Electronically variable time delays using cascaded magnetostatic delay lines", To be published at J. Appl. Phys.

9. J.D. Adam, M.R. Daniel, and D.K. Schroder, "Magnetostatic-wave devices move microwave design into gigahertz realm", Electronics, May 8, 1980, pp.123.

10. K.W. Chang, J.M. Owens, and R.L. Carter, "Linearly designs in Time-Delay Control of Magnetostatic Surface wave by variable Ground-Plane Spacing", Electron. Lett. 19, 1983, pp.546.

11. K.W. Reed, C.V. Smith, Jr., J.M. Owens, and R.L. Carter, "Microwave Pulse Compression Loops Using Magnetostatic Wave Delay Lines", Proceedings of the 1981 RADC Microwave Magnetics Technology Workshop, RADC-TR-83-15, Rome Air Force Base, NY 13441, pp. 277-289 (1983).

12. H.J. Wu, "Magnetostatic Wave Transducers", Ph.D. Thesis, University of Texas at Arlington, December, 1978.

13. K.W. Reed, "Magnetostatic Ion Implanted Reflected Array Filters, PhD Dissertation, UT Arlington, 1985

3. MSW TRANSVERSAL FILTER

3.1 MSSW Transversal Filter Based on Open Circuit Transducer Arrays

Although some limited types of bandpass shaping are possible using multibar transducers or reflective arrays, the performance of these devices exhibit high insertion loss. The complexity of the theoretical multibar transducer response using the reflective array techniques (etched metal film patterns, ion implanted zone, etc.) is the main reason for this group to seek alternative techniques.

The first approach was to investigate the practicality of the design of transversal filters by current weighting of multibar transducers. To do so, two sets of single bar, 3mm I/O transducers were built. One set was made using the standard photolithography and gold up-plating technique which resulted in a circuit pattern with gold thickness of about 3 μm. The ohmic resistance of the transducer was approximately 0.5 Ohms. For the other set, the transducers were covered with photoresist before gold plating the circuit to prevent it from plating, so only the 50 Ohm transmission line was gold plated to a thickness of 3 μm. The transducers had a thickness of about 800 Angstroms and the ohmic resistance was about 200 Ohms. The theoretical and experimental insertion loss vs. frequency response of the two devices are shown in Figure 3.1. The same procedure was repeated for a two parallel I/O bar and a four parallel I/O bar delay lines with transducer spacing of 300 μm for all of them. The results are shown in Figures 3.2 and 3.3.
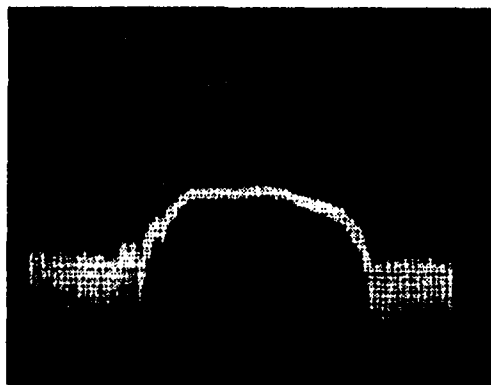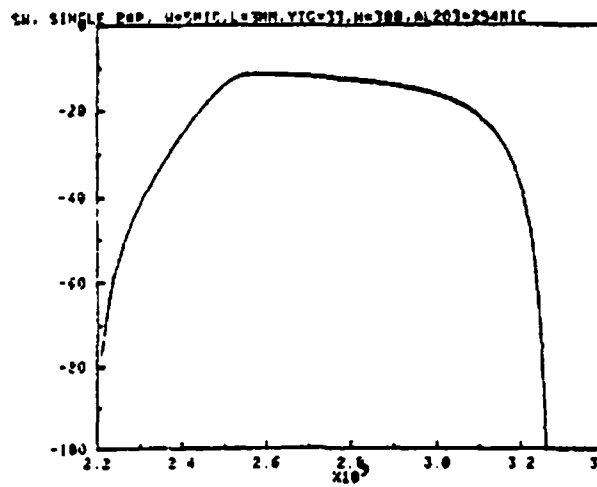
Figure 3.1 The theoretical frequency response of a singlebar I/O (TOP) and
the experimental result for 3 micron thick transducer (MIDDLE)
and 800 angstrom thick transducer (BOTTOM).
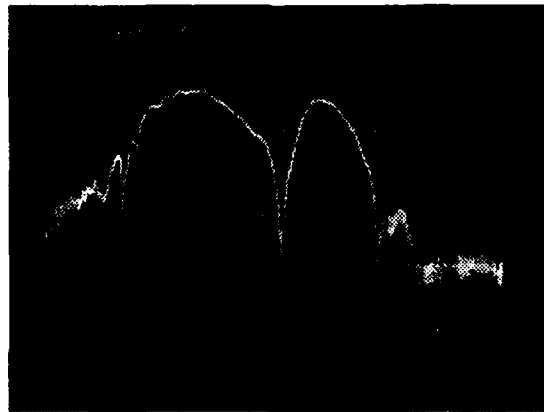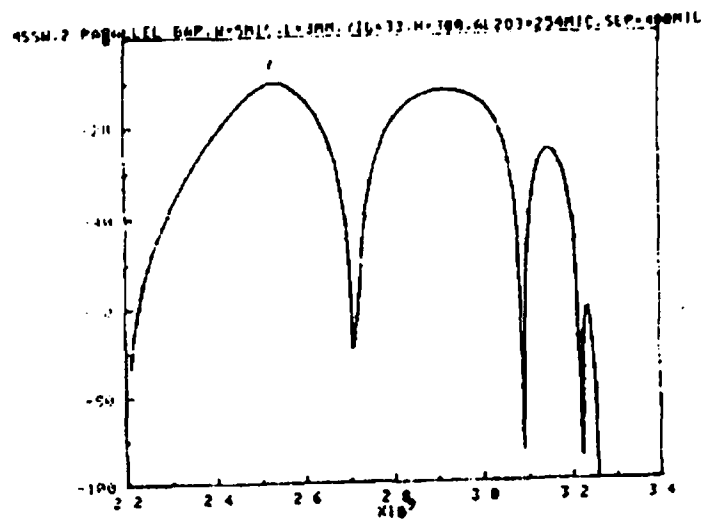
Figure 3.2 The theoretical frequency response of a 2 parallel Ibars I/O delay line
(TOP) and the experimental results for 3 micro thick transducers
(MIDDLE) and 800 angstrom thick transducers (BOTTOM).

47

Figure 3.3 The theoretical frequency response of a 4 parallel bars I/O delay line
(TOP) and experimental results for 3 micron thick transducer (MIDDLE)
and 800 angstrom thick transducer (BOTTOM).

48

The next step was to see if some kind of current weighting could be done by having thin gold in a portion of the transducer while the rest of the transducer length had thick gold. As an example, consider two delay lines, each having a single bar in the input and the output with one device having thick transducers and the other with thin transducers. If the average current in the thick transducer is I and the average current in the thin transducer is I_o (where obviously $I > I_o$), then the minimum current weighting factor is equal to $I_o/I=a$ where $0<a<1$. If the thickness in the thin transducer is very small, then $0\leq a<1$. Therefore any current weighting could be obtained by dividing the transducer into two specified regions of thick and thin films. Three sets of 5 bar I/O transducers were fabricated. One set had thick gold on the entire length of each transducer, and was used as the control sample. The responses of the other devices were compared with this control. In the other two sets, a portion of each transducer was made to have a thickness of about 800 Angstroms (shown as the white area in Figure 3.4), and the remaining length had a thickness of about 3 μm (black region).

It should be pointed out that at this point no attempt was made to precisely control the ratio of the thick and thin gold regions. The main interest was to experimentally investigate the effect of current weighting (although unknown), on the frequency response of the multibar transducers. The insertion loss responses of the three devices are shown in Figure 3.4. As can be seen a dramatic change can occur if the current is not distributed evenly in each finger of a multibar transducer delay line. These results indicate that the frequency response can be changed with proper current weighting

49
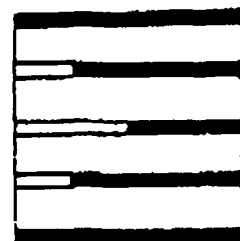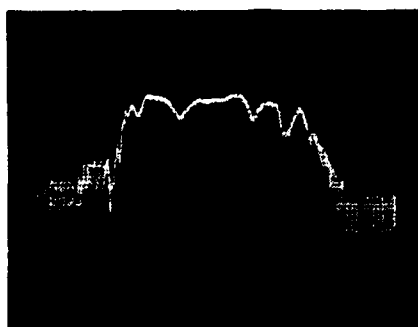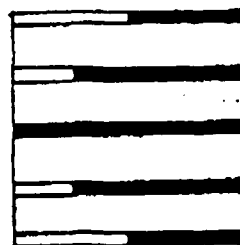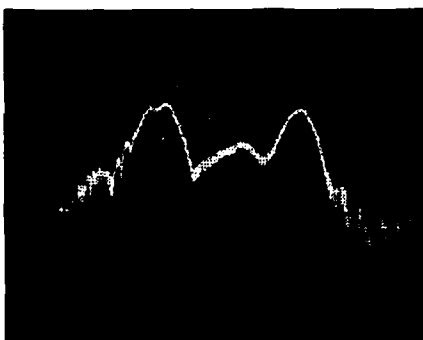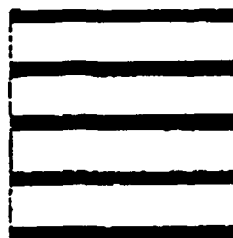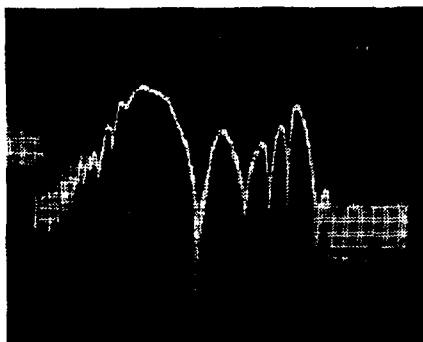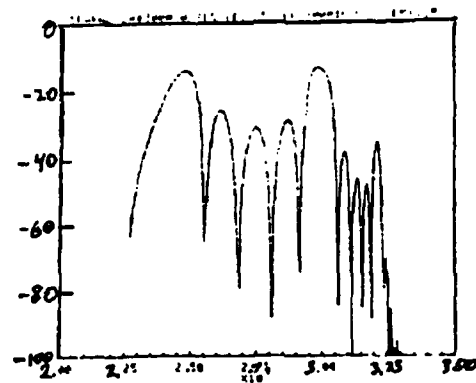
Figure 3.4 The theoretical frequency-I.L response for a 5
parallel bars I/O delay line (TOP). The experimental response
for three dufferent current weighting configurations are
shown here.

50

technique.

The theoretical approach for designing a filter is given in Appendix 1. The set of computer programs used for synthesizing a filter is printed in Appendix 2. All the programs were written in FORTRAN and were run on a DEC-20 system. The first program gives the linear insertion loss vs. frequency response (total of 152 points) for a single bar delay line with zero path length in the MSSW mode. The second program, [13] calculates the complex K values for the frequency range determined from running the first program. Finally, the synthesis program was run which used linear frequency vs. insertion loss data and complex K data from the two previous programs to generate normalized current weighing factors for an N bar transducer. The shape of the filter was in this case predetermined to have a square passband. In this program, one can change the shape of the passband, the bandwidth, the center frequency, the sidelobe suppression and the number of transducers. As an example, the program was run for synthesizing a bandpass filter centered at 2.8 GHz. This showed the effect of the passband and also the number of transducers on the frequency response of the filter. The passbands being considered are 100 MHz, 150 MHz and 200 MHz. For each case the number of transducers varied as 5, 7, 9, 11, 13, 15 and 25. From the results shown in Figure 3.5, it is clear that for a given bandwidth there is an optimum number of transducers. Increasing the number of bars beyond this point will not improve the response of the filter any further. Figure 3.6 is the theoretical response of a 21 bar transducer programmed to be a 100 MHz bandpass filter centered at 2.8 GHz with sidelobe suppression of 100 dB. As can be seen the maximum theoretical
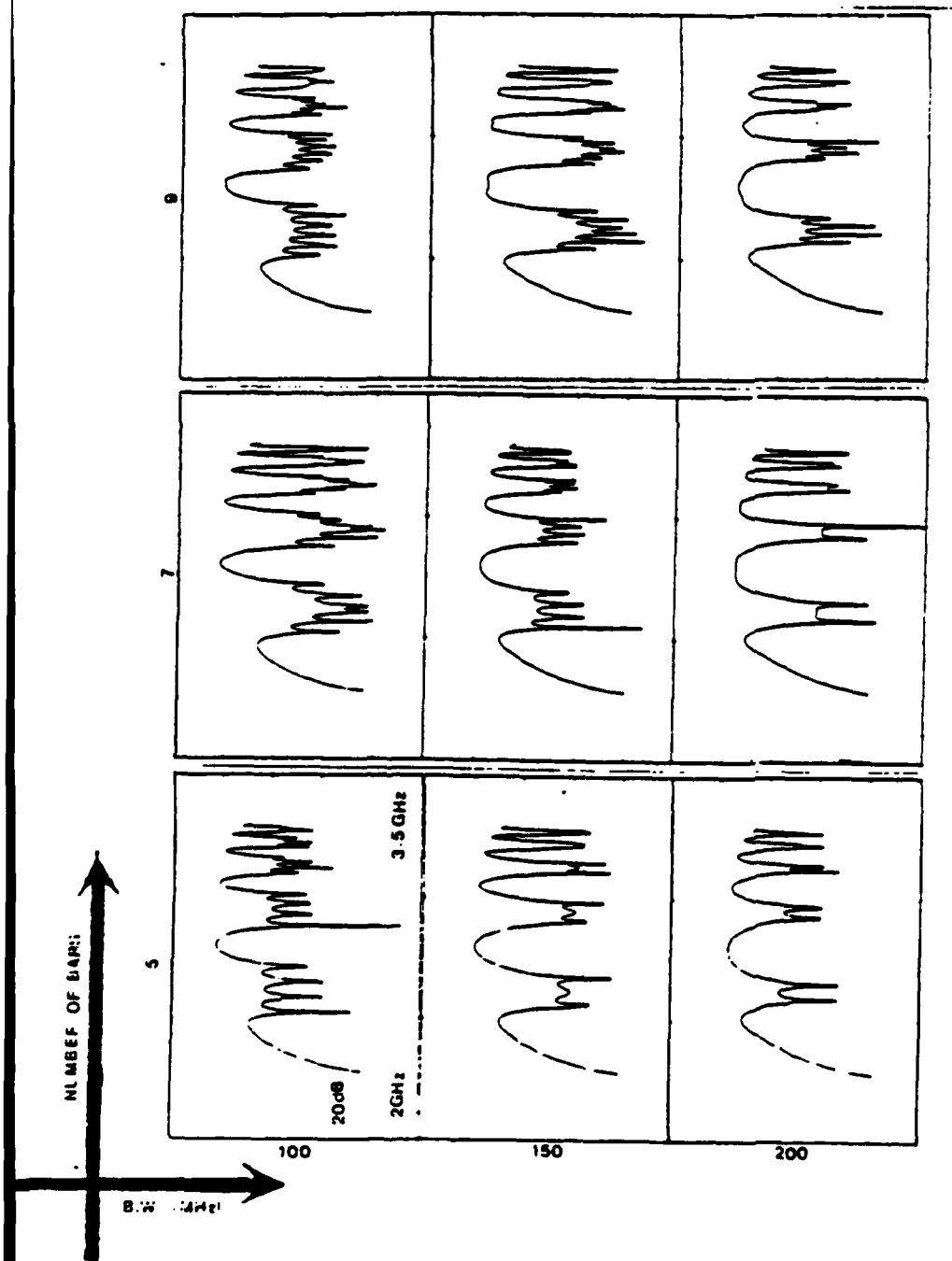
Figure 3.5 The frequency response of a bandpass filter when the bandwidth and the number of transducers are varied. These sets of plots indicate that there is an optimum number of the bars for a given bandwidth.

Figure 3.5 continued.

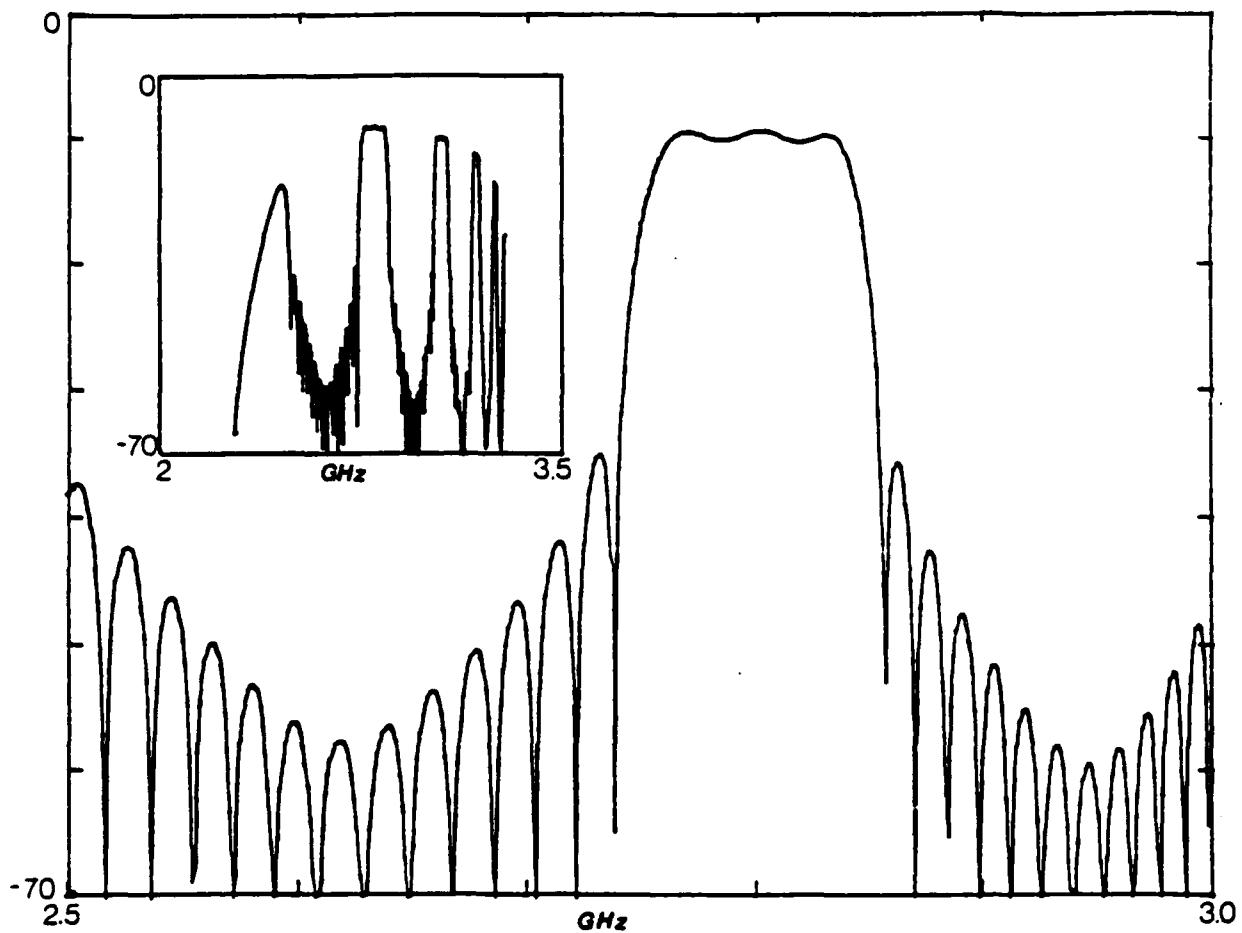NUMBER OF BARS

B.W. MHz

11   13   15   28

53
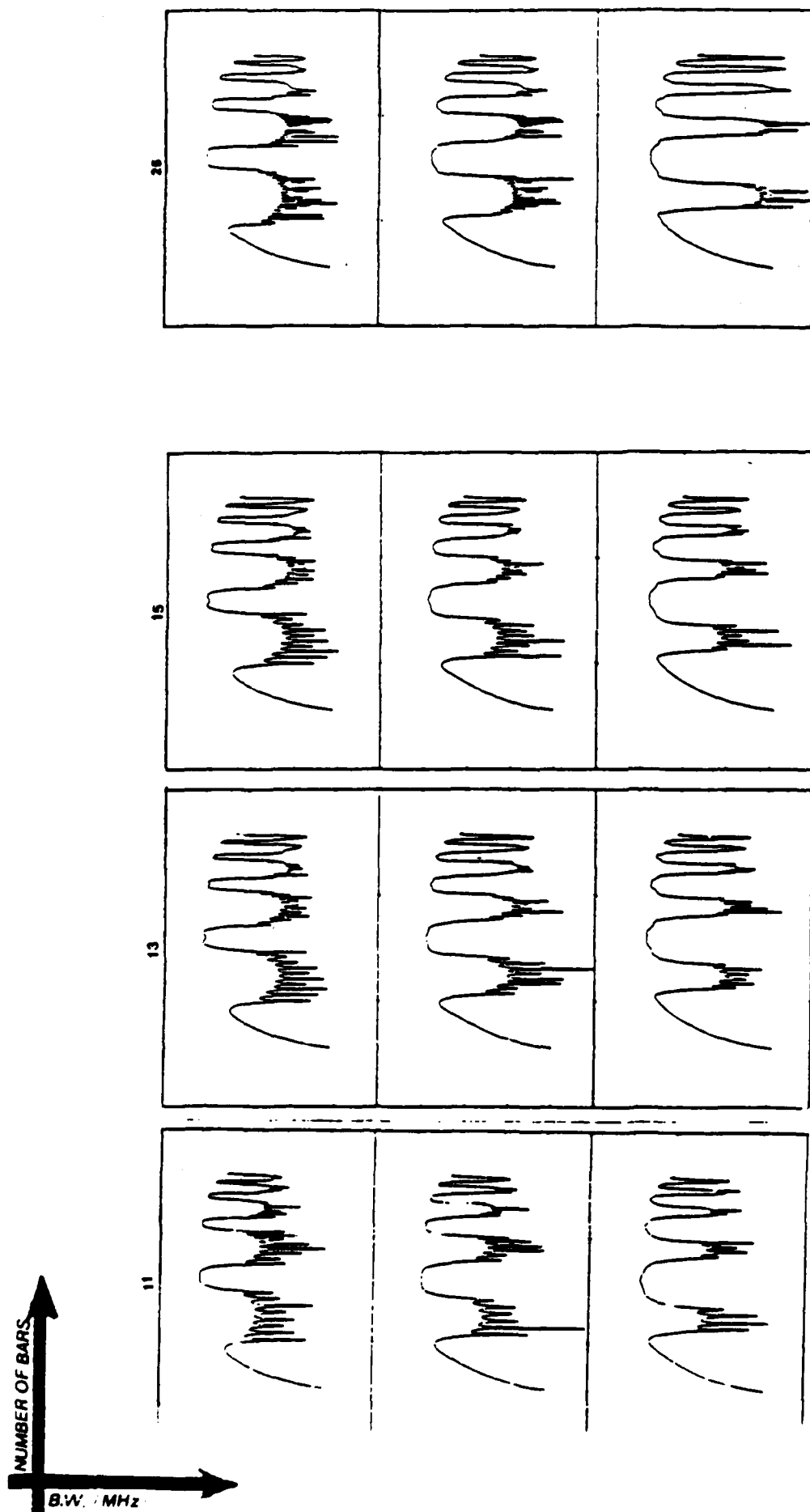
Figure 3.6 The theoretical frequency response and its expanded form of
a 21 bar filter designed to have a bandwidth of 100 MHz,
centered at 2.8 GHz and to have a sidelobe suppression of 100
dB.

sidelobe suppression is about 30 dB.

This synthesis program outputs the normalized current weighting factors ($-1 < a < +1$) and does not determine or depend on the technique being used to achieve the weighting. To experimentally check the synthesis program, four sets of devices were constructed (named CHECK5-A, CHECK5-B, CHECK7-A, and CHECK7-B) which are shown in Figure 3.7. In all four patterns, the transducers were 3 mm long and 30 μm wide and the 50 Ohm transmission lines feeding each element were equal in length for each device. This was done to equalize the phase for each bar. The devices had either 5 or 7 bars at the input and one at the output. MSW delay line is bilateral so that the input and output can be interchanged when the direction of the magnetic field is changed. For the two cases of CHECK5-B and CHECK7-B the patterns were designed so two of the elements could have current flowing in the opposite direction of the current in the other bars.

In addition, different attenuators having different values were connected to each port to control the current passing through each finger. Using equal length 50 Ohm coaxial cables, the attenuators were connected to an 8-way power divider where its unused ports were terminated by 50 ohm loads. A computer program (Appendix 3) was written to compute the insertion loss response of an N bar transducer with external attenuators for current weighting. The theoretical and experimental responses for these devices with different cases are shown in Figure 3.8. These figures demonstrate very good correlation between the theory and experiment.

The next step was to construct the filter and use a current

55
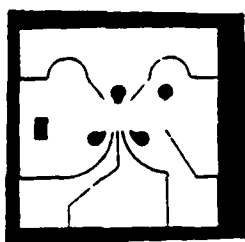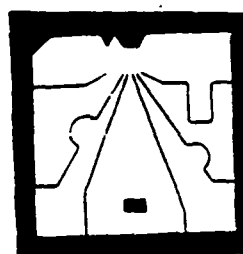
CHECK5-B

CHECK5-A
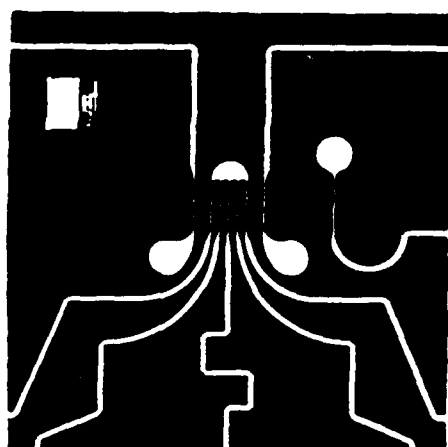
CHECK7-B
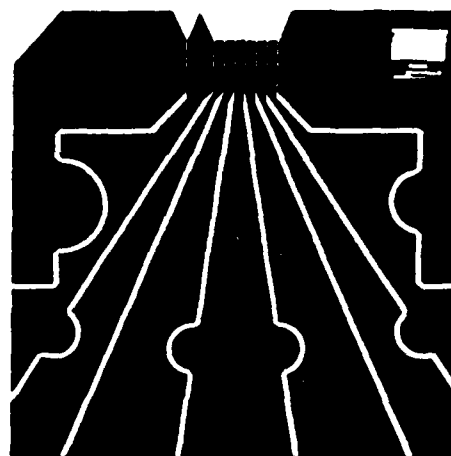
CHECK7-A

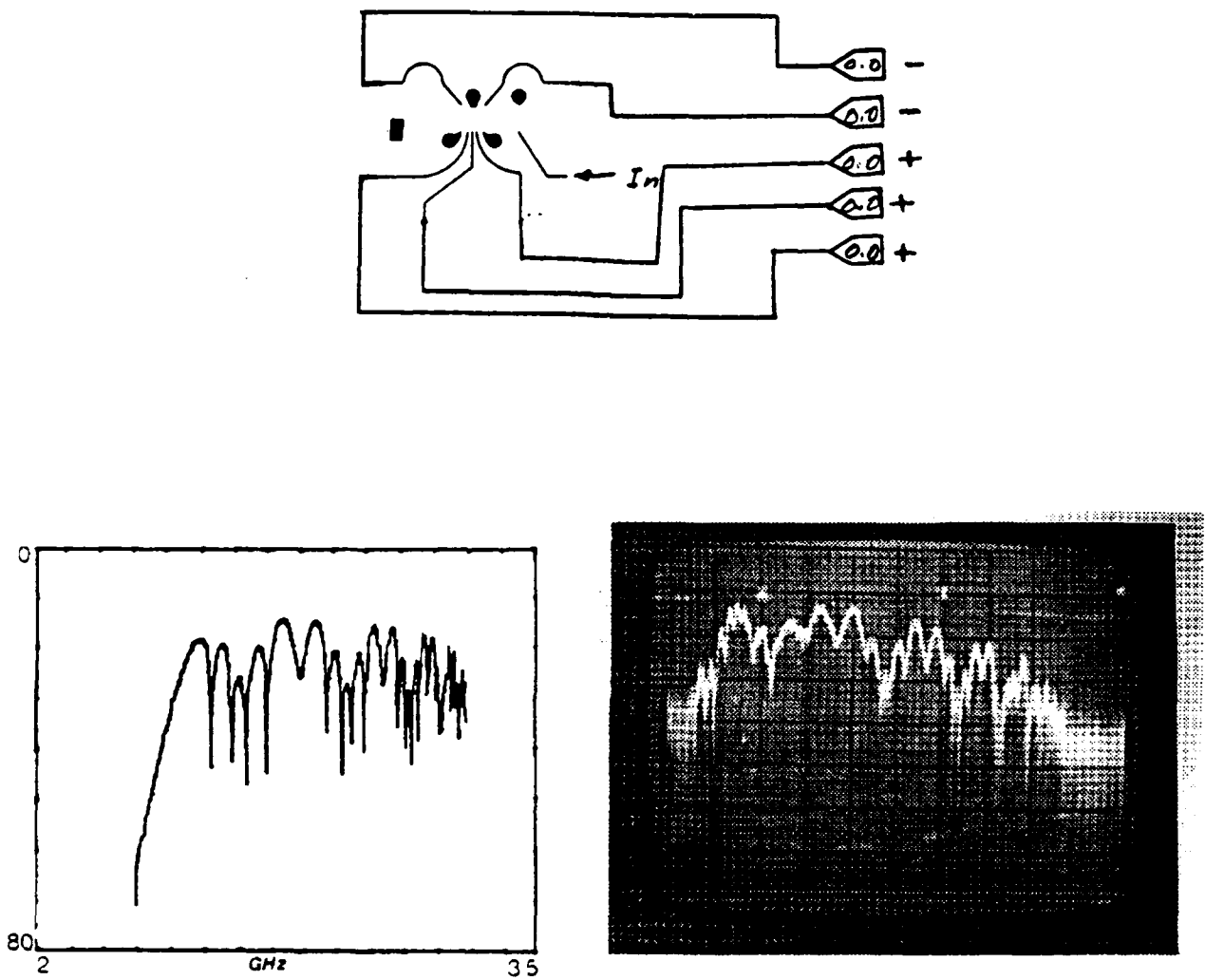Figure 3.7   See text for explanations.

Figure 3. 8 The values of the external atternuators, the theoretical predtiction
of the frequency response, and the experimental results for
several devices with different configurations. (Notice the values
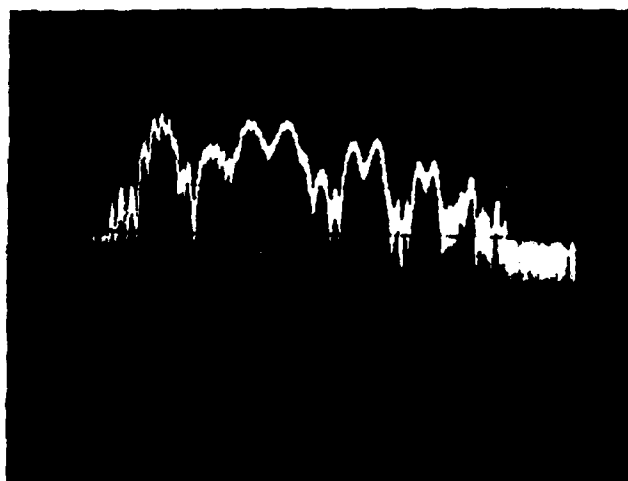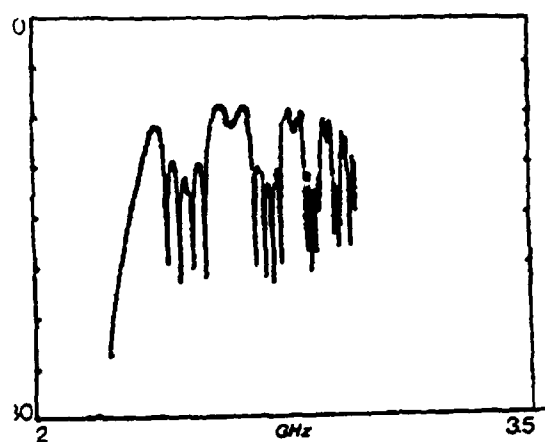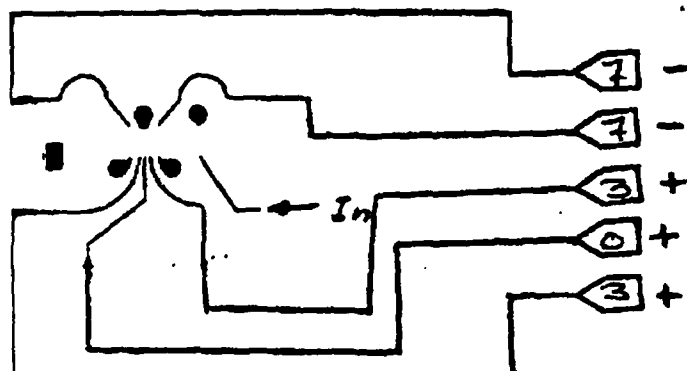of the attenuators given in dB for each case).
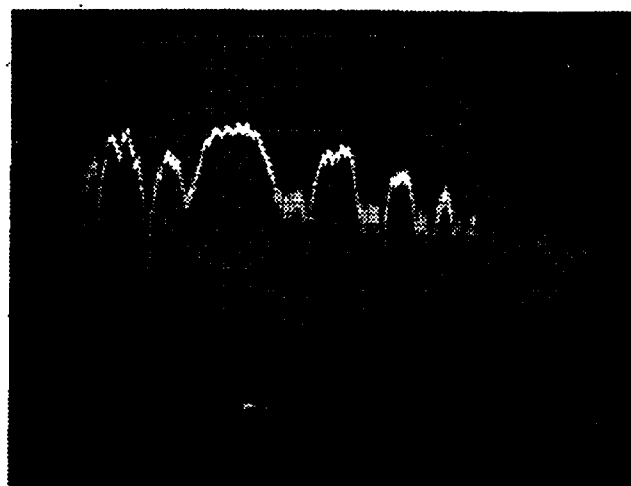
57

Figure 3.8 continued.
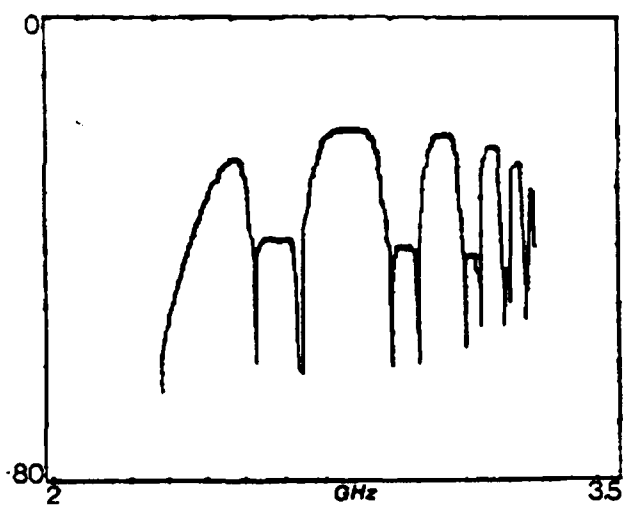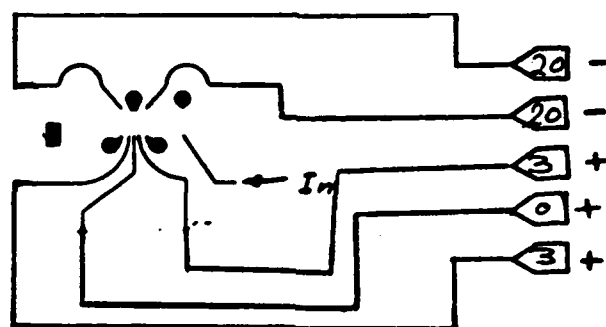
Figure 3.8 continued.
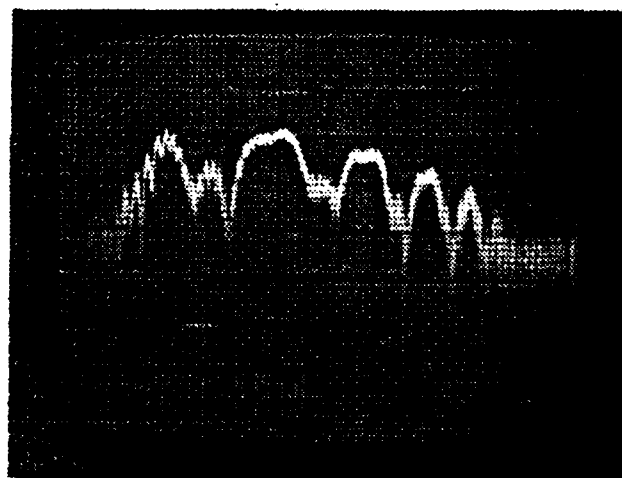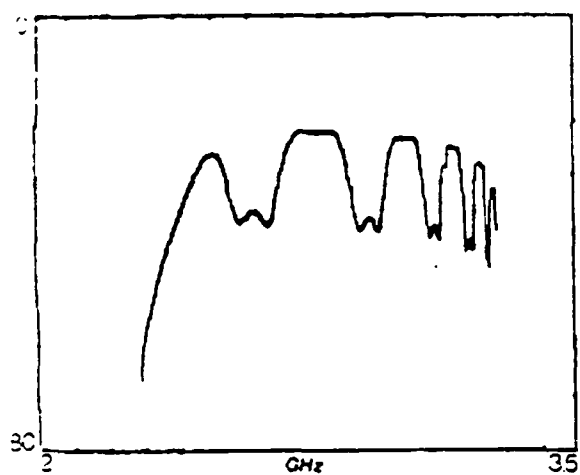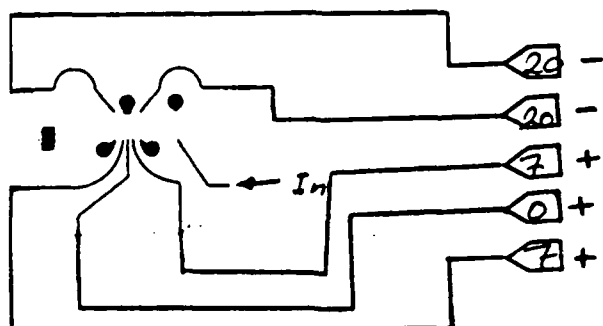
Figure 3.8 continued.
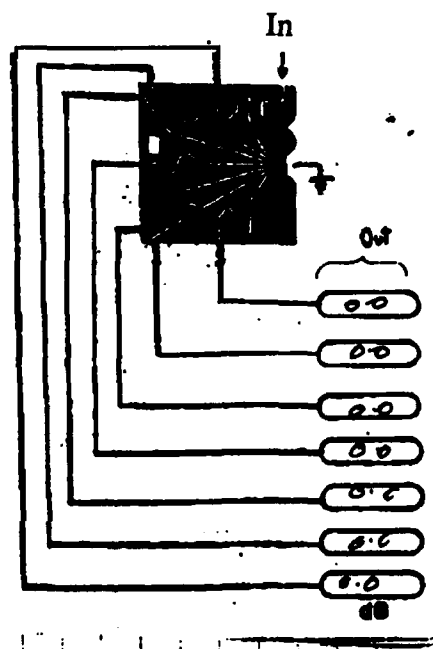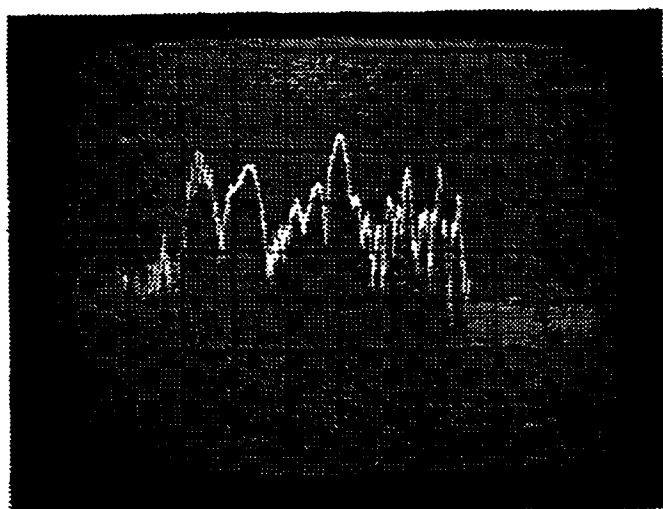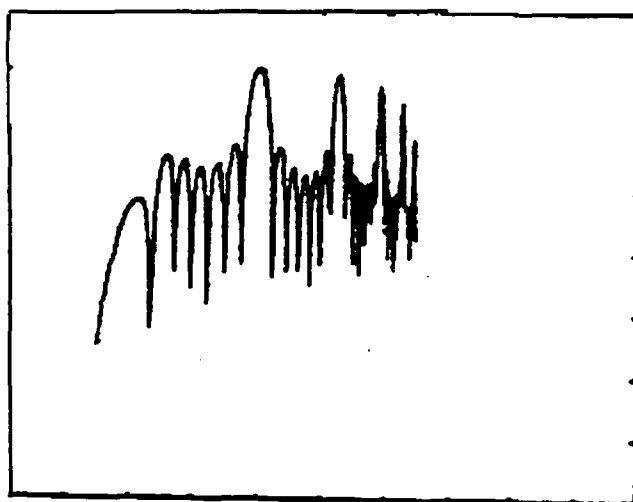
Values of the external attenuators (right), theoretical prediction (top-left),
and the experimental results (bottom-left).

Figure 3.8 continued.

61

Values of the external attenuators (right),
theortetical predition (top-left), and the
external results (bottom-left).

Figure 3.8 continued.
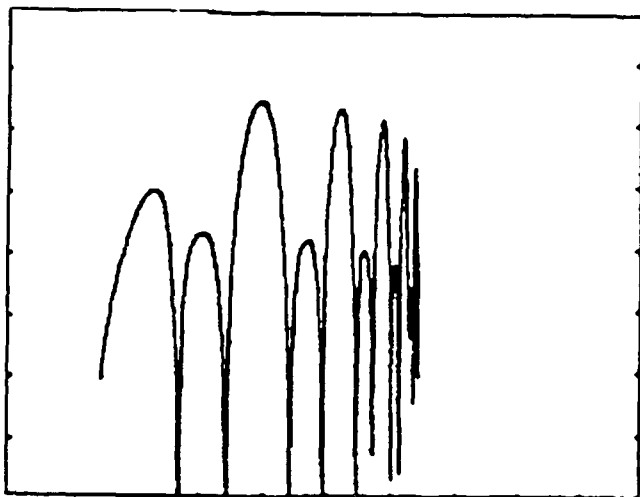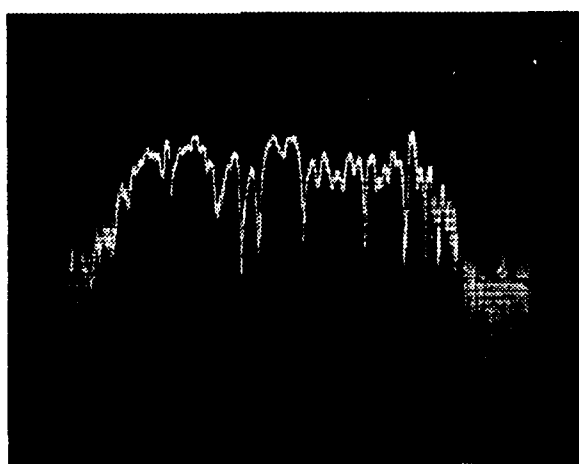
Values of the external attenuators (top), theoretical prediction (middle), and the experimental results (bottom).

Figure 3.8 continued.

Figure 3.8   continued.

64
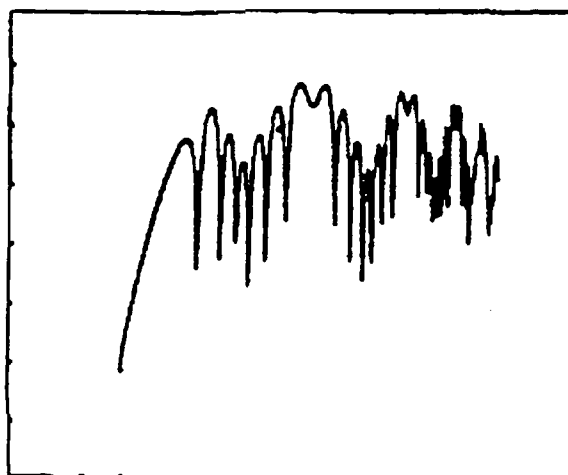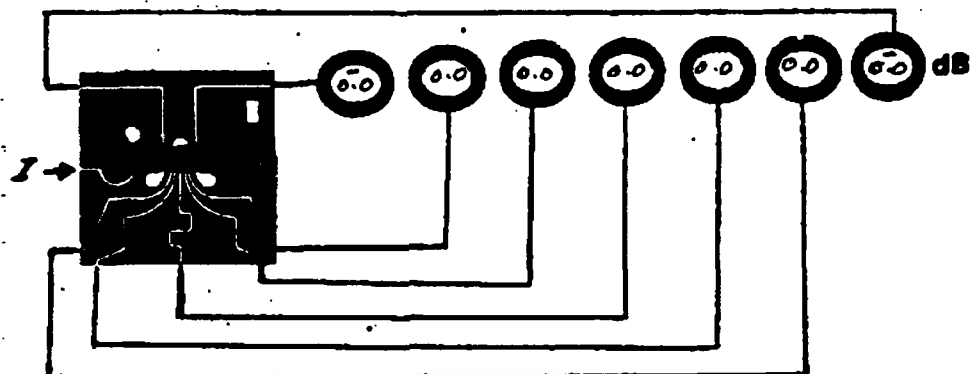
Values of the external attenuators (top), theoretical prediction (middle)
and the experimental results (bottom).

Figure 3.8 continued.
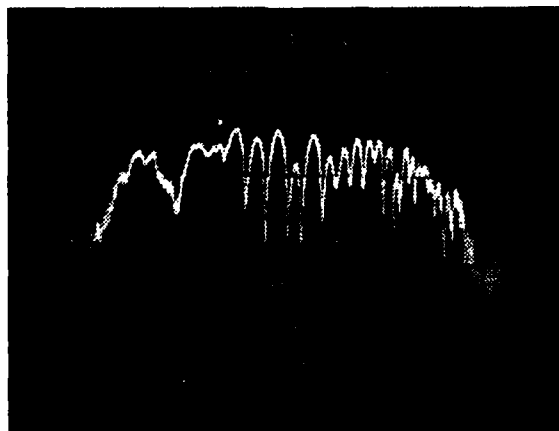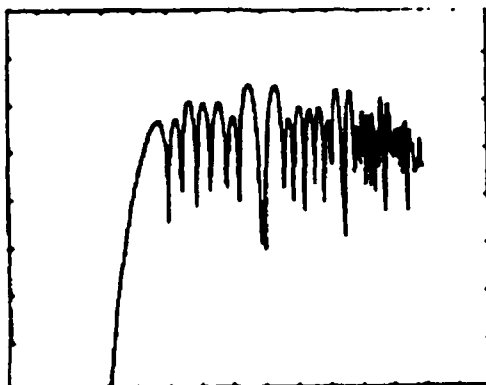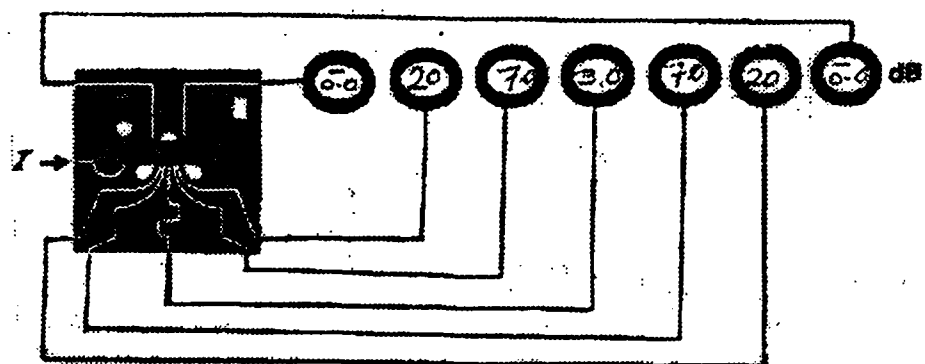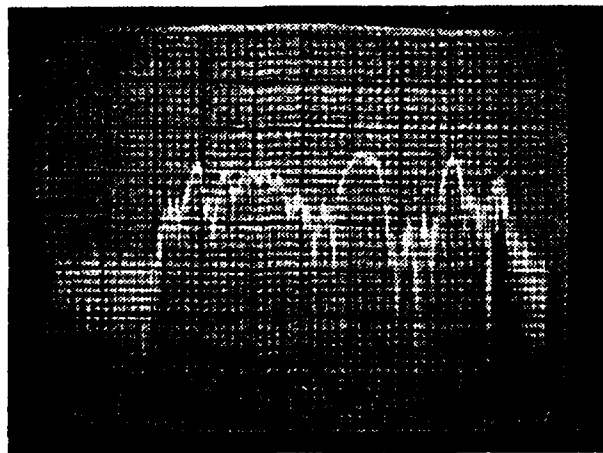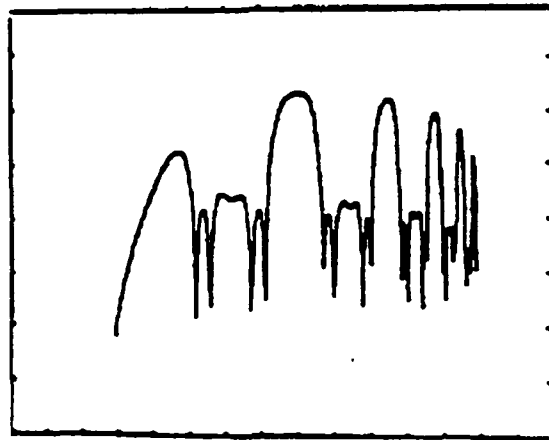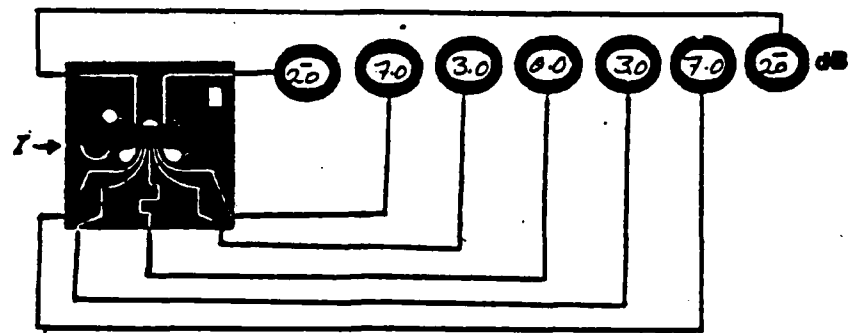
weighting technique that can produce any current weighting factor in the range of -1 to +1.

The earlier method of weighting the transducer by thick and thin gold plating has several shortcomings. First of all, it is practically limited by the precision of controlling the thickness. Second, one can only achieve positive weighting factors, and even then, it is impossible to have a practical current weighting of zero.

To overcome these problems, another approach to the distribution of current was taken by using an open gap transducer. technique. In an open ended transducer bar the current at the position of the gap is zero and increases in the sinusoidal form as distance away from the gap increases. If the length of the transducer is very small in comparison with the wavelength, the current distribution can be considered to be linear. If a transducer is fed from both ends and a gap is placed in the center of the transducer, the .net current of the transducer will be zero. By varying the position of the gap along the length of the transducer, it is possible to have a normalized current of any value from -1 to +1 (see Figure 3.9). Figure 3.10 shows the circuit pattern and the frequency response of a 21 bar bandpass filter (named FILTER-A) designed to have 100 MHz bandwidth centered at 2.8 GHz. Two other designs (FILTER-B and FILTER-C) and their frequency responses are shown in Figures 3.11 and 3.12.

All these filters seemed to work only at a single frequency and when the tuning was attempted, the response became disturbed as shown in Figure 3.13-d. The following explanation is believed to cause the distortion. As shown in Figure 3.13-a, in addition to the

66

SIN(X)/X current distribution of the transducer, there is also an additional current distribution due to the transmission line feeding the fingers. The combined effects are shown in Figure 3.13-b, and the frequency response for this kind of current distribution is plotted in Figure 3.13-c. This is very similar to Figure 3.13-d. Effects of the addition of different types of current distributions on the main SIN(X)/X curve are shown in a series of plots in Figure 3.14.

A power divider to distribute current evenly to each bar was needed to overcome this problem. A simplified current divider was used to design a 16 finger bandpass filter which is shown in Figure 3.15. The tuning capability of this device is demonstrated in Figure 3.16.

Next, to suppress the other harmonics of the filter, a loop transducer was used instead of the single bar transducer. As shown in Figure 3.17, when the response of a single bar-loop delay line (curve # 2) is superimposed on the frequency response of a weighted multibar-single bar filter (curve # 1), the result is suppression of the harmonics (curve # 3). The procedure to theoretically calculate the loop-multibar response follows. First, program 1 of Appendix 2 is run for single bar-single bar mode. Then the same program is run for loop-loop mode. The two outputs are then used by program 4 of Appendix 2 to obtain the linear frequency vs. insertion loss response of single bar-loop delay line with zero path. The last data can now be used for synthesizing a filter in the manner described earlier. Figure 3.18 shows the circuit pattern and a photograph of the constructed 16 bar filter with loop transducer.

Current Weighting
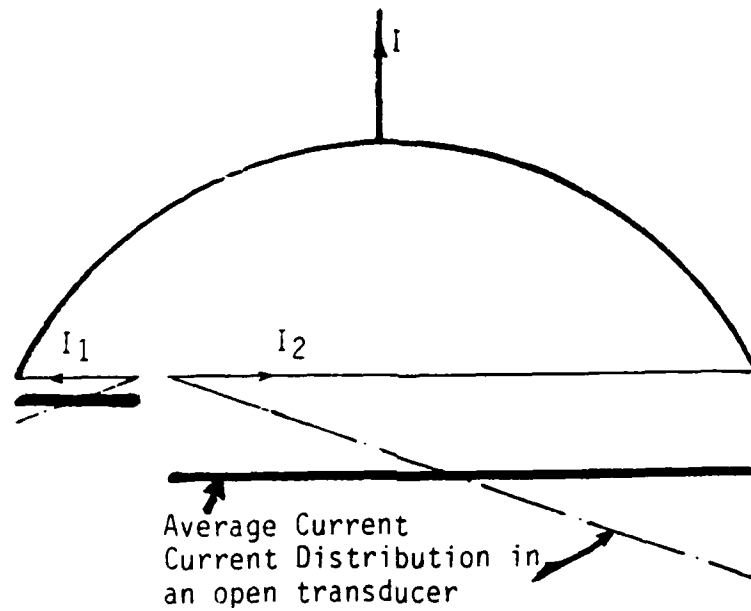
Current weighting of an open circuited gap transducer assuming $\ell \ll \lambda$.

Current weighting in the form of $\dfrac{\sin(x)}{x}$ in a 16 element filter.
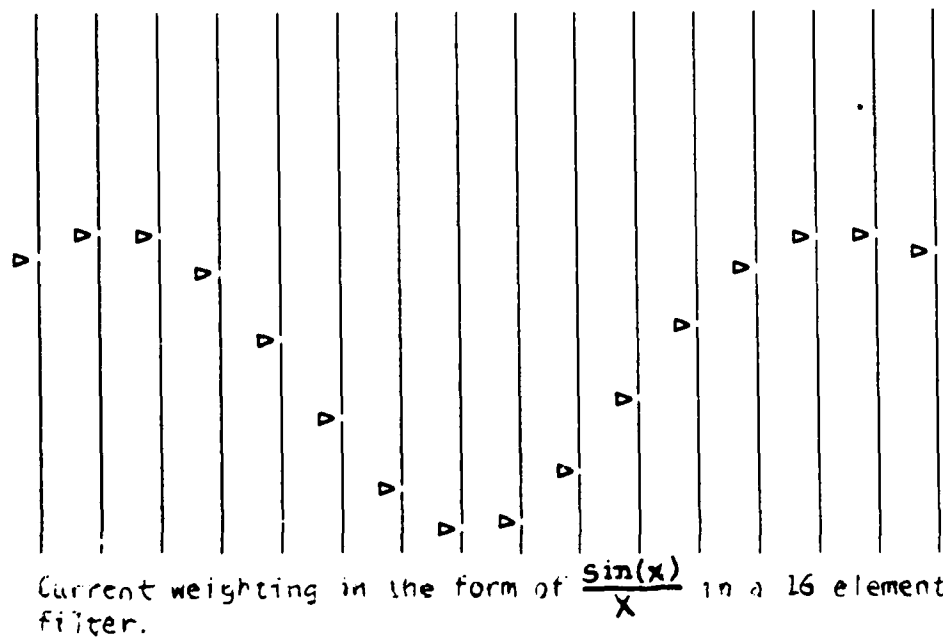
Figure 3.9 Current Weighting Filter
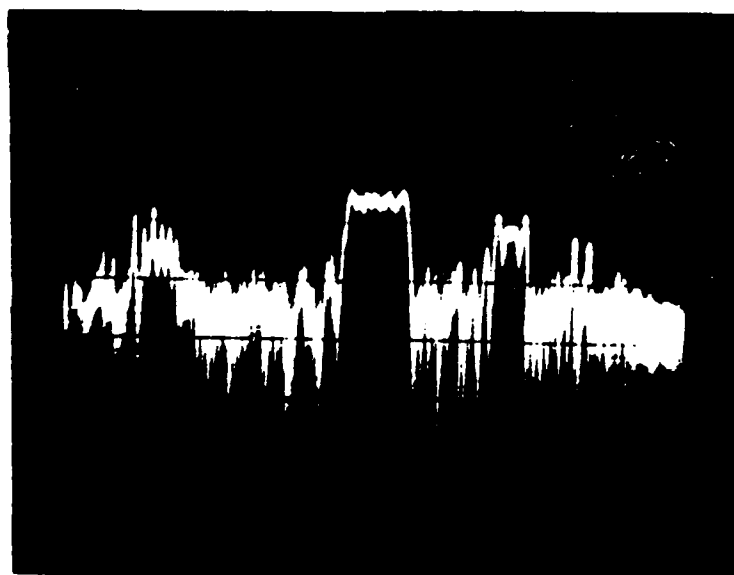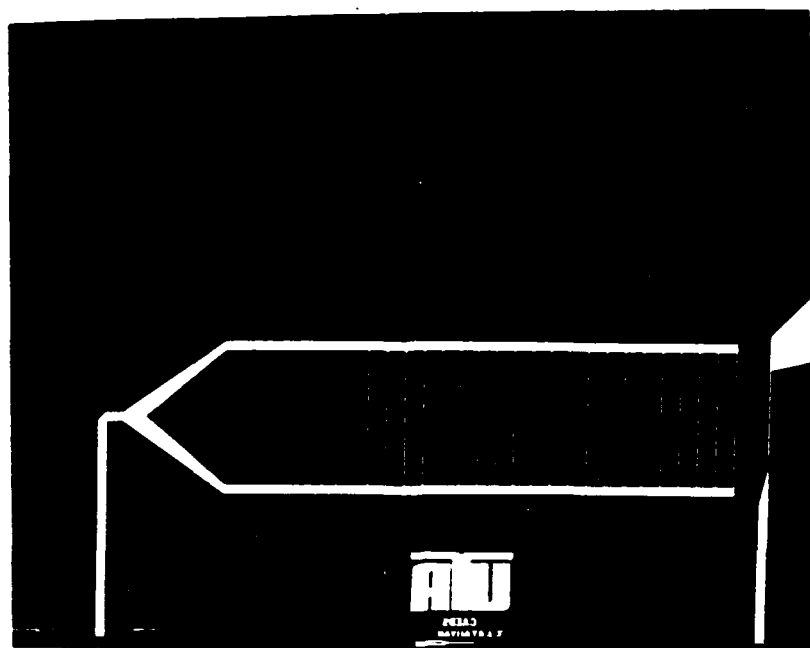
C.F. : 2.4 GHz
Δ F. : 1.5 GHz

Figure 3.10   The circuit pattern and the frequency
             response of FILTER-A.
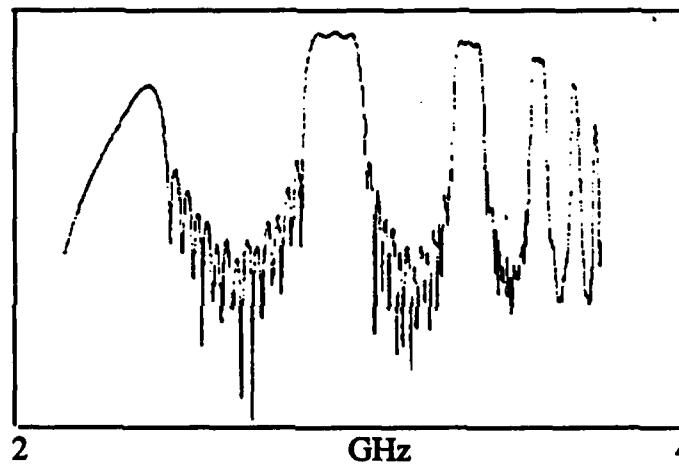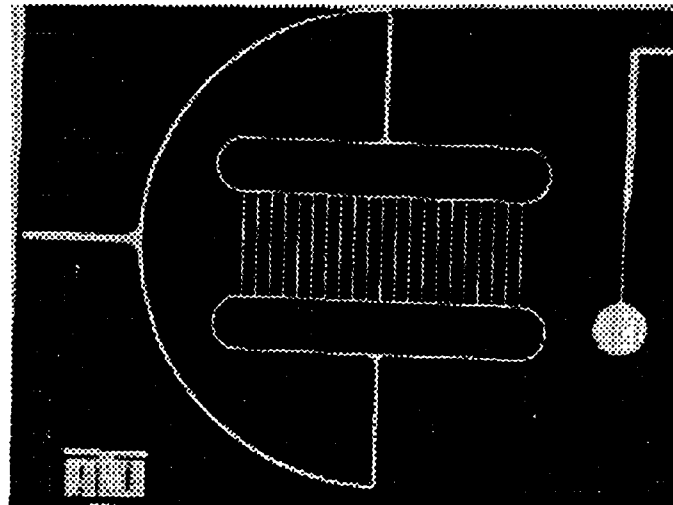
Figure 3.11 The circuit pattern (TOP), theoretical (MIDDLE) and the experimental response (BOTTOM) of the device FILTER-B. The response is amplified to show the suppression of the sidelobes.

70
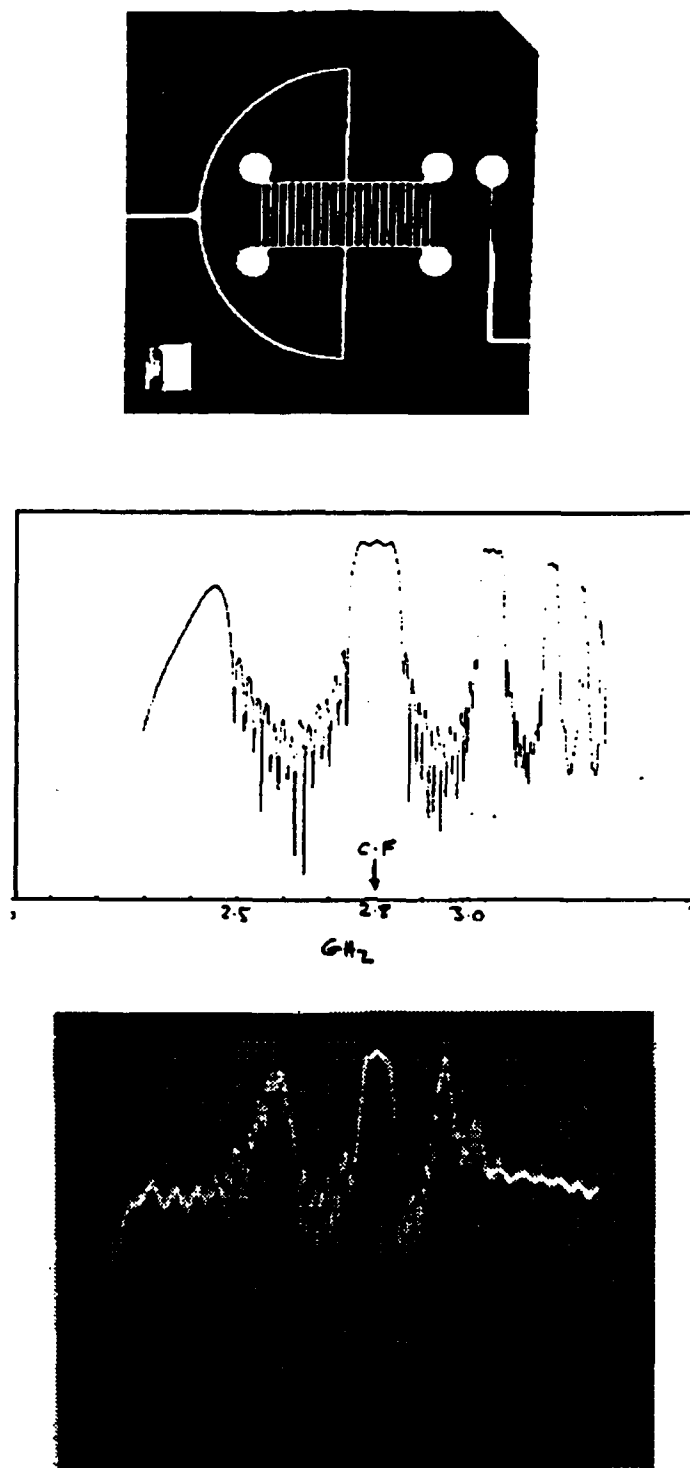
Figure 3.12 The circuit pattern (TOP), theoretical prediction (middle) and
the experimental response (bottom) of FILTER-C. The output is amplified
to show sidelobe suppression.

71
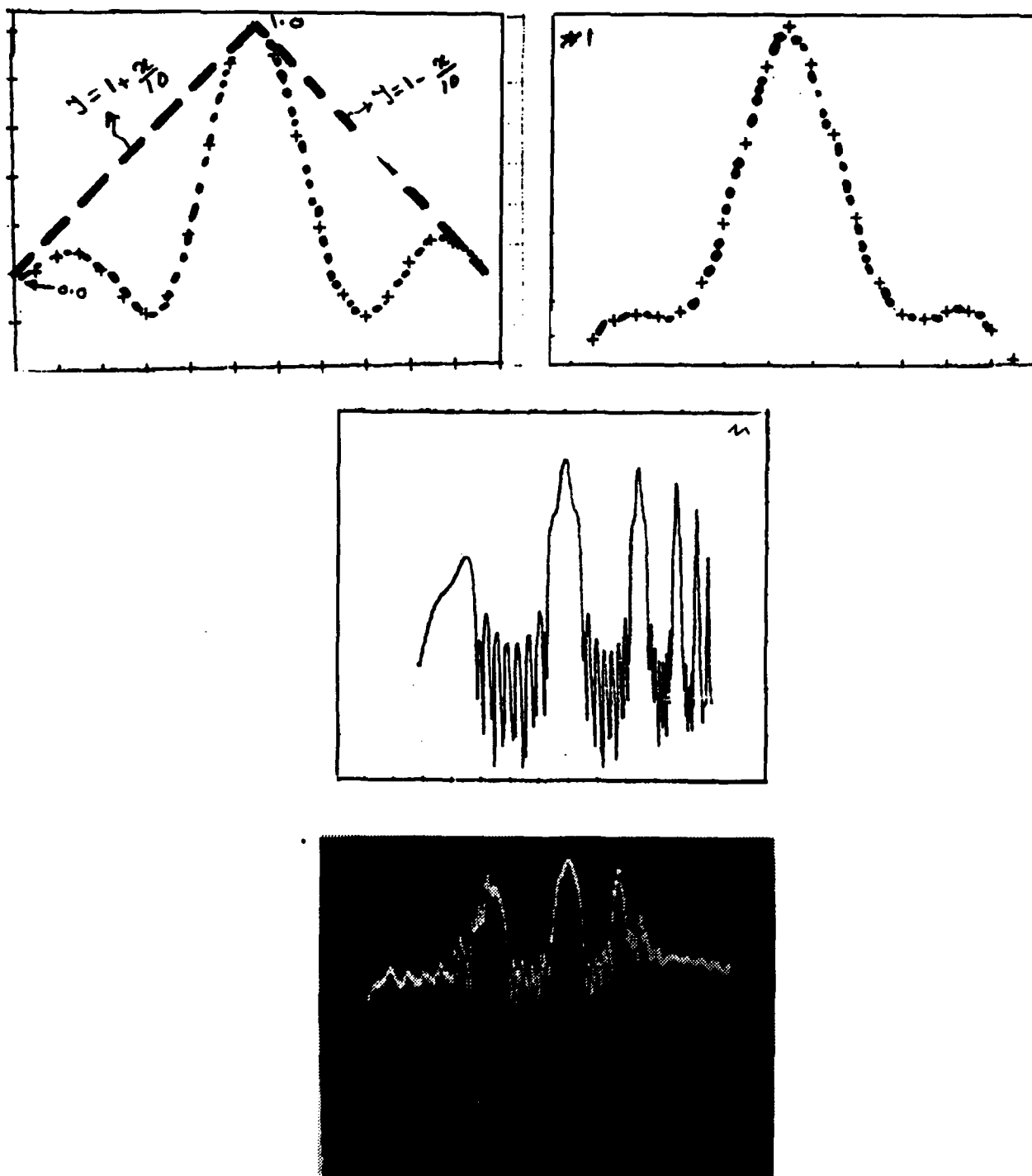
Figure 3.13 The current disctribution of the fingers and the feeders
(13-1) combined to form a current distribution shown in figure 13-b.
The predicted frequency response (13-c) is very similar to the
experimental response of the devise tuned at a frequency defferent
from the one designed for.
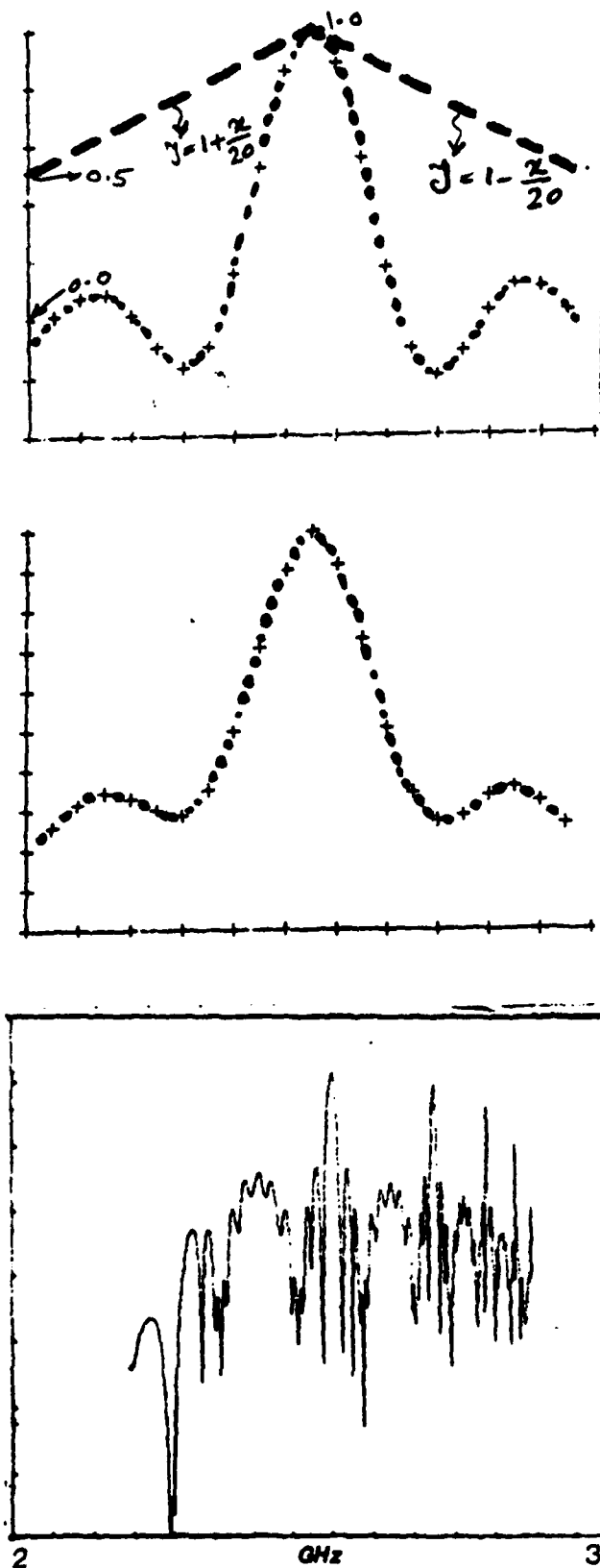
Figure 3.14 The theoretical prediction of the frequency response of
a 100 MHz bandpass filter when the feeders contribute to
the main SIN(X)/X current distribution. (3 different
combinations are being considered.)

Figure 3.14 continued.

74

Figure 3.14 continued.

75
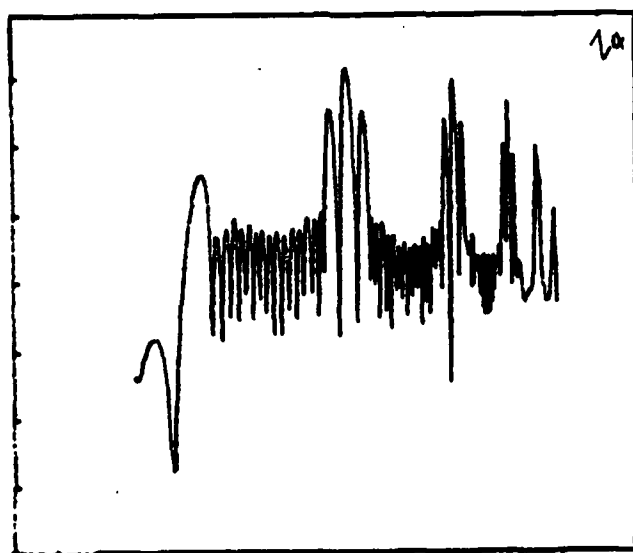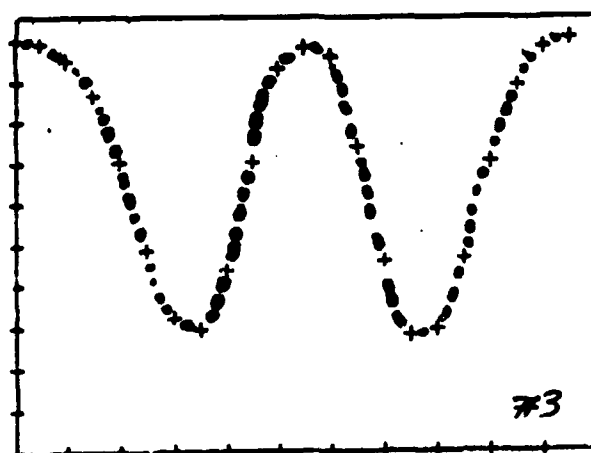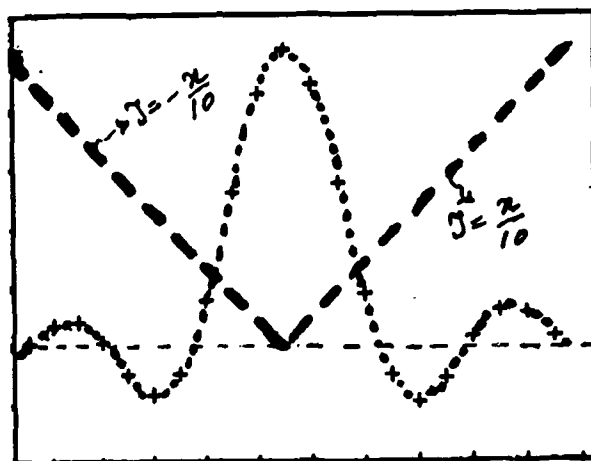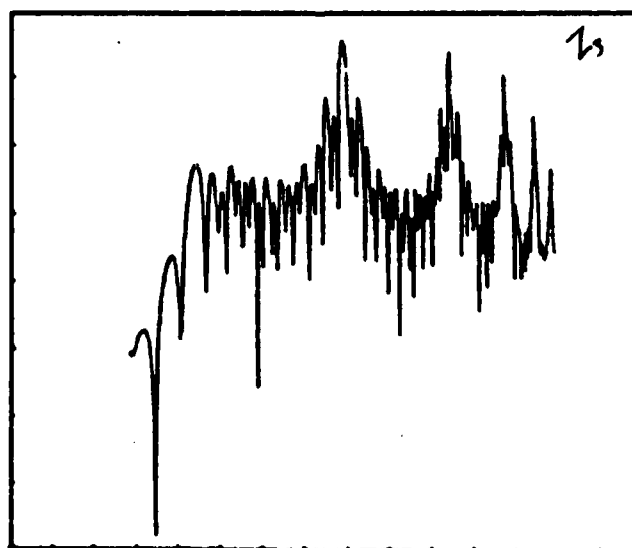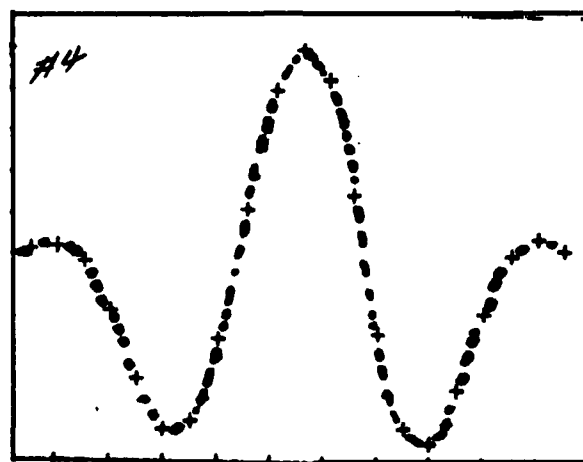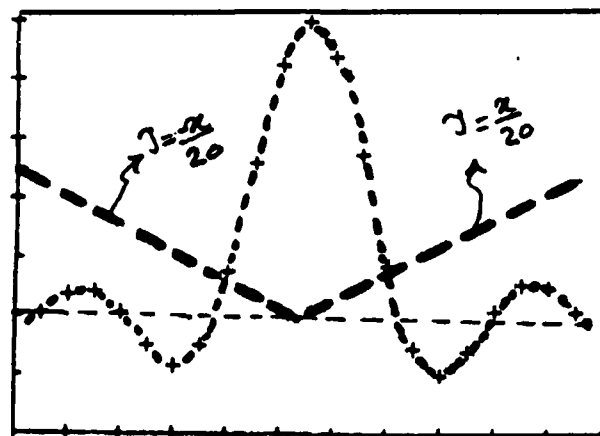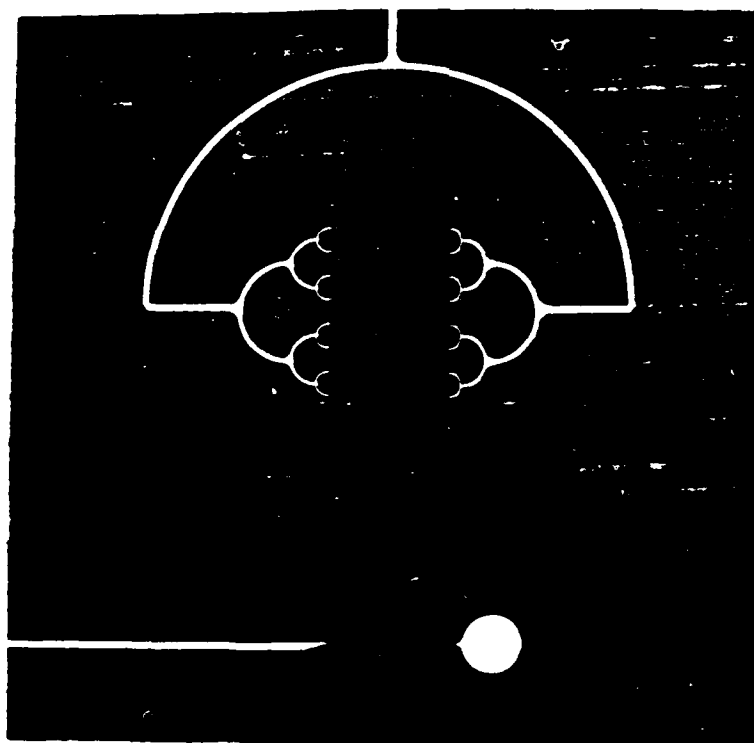
Figure 3.15   The circuit pattern of a 16 bar bandpass
filter with a simplified power divider.
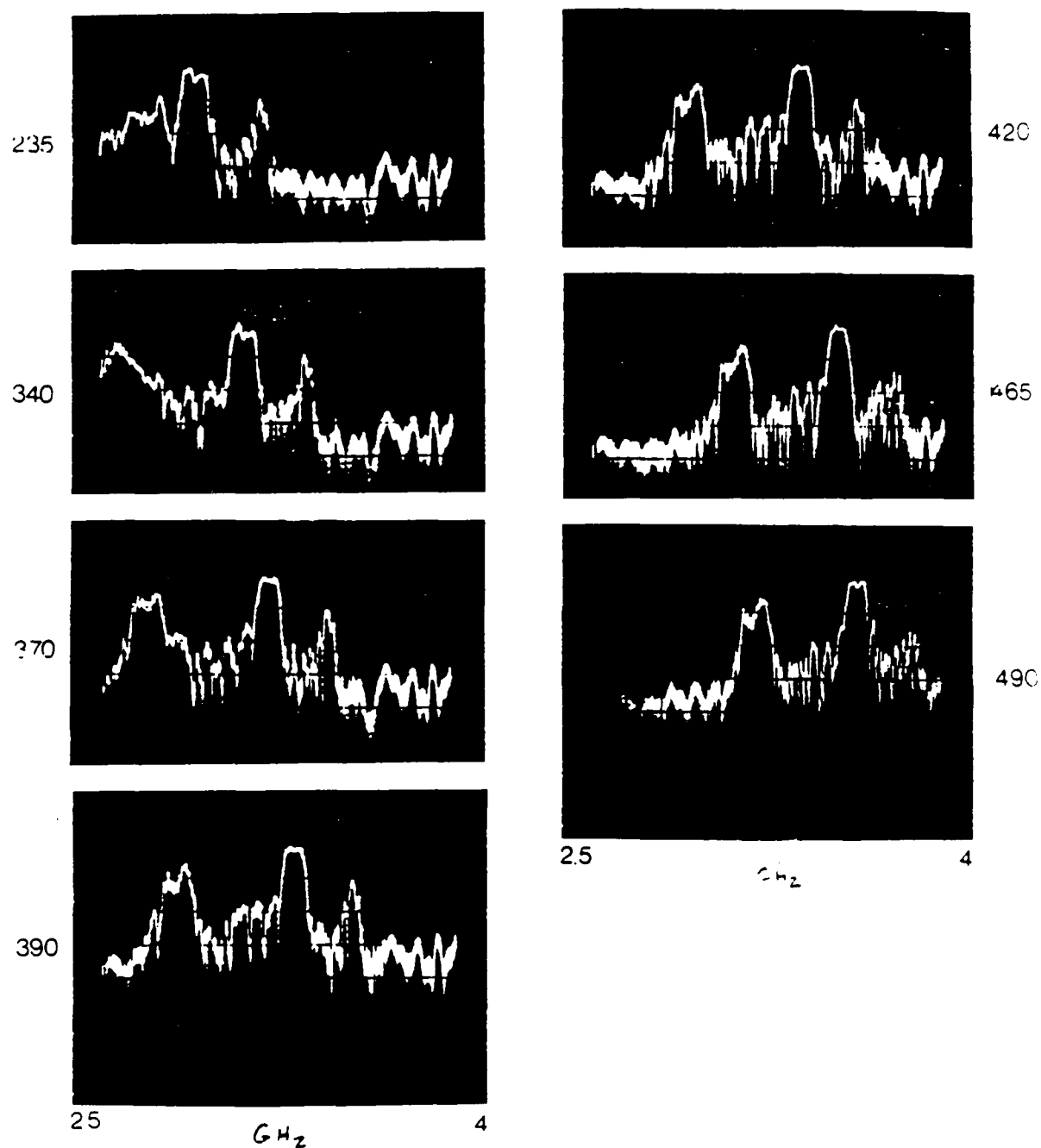
Figure 3.16 The frequency response of the filter shown in Figure 3.15, tuned at different frequencies by varying H from 235 to 500 Oe.

77
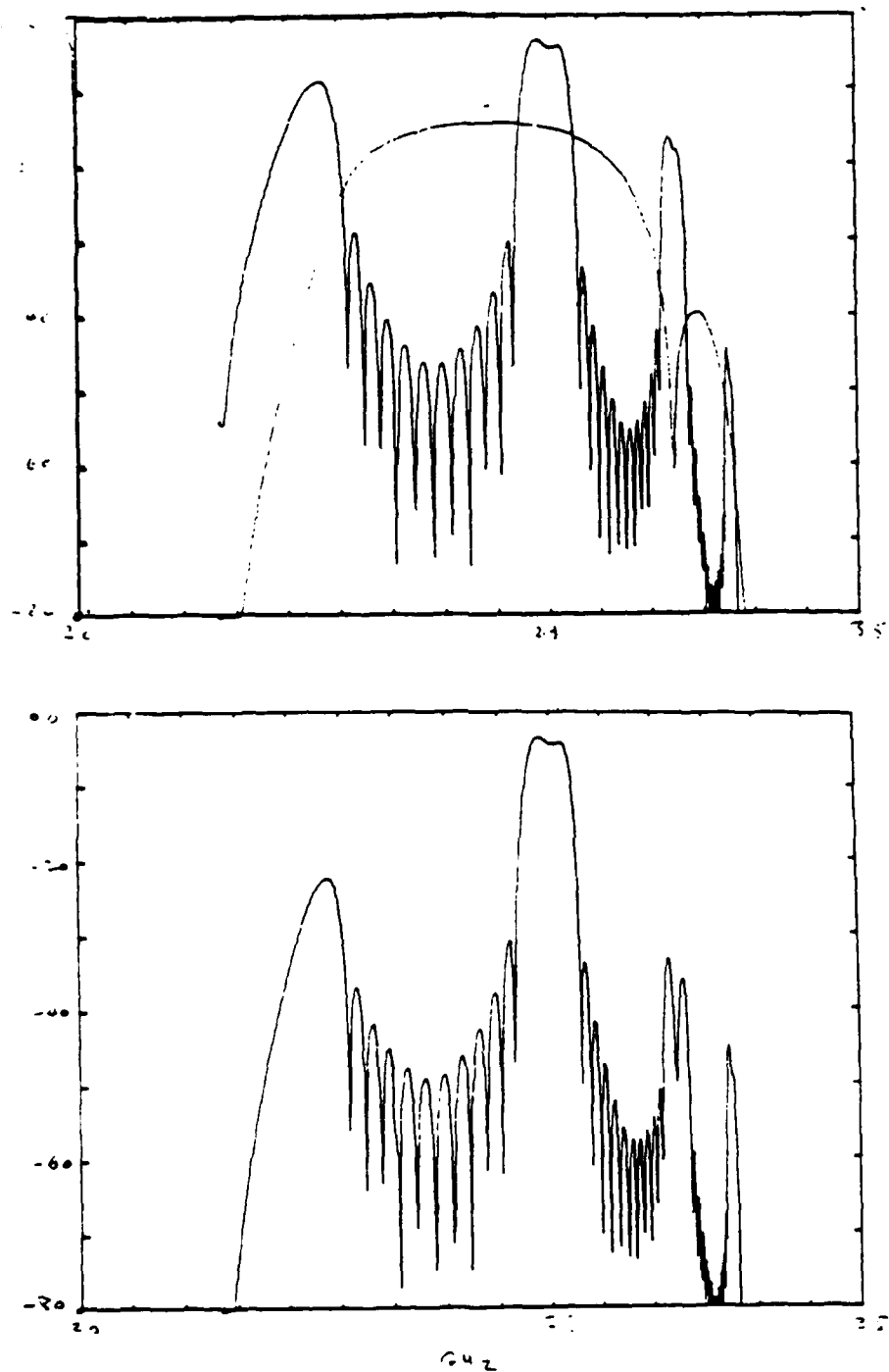
Figure 3.17 Combining the frequency response of a multibar-single bar
filter with a single bar-loop delay line (TOP) can result
in suppression of the harmonics.
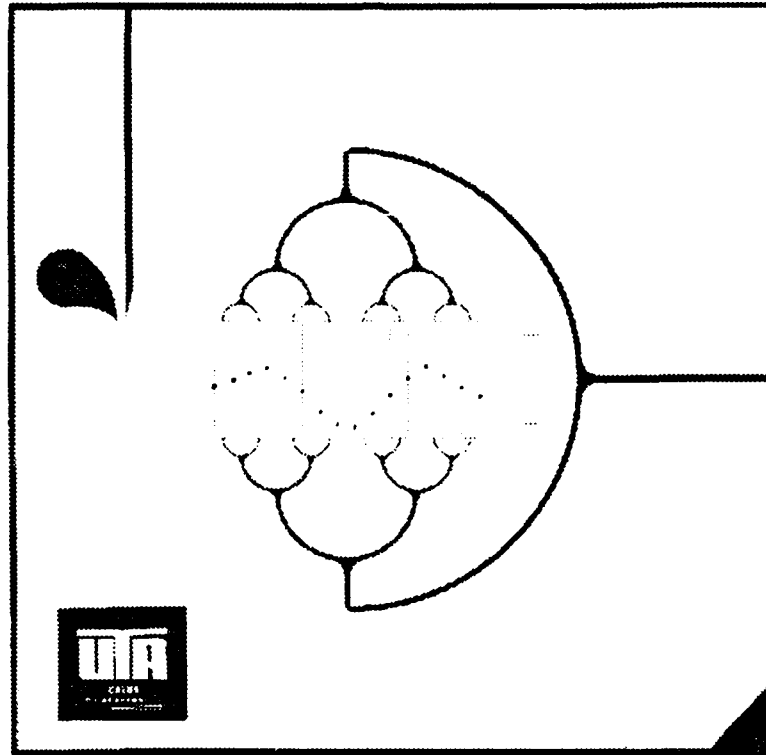
Circuit pattern of the 100 MHz tunable bandpass filter.
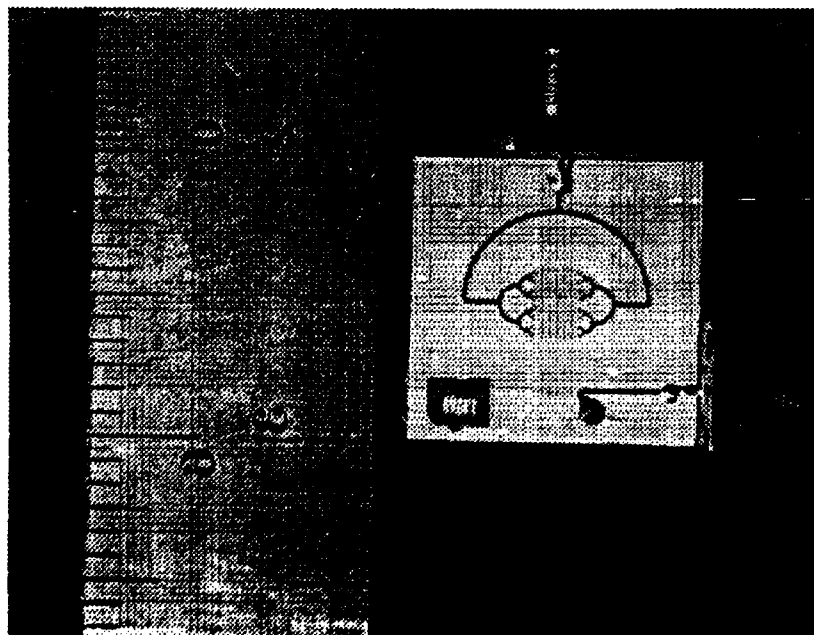
Photograph of the constructed 16 element bandpass filter.

Figure 3.18

79

The frequency response and its tunability are shown in Figures 3.19 and 3.20.

To improve the insertion loss, an attempt was made to narrow band match the power divider. The pattern and the frequency response is shown in Figure 3.21. As can be seen an improvement of about 10 dB can be achieved by having a matched power divider. Another filter was constructed with transducer length of 5 mm and was operated at higher frequency (4.5 - 5.5 GHz). The theoretical and experimental responses are shown in Figure 3.22. With this device, the minimum insertion loss was as low as 6 dB.

A matched power divider, was needed to gain information about the transducer coupling at different frequencies and with different lengths of transducer being under the YIG. A single bar I/O delay line was used. The S_{11} response of the device at 2 GHz, 3 GHz, 4 GHz and 5 GHz are shown in Figure 3.23 as points A through D. In this case the YIG was on the entire 3 mm length of the transducer. Next, the effect of transducer length on S_{11} was investigated by using 25 um thick YIG covering 3 mm (point D), 2 mm (point E), 1 mm (point F) and 0 mm (point G) of the transducer operating at 5.0 GHz.

As shown in these two figures, constructing a matched power divider is a difficult task because of the complexity of the load on each transducer.

Finally, instead of a single bar in output, the same filter pattern was used both in the input and the output ports. The theoretical response of this kind of filter is compared with the one which has single bar as an output (Figure 3.24). As can be seen, theoretically it is possible to suppress the sidelobe as much as 45

80
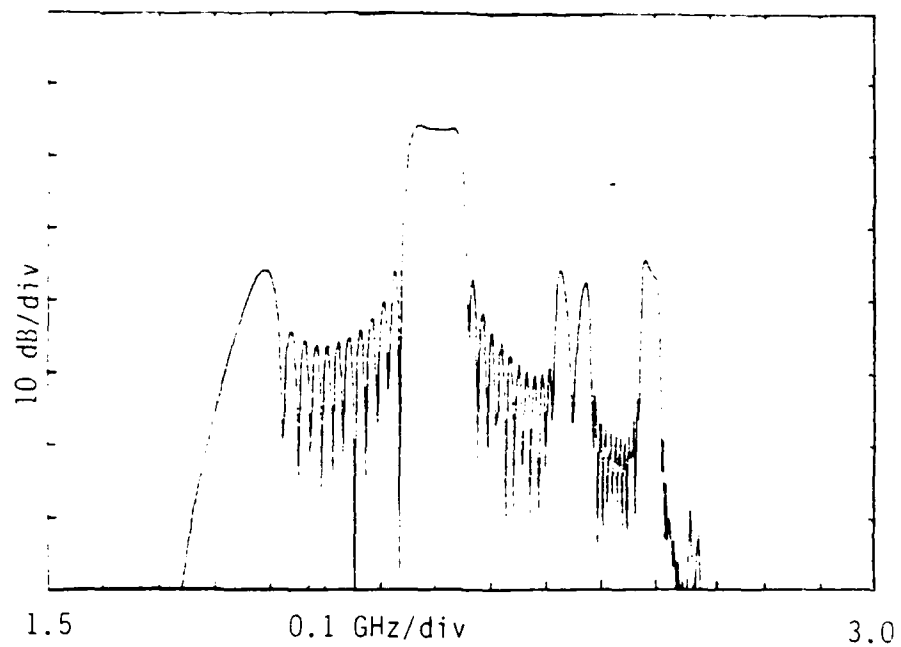
Theoretical prediction of the I.L. vs frequency.
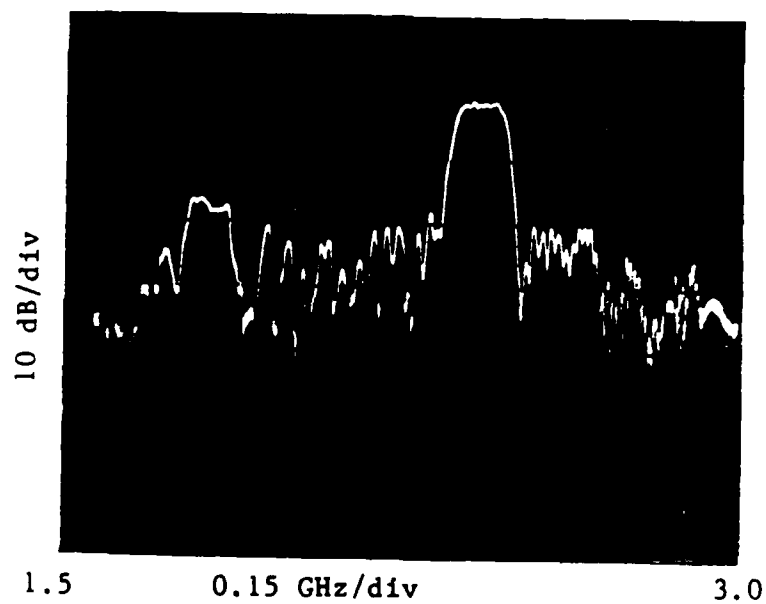
The experimental I.L. vs frequency response of the device.

Figure 3.19

81

2.0   0.1 GHz/div   3.5
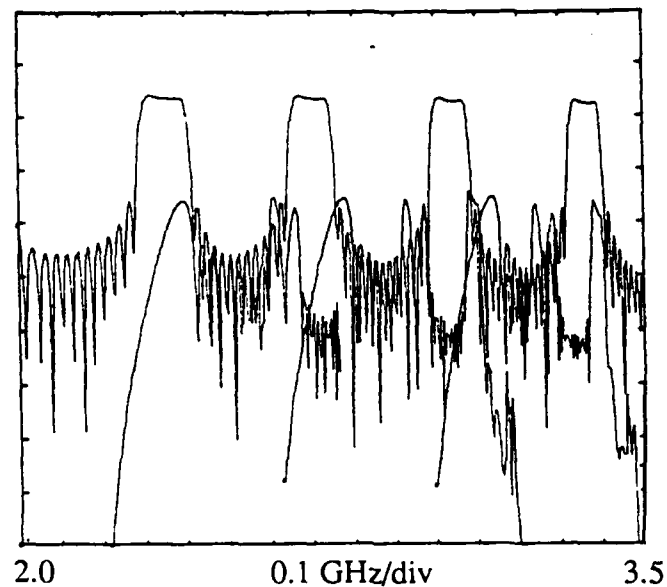
The theoretical simulation of the tunability of the filter.
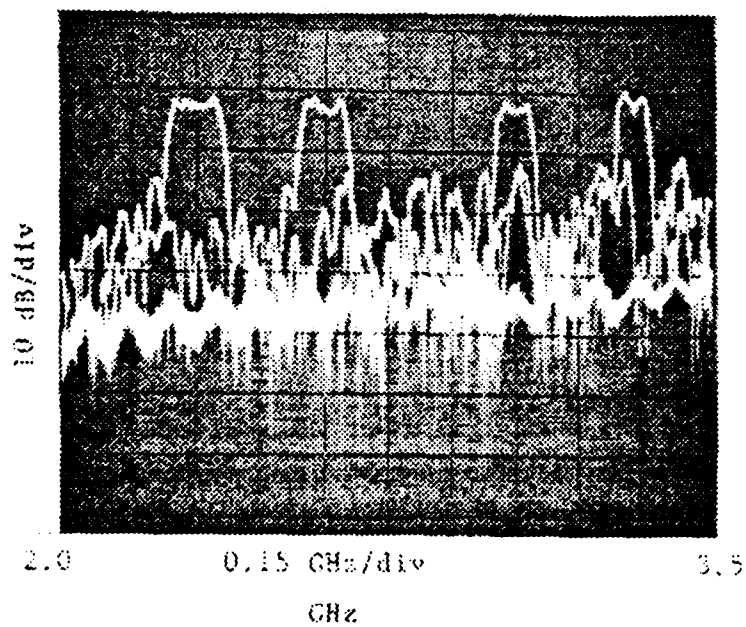
The experimental results of the filter tuned at different bias fields.

Figure 3.20
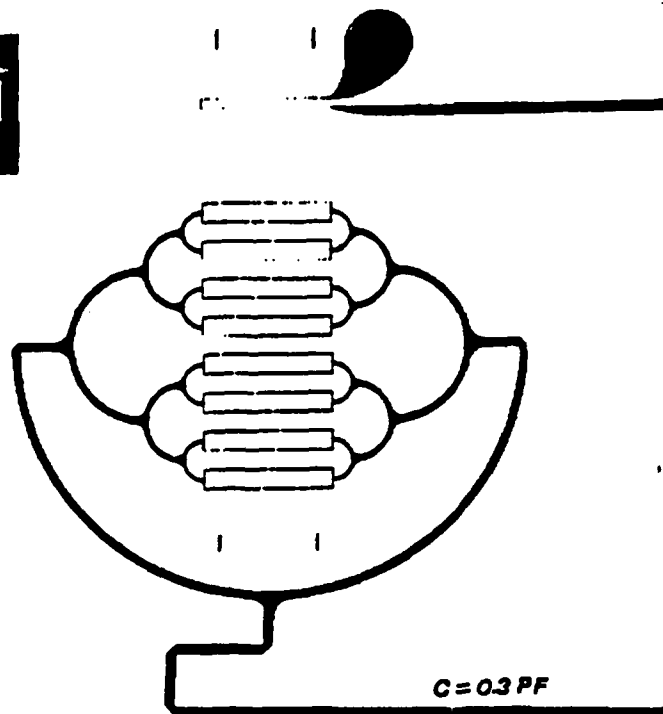
Narrowband matching circuit.

Improvement of the minimum insertion loss.

Figure 3.21

OUT

IN

3MM WIDE
YIG FILM

MICROSTRIP CIRCUIT
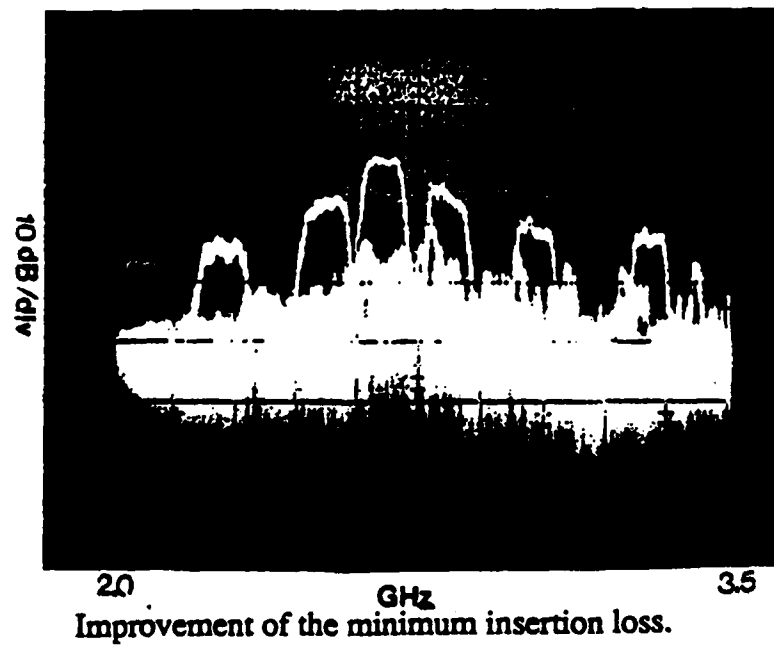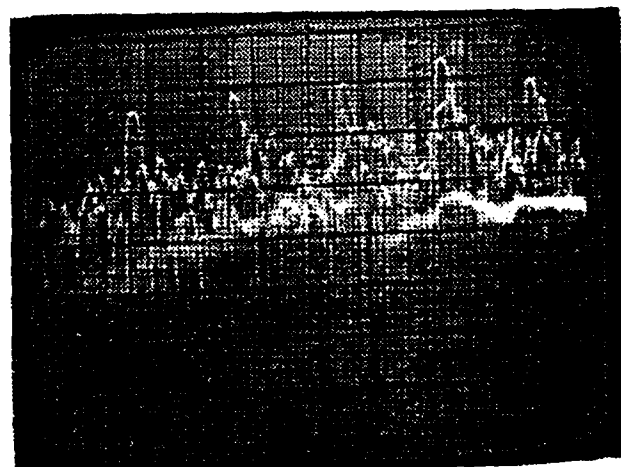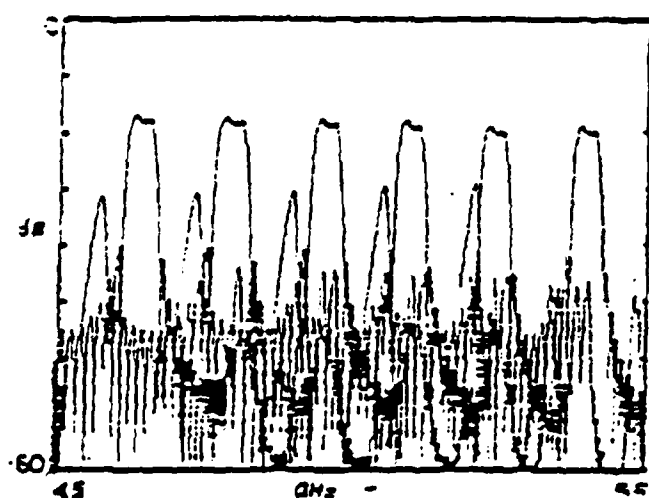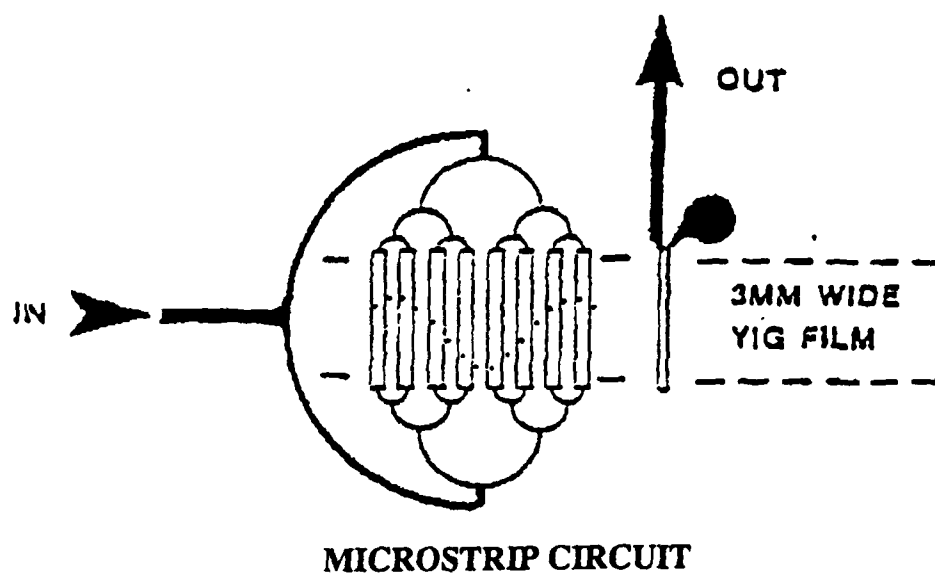
Figure 3.22 The circuit pattern of the 16 finger filter with 5 mm transducer
length (TOP) and its theoretical simulation of frequency response
in tunning (BOTTOM-LEFT) and the experimental result
(BOTTOM-RIGHT).
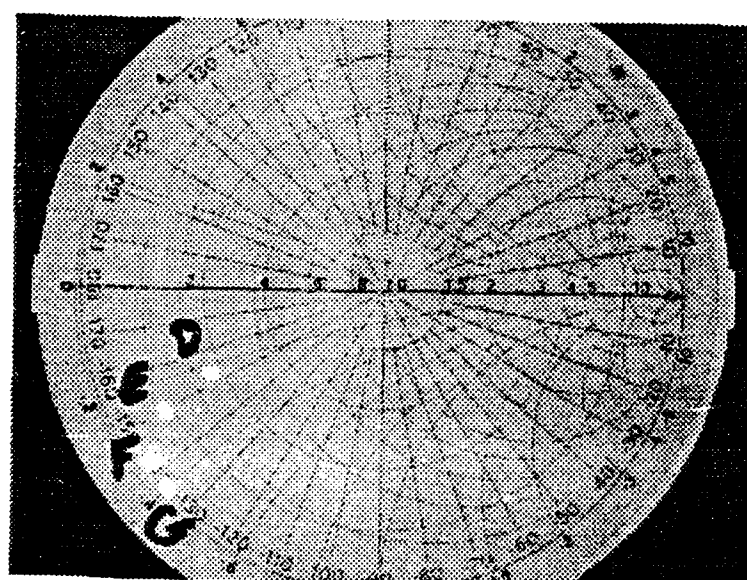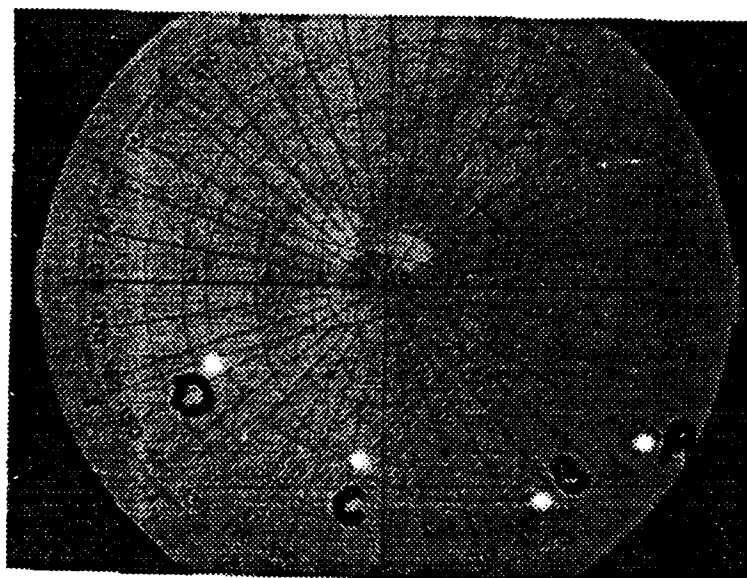
Figure 3.23 TOP- the measured S_{11} of a single bar delay line with the YIG covering
entire length of the transducer and tuned at 2 GHz (point A), 3 GHz
(point B), 4 GHz (point C) and 5 GHz (point D).
BOTTOM- the measured S_{11} response of the same device tuned at 5 GHz
with the YIG covering entire 3 mm transducer (point D), covering
2 mm (point E), covering 1 mm (point F) and removed (point G).
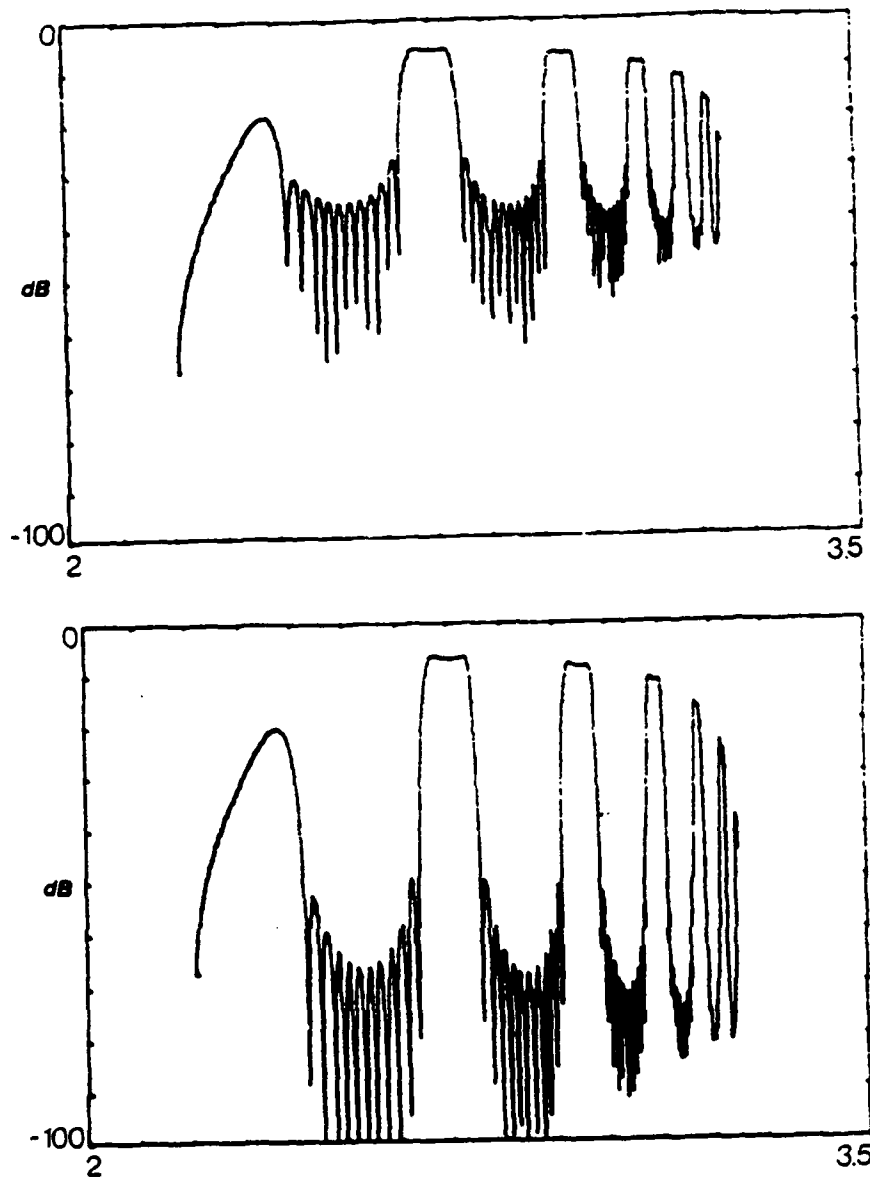
Figure 3.24 The theoretical frequenc:-I.L response of a multibar-single bar
filter (top) and multibar-multibar filter (   ).

dB. But when a device was made (Figure 25) with a semimatched power divider, the results were not satisfactory. A paper describing the theory and the experimental results of the first MSW transversal filter based on the work described so far, was presented at the IEEE-MTT (1986) meeting and was published in the proceedings of that meeting. A copy of this paper is given in Appendix 4.
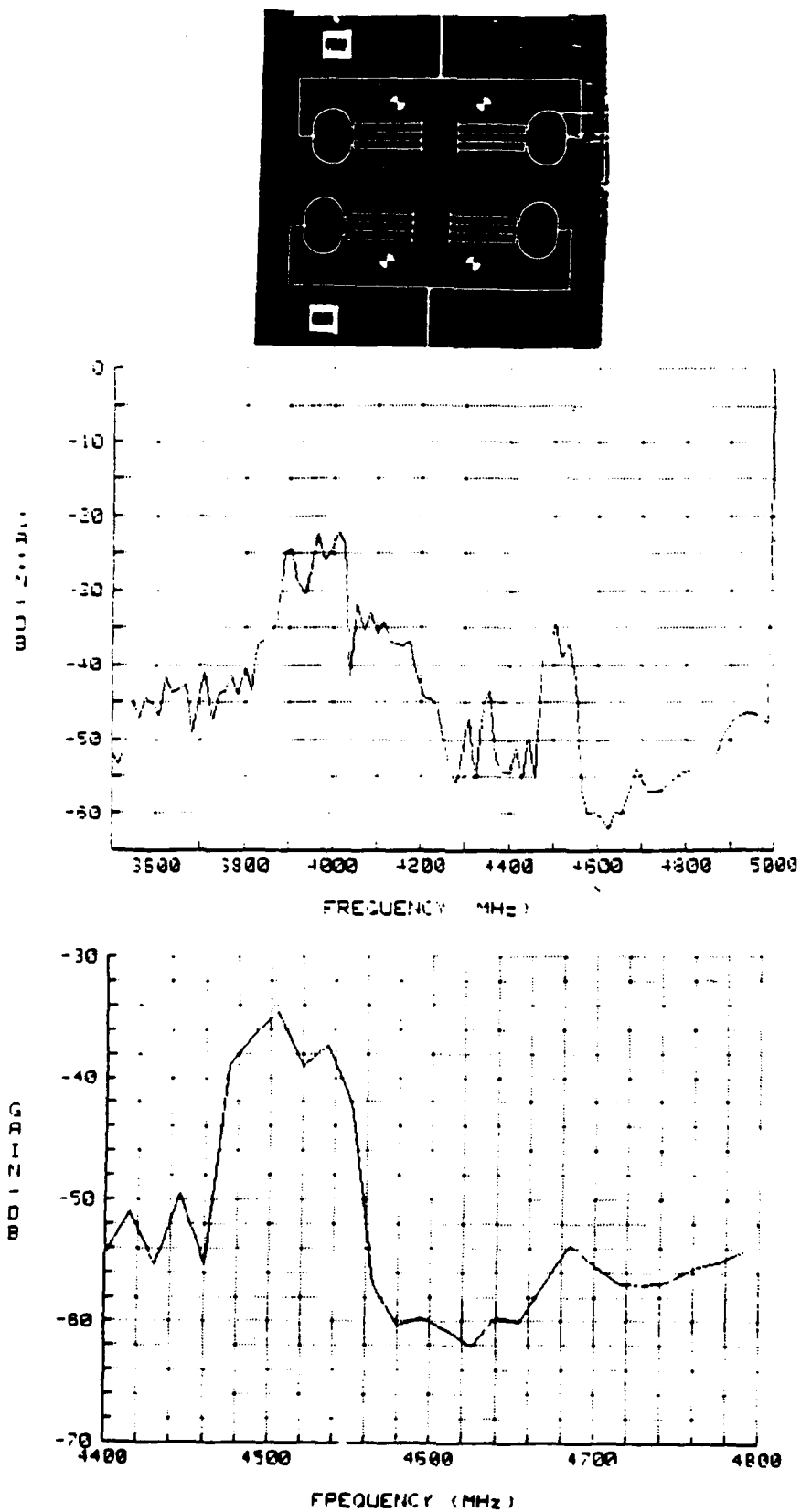
Figure 3.25 Photograph of the device with synthesised filter pattern
both in the input and the output, and the frequency
response.

88

4. DELAY LINES

4.1   **S Band Linear Delay Line**   The research for the construction of linearly dispersive MSSW delay line was continued. Several attempts were made for miniaturization of the device and improvement of its insertion loss and group delay. One of the devices is shown in Figure 4.1 along with the measured S_{11} and S_{21} responses.

The magnet package shown in Figure 4.2a, provided by Rockwell International was designed to house the MSSW delay line. It had a constant field of 400 Oe at the center. The device (Figure 4.2b) was designed to have the transducers located in the center of the device. Figure 4.2c is the photograph of this device with the graded ground plane and the YIG placed on it. Figure 4.3 shows the insertion loss vs. frequency response in the frequency range of 2.4-3.9 GHz (top-left), the reflection coefficient (S_{11}) for 2.8-3.2 GHz range (top-right), and the phase - magnitude response in the 2.9-3.15 GHz range (bottom).

Several graded ground planes were tested and the R.M.S. deviation from quadratic phase for different frequency ranges were calculated. The results are shown in Figure 4.4.

Our earlier experience had shown that a few dB improvement in the insertion loss can be achieved if the graded ground plane and the ground block are both gold plated, and if indium solder is used for grounding the Al_2O_3 substrate instead of silver paste. In the final stage, when the repeated measurements of the insertion loss response and the group delay was satisfactory, the graded ground plane was permanently soldered to the block and the YIG strip was

89

S_{11} S_{21}

Figure 4.1   Photograph of a matched MSSW delay line with graded ground
              plane (TOP), S_{11} in the frequency range of 2.8-3.3 GHz
              (BOTTOM-LEFT), and S_{21} for 2.5-4 GHz (BOTTOM-RIGHT).

90
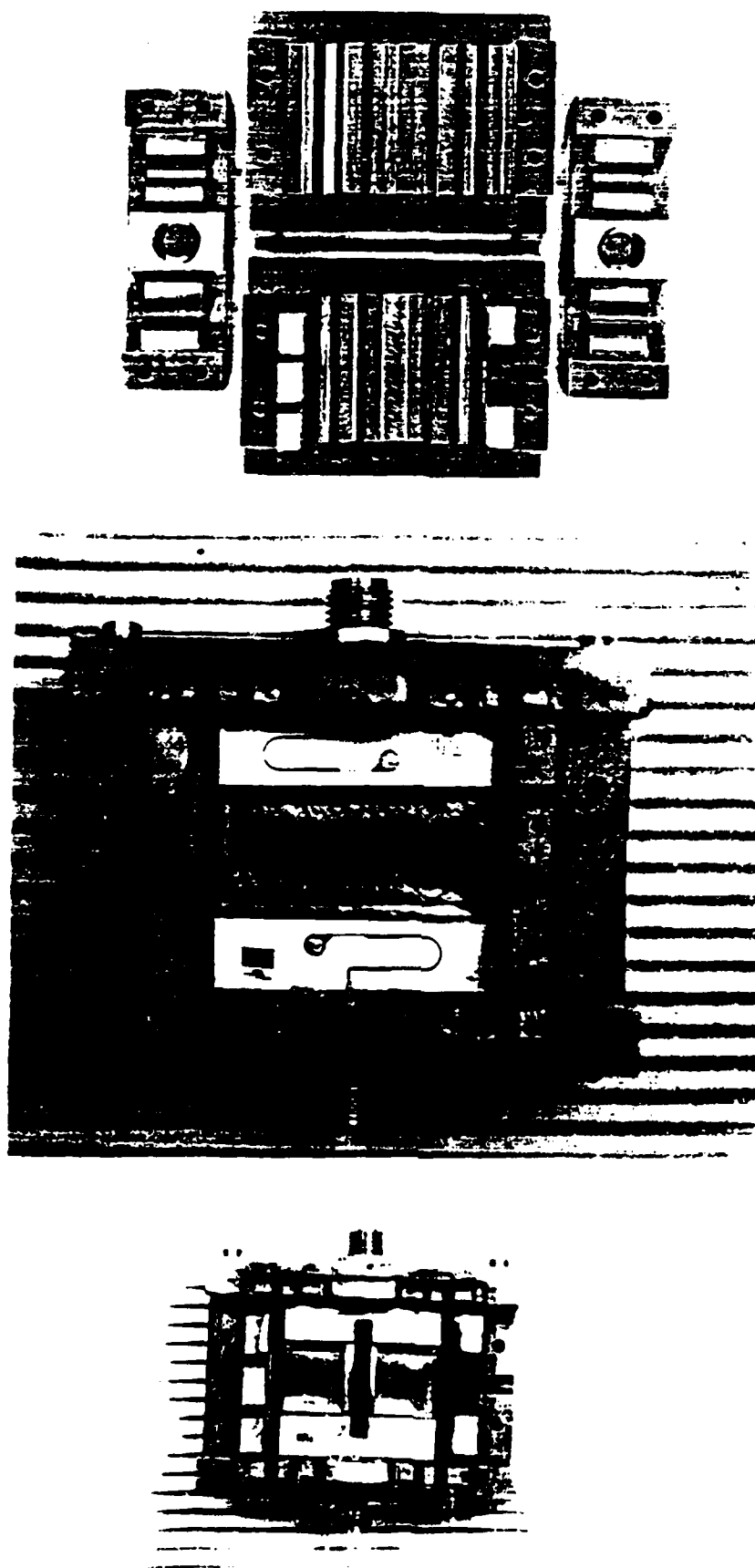
Figure 4.2 Photographs showing disassembled view of the magnet package and the position of the device.
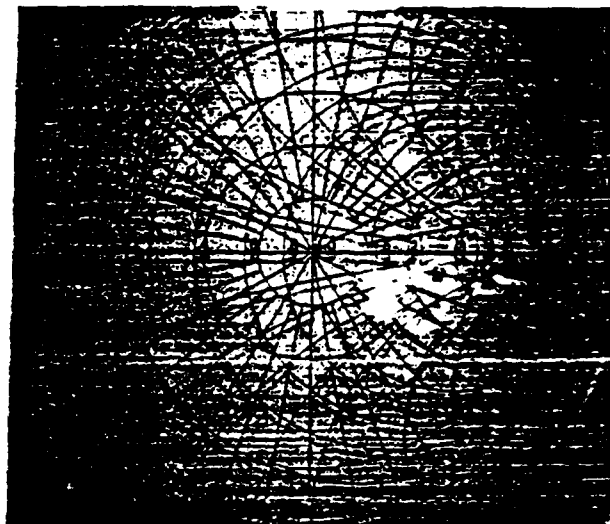
S_{21} S_{11}
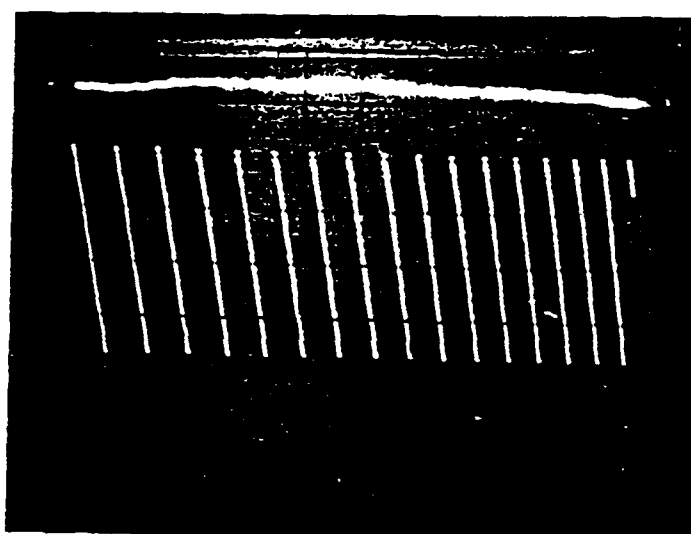
S_{21} & S_{11}

Figure 4.3 S_{21} in the frequency range of 2.4-3.9 GHz and S_{11} for 2.8-
3.2 GHz (TOP) and phase-magnitude response for 2.9-3.15 GHz
range (BOTTOM).
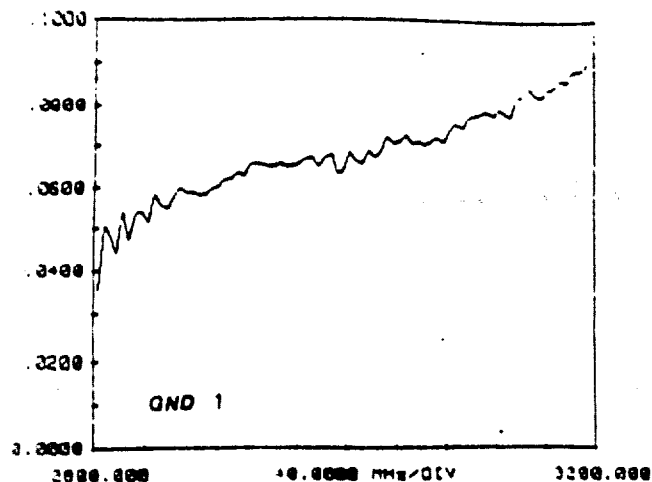
Figure 4.4   Time delay response and analysis of the linearity of the
group delay for several types of graded ground planes.

Figure content:

```
.1000

.0820

.0600  DELAY - uSEC

.0400

.0200

0.0000

        GND 4

2800.000    40.0000 MHz/DIV    3200.000
```
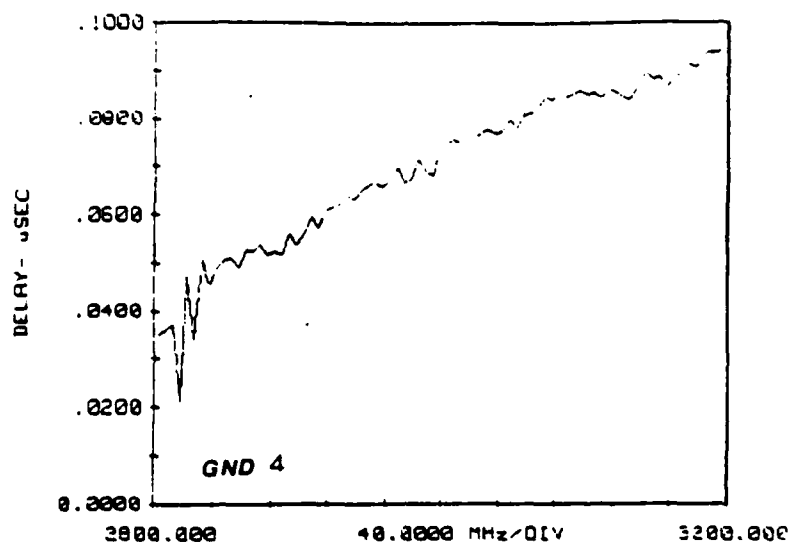
*****MSSW5*****
B.W= 2.8000 TO 3.0550 GHz
A= 181.4271 B=-470.4292
Phase(QUADRATIC)=.5A(F^2-F_0^2)-B*(F-F_0)
THE R.M.S. DEVIATION FROM QUADRATIC PHASE IS: 20.8681

*****MSSW5*****
B.W= 2.8500 TO 3.1850 GHz
A= 154.2979 B=-390.4362
Phase(QUADRATIC)=.5A(F^2-F_0^2)-B(F-F_0)
THE R.M.S. DEVIATION FROM QUADRATIC PHASE IS: 7.5878

*****MSSW5*****
B.W= 2.9000 TO 3.1550 GHz
A= 133.6094 B=-328.6460
Phase(QUADRATIC)=.5A(F^2-F_0^2)-B(F-F_0)
THE R.M.S. DEVIATION FROM QUADRATIC PHASE IS: 13.8825

*****MSSW*****
B.W= 2.9450 TO 3.2000 GHz
A= 112.3049 B=-264.0575
Phase(QUADRATIC)=.5A(F^2-F_0^2)-B(F-F_0)
THE R.M.S. DEVIATION FROM QUADRATIC PHASE IS: 16.0892

Figure 4.4 continued.

94

secured with glue applied at both ends. This linearly dispersive (positive slope) MSSW delay line was intended to be cascaded with another linearly dispersive (negative slope) MSBVW delay line to produce an electronically tunable constant delay line. The MSBVW device was constructed at Rockwell International. A paper describing the theory of operation and the experimental results was presented at the Phased Arrays, 1985 Symposium and was also published in the 1986 March issue of the MICROWAVE JOURNAL. A reproduction of this paper is given in Appendix 5.

4.2 **Ka Band Delay Lines** To explore the usefulness of MSW devices at higher frequencies, the response of simple delay line at Ka band (26.5-40 GHz) was investigated. The first sample was an open ended single bar I/O delay line with transducer length of 3 mm and 10 μm width constructed on quartz substrate.

Figure 4.5 shows photographs of the S_{21} for the zero line (no device) and also the direct break-through (device with no H field). Figure 4.6 is the frequency response of the device operated in the forward volume wave mode for different YIG widths and different positions. The same procedures are repeated for the backward volume wave mode and the results are shown in Figure 4.7. All the pictures in Figures 4.5, 4.6 and 4.7 were taken for center frequency of 27 GHz and frequency sweep of 1 GHz with 50 μm thick YIG.

The tunability of the device in the frequency range of 27 GHz-33 GHz is shown is the series of photographs displaying S_{11} and S_{12} in Figure 4.8. For these pictures the 1.5 mm wide and 50 μm thick YIG covered the second half (close to the transmission line) of the 3 mm long transducer. For all the pictures the frequency sweep was 1

95
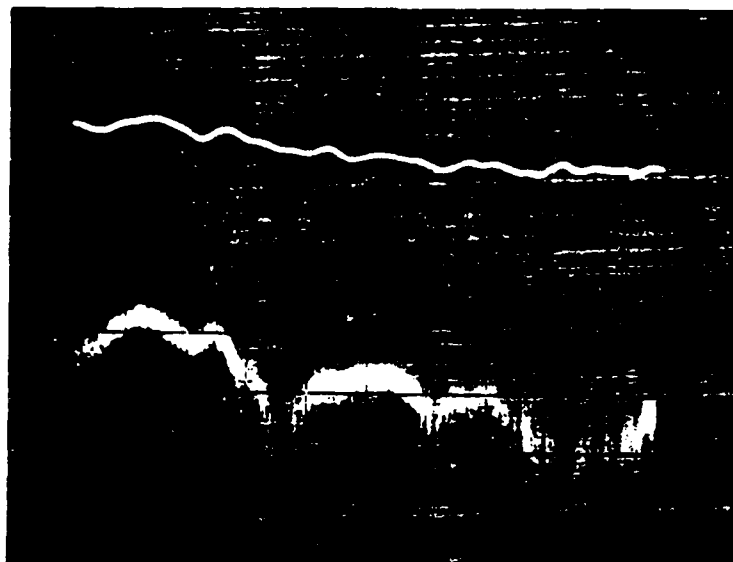
CF 27 GHz

ΔF 1 "

Figure 4.5   S₂₁ response for zero line (no device) and direct-through (device without the field).

S_{21} - NO DEVICE

S_{11} - DEVICE, NO FIELD

S_{11} - DEVICE, TUNED

S_{21} - DEVICE, TUNED

CF 27 GHz

ΔF   ''
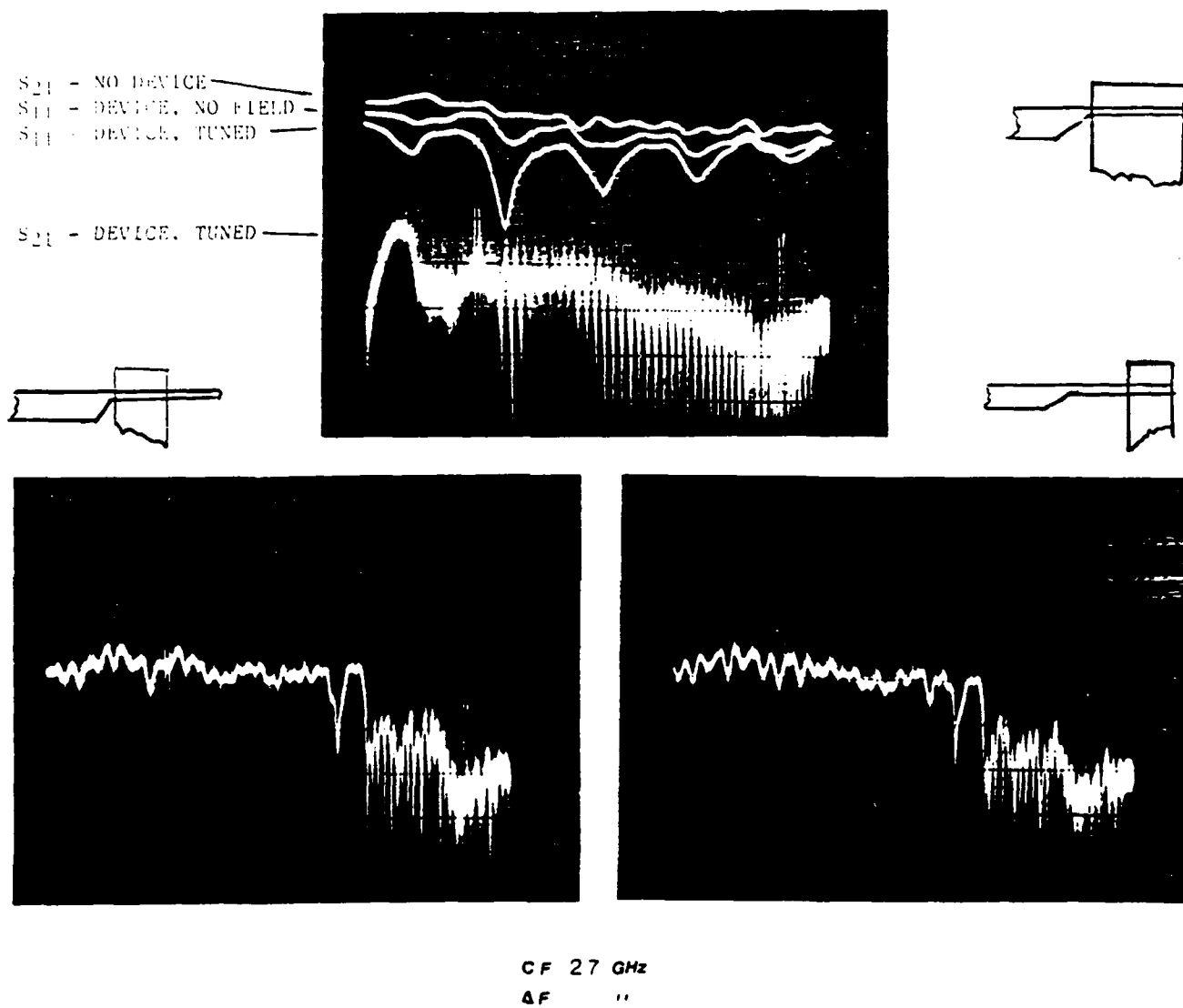
Figure 4.6 I.L vs frequency response for different YIG widths and positions for MSFVW mode.

97

S_{21} - NO DEVICE
S_{11} - DEVICE, NO FIELD
S_{11} - DEVICE, TUNED

S_{21} - DEVICE, TUNED
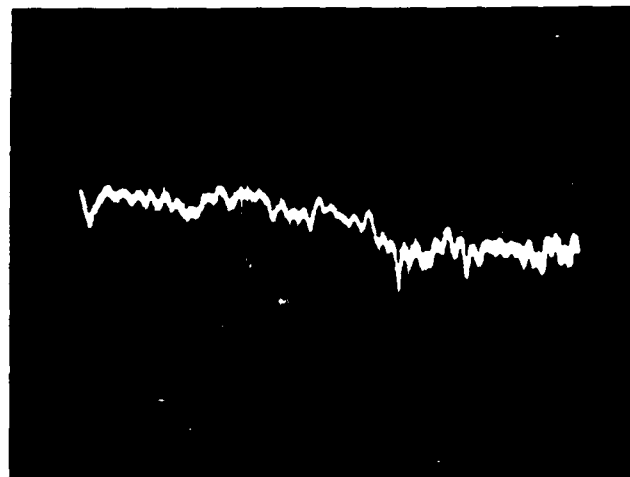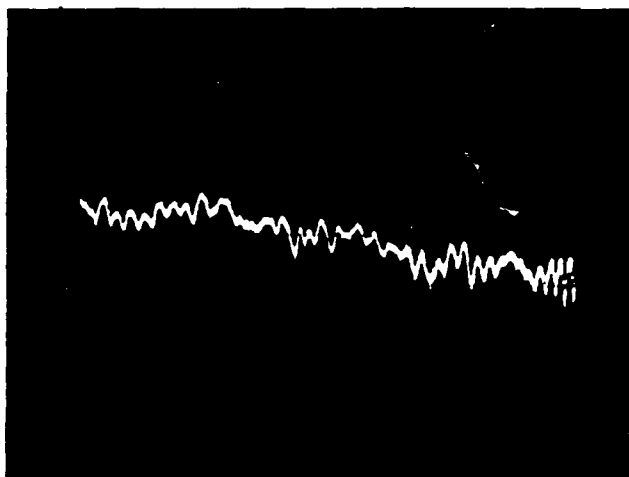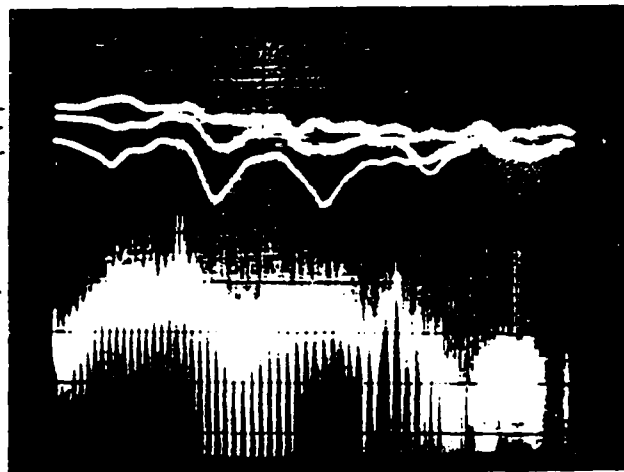
Figure 4.7 Same as Figure 4.6, but for MSBVW mode.
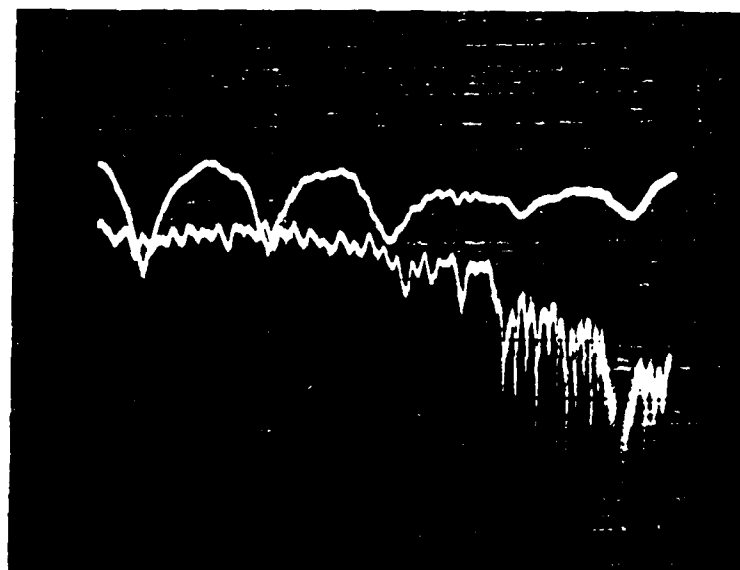
CF 27 GHz
H 8.7 k
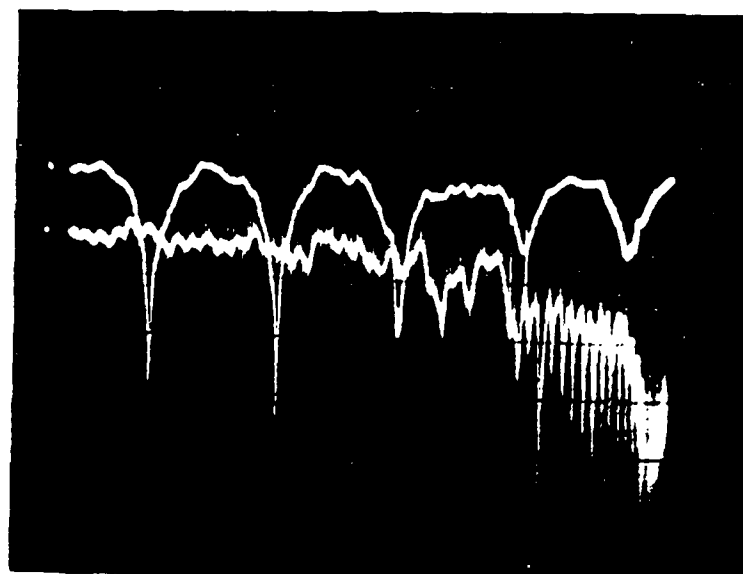
CF 29
H 9.5 k

Figure 4.8   Series of Photographs displaying S_{11} and S_{21} responses for
various H fields for the delay line operated in the MSFVW mode.
ΔF=1 GHz

CF 6.
H 4.5 k
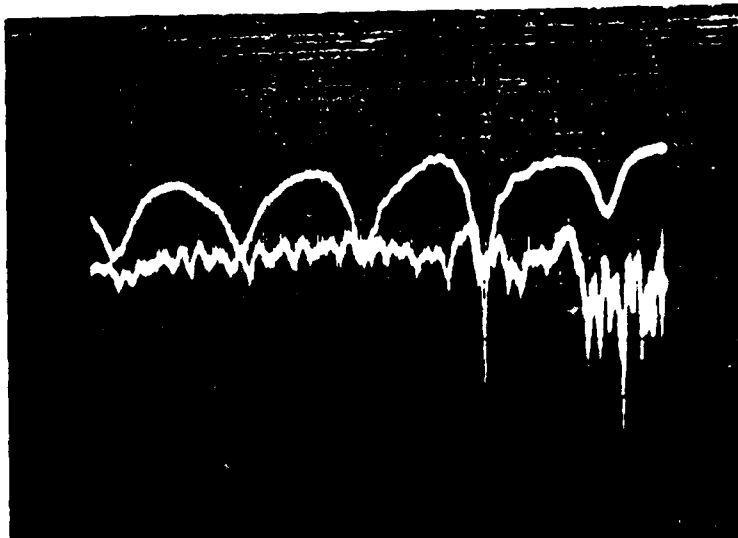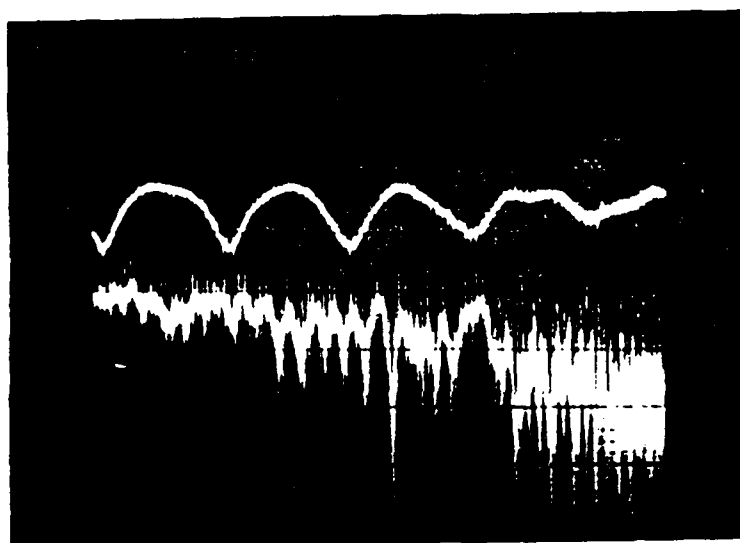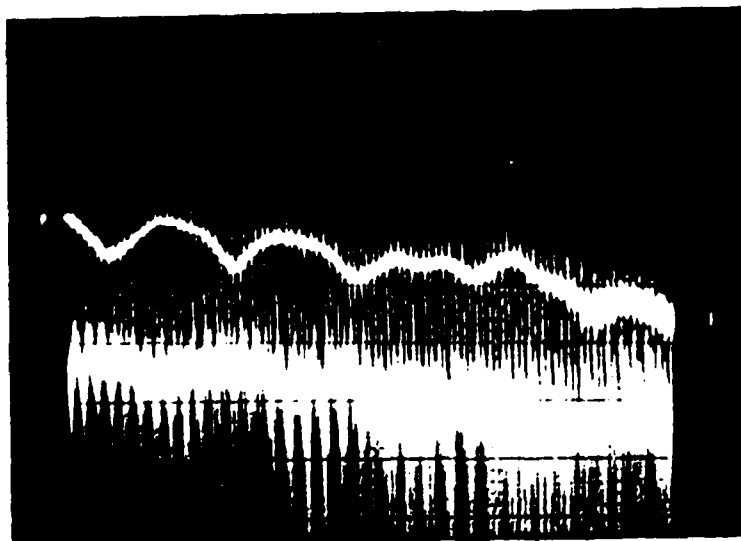
CF 33
H 1.5 k

CF 33
H 11 k

Figure 4.8 Continued.

100

GHz. The second device was a 150 μm loop I/O delay line (with 1 mm center/center spacing) constructed on quartz substrate. A photograph showing the pattern and also the frequency response of the device is shown in Figure 4.9. In the picture showing the response, the top line is the zero line, the bottom line is the direct break-through and the middle line is S_{21} of the device, all in the frequency range of 27.5-28.5 GHz operated in the MSFVW mode with 50 μm thick YIG.

After subtracting the zero line from the S_{21} of the MSFVW mode in the frequency range of 27-29 GHz, a sample plot of insertion loss vs. frequency for another device is shown in Figure 4.10. This figure shows there is a promise of designing MSW delay lines at high frequencies.

Another device (Figure 4.11) was designed with open ended transducers of width 30 μm and length 4 mm. In order to reduce the mismatch, special semi-rigid cables with type K connectors were used to interface the device with the test instrument.

Several experiments were performed with YIG strips of different thicknesses and widths, and positioned at various places on the transducers. The results showed that narrower strips (less than 1 mm) with YIG thicknesses > 50μm positioned 2/3 of the way away from the open end of the transducer resulted in the lowest insertion loss and the smoothest response. Figure 4.12 shows the insertion loss vs. frequency and phase response operated in the MSFVW mode. The pictures are for the center frequency of 30 GHz and a bandwidth of 1.5 GHz. For the same center frequency, but with the sweep bandwidth of 500 MHz, the magnitude and the phase responses in the same mode are shown in Figure 4.13. The magnitude and the phase

responses of the device operated in the forward and reverse modes

of MSSW are shown in Figures 4.14 and 4.15, respectively.

5. SUMMARY

In summary the primary accomplishments of this final program period have been:

1. A variable time delay device with an R.M.S. phase error of as low as 6.40°R.M.S. has been built and tested. Time variation of 42 nsec was achieved. the design procedures for dispersion control utilizing a variable and backward wave delay line with linearized dispersion, and thus matched dispersive line have been developed with significant potential in signal processing applications.

2. The current weighting technique using open gap transducers to realize MSSW filters, has demonstrated good correlation between the theoretical prediction and measured response. Using this technique, filters were realized. Tunable bandpass filters with sidelobe suppression greater than 20 db and passband ripple of less than 3 db, and insertion loss of 6 db have been realized.

3. Ka Band delay MSFVW lines with insertion losses of less than 16 db and bandwidth of greater than 1 GHz have been realized.

ZERO LINE ——————

S_{21} ——————

DIRECT THRU ——————
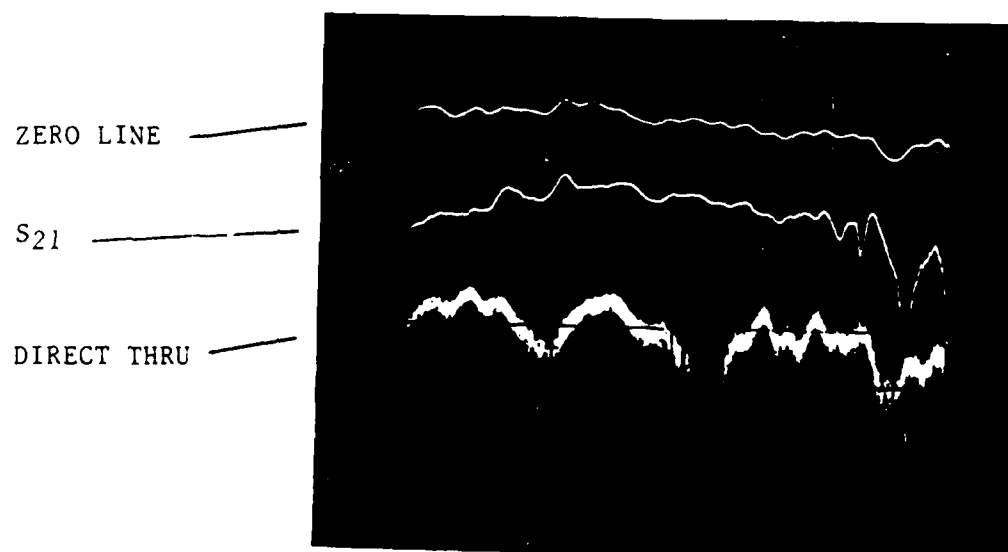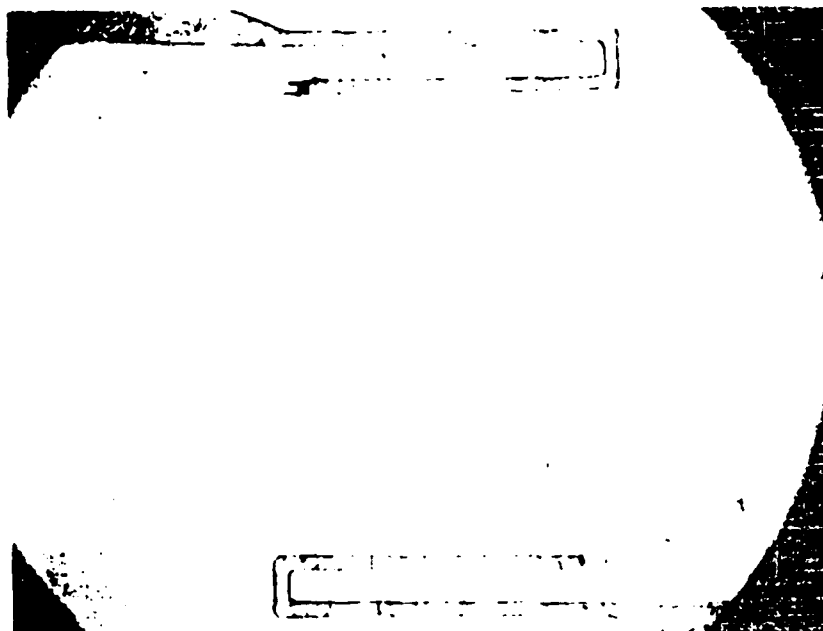
CENTER F=28 GHz
SWEEP =1 GHz

Figure 4.9 Photograph of loop-loop delay line and its frequency response
in the MSFVW mode.

104
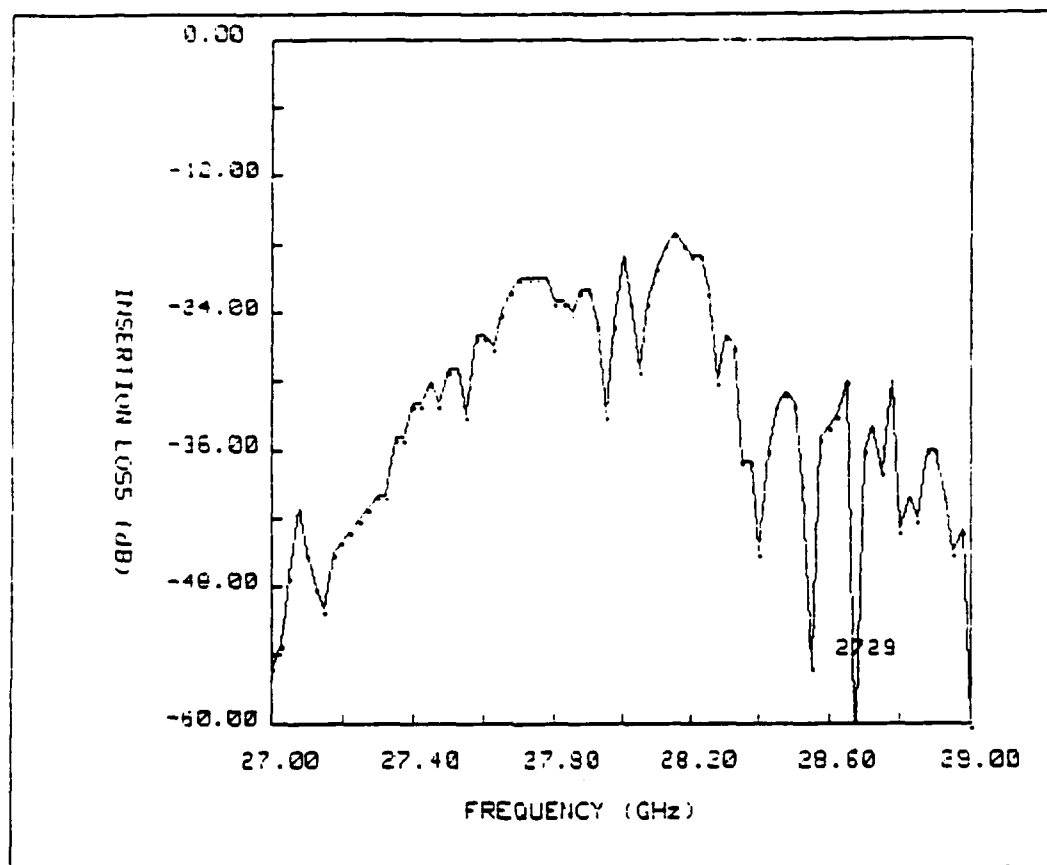
Figure 4.10   Plot of I.L vs F for device operating in the MSFVW mode
               corrected for the zero line.
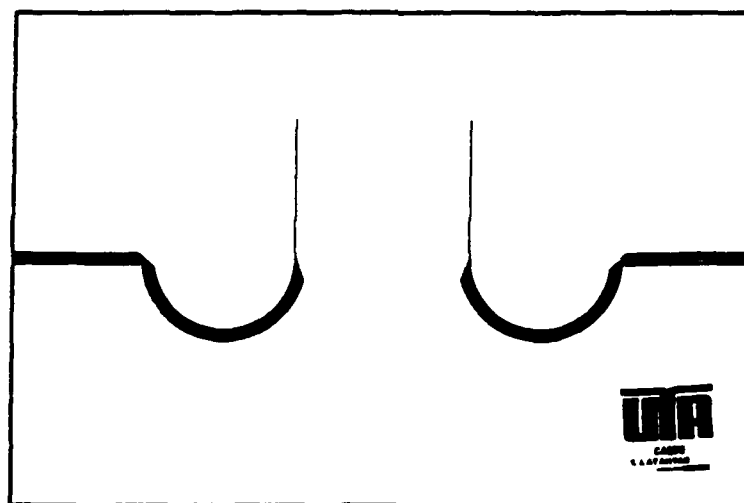
Figure 4.11   Photograph of open-ended single bar I/O delay line.

CF 30

ΔF 1.5
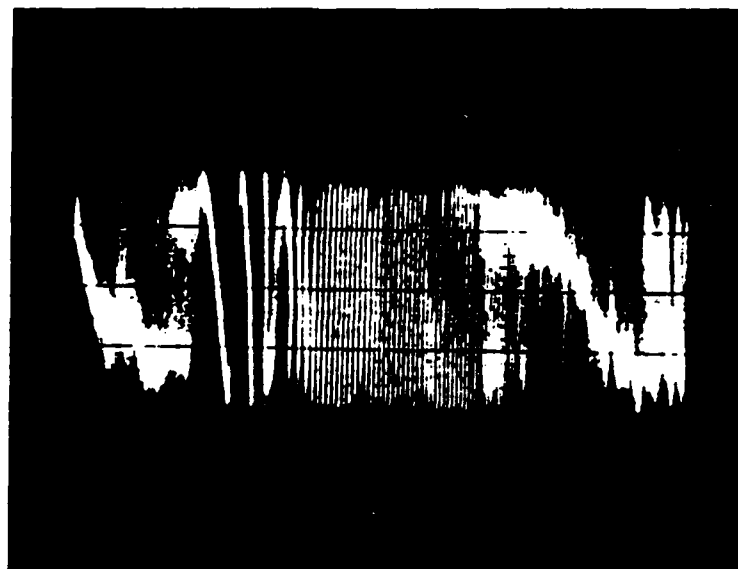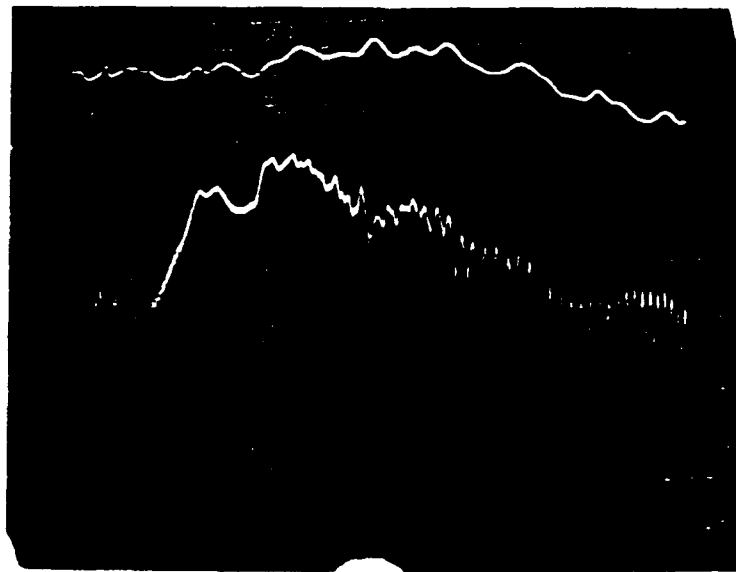
H 12.1

Figure 4.12   I.L vs F and the phase response of the device operated
in the MSFVW mode.

CF 30

ΔF 0.5

H 12.1
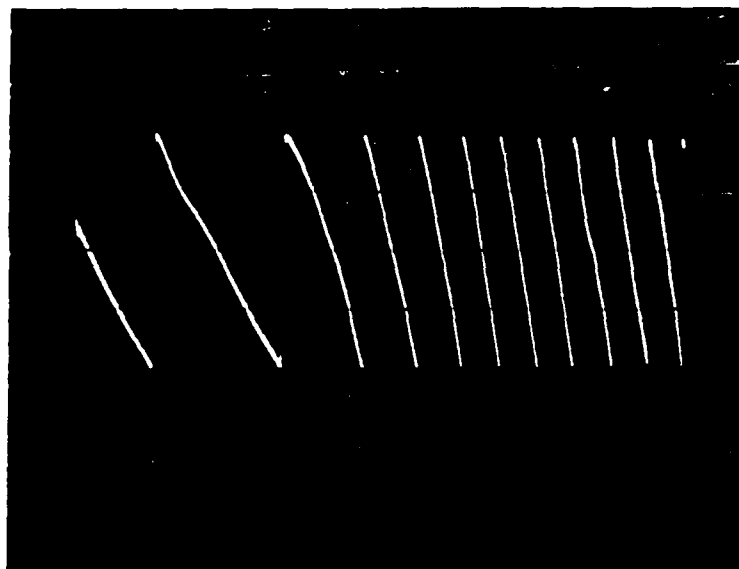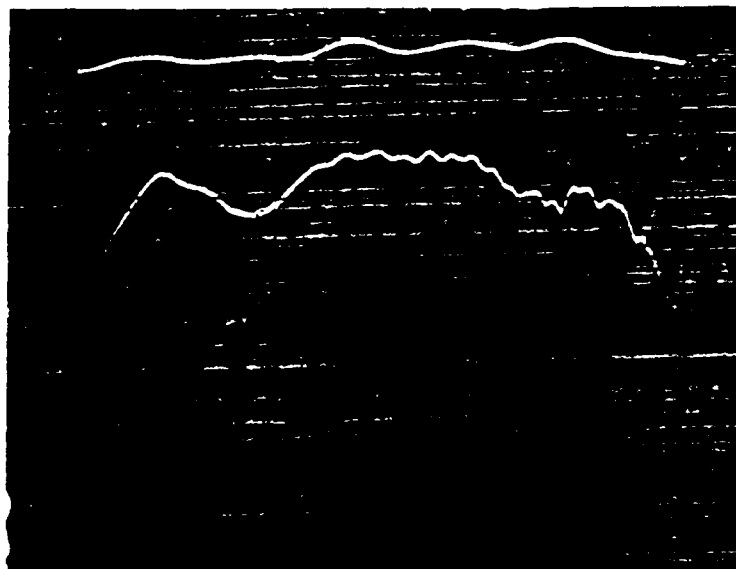
Figure 4.13   The expanded view of Figure 4.1.2.

CF 27

ΔF 0.4

H 8.6
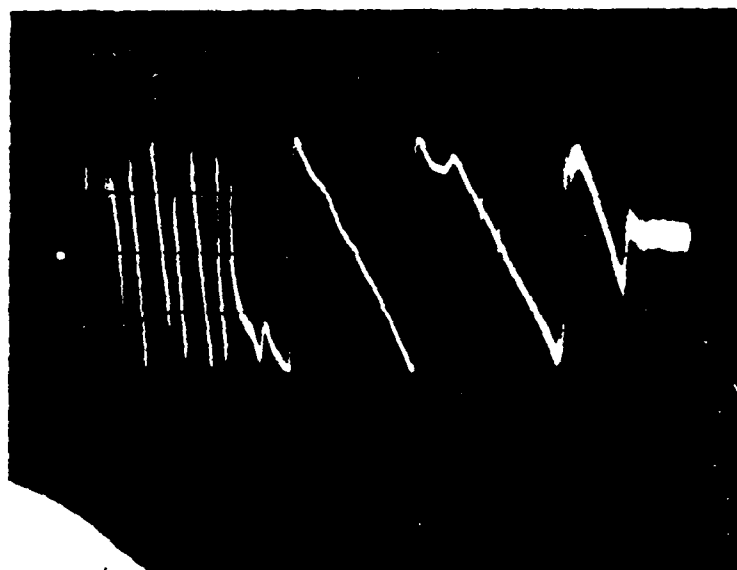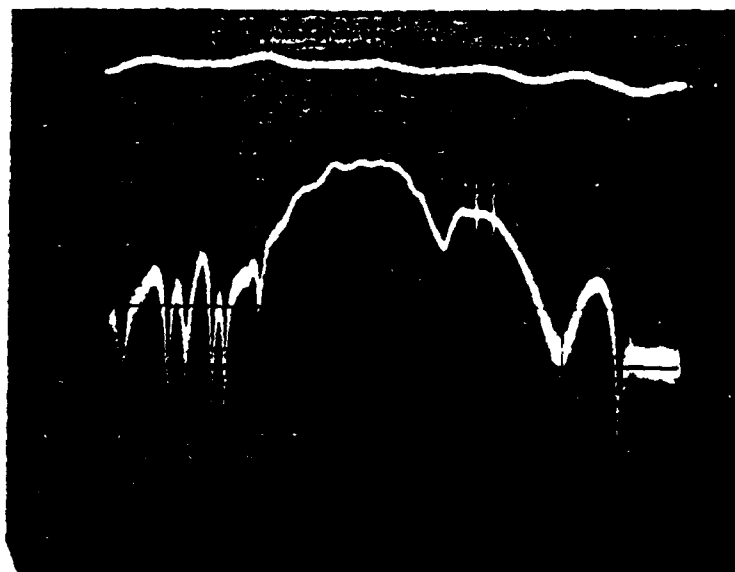
25 MHz

Figure 4.14   Magnitude and the phase of the device operated in the forward MSSW mode.

109

CF 2⁻

ΔF 0.15

H - ﹖
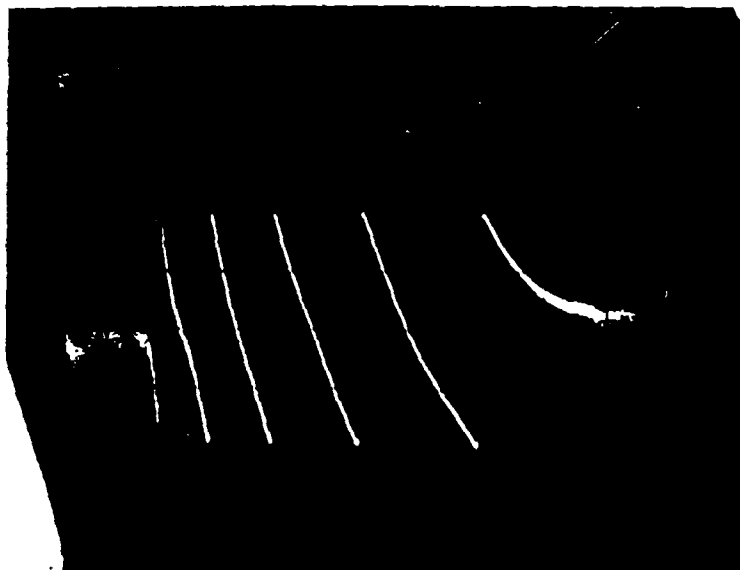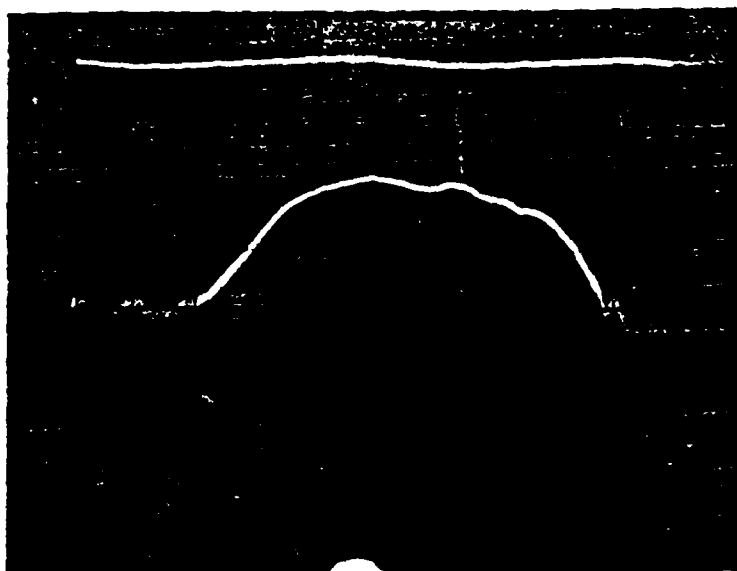
Figure 4.15   Magnitude and the phase response of the device operated in the reverse MSSW mode.

6.0 PUBLICATIONS
FROM AFOSR SUPPORT

1. R. L. Carter, C. V. Smith, Jr., and J. M. Owens, "Magnetostatic Forward Volume Wave-Spin Wave Conversion by Eteched Grating in LPE-YIG," IEEE Trans-Mag, Vol. Mag-16, 5, 1159-1161, September 1980.

2. J. M. Owens, "Magnetostatics Join SAW's" Microwave Systems News, May 1980 v. 10, No. 5, pp. 112-113.

3. C. V. Smith, Jr., J. M. Owens, R. L. Carter and J. H. Collins, "Magnetostatic Waves, Microwave SAW," Ultrasonics Symposium Proceedings, IEEE Cat. No. 80CH1602+2, pp. 506-513, November 1980.

4. J. C. Sethares, J. M. Owens, C. V. Smith, Jr., "MSW Non-dispersive, Electronically Tunable Time Delay Elements," Electronics Letters, Oct. 1980, V. 16, No. 22 pp. 825-826.

5. J. C. Sethares, C. V. Smith, Jr. and J. M. Owens, "MSW Time Delays," Symposium Proceedings, IEEE Cat. No. 80CH1602-2, pp. 518-521, November 1980.

6. J. M. Owens, R. L. Carter, C. V. Smith, Jr., and G. Hasnian, "A 3-Port Model for Magnetostatic Wave Transducers," Symposium Proceedings, IEEE Cat. No. 80CH1602-2, pp. 538-542, November 1980.

7. W. R. Brinlee, J. M. Owens, C. V. Smith, Jr., and R. L. Carter, "Two-port Magnetostatic Wave Resonators Utilizing Periodic Metal Reflective Arrays" J. Appl. Physics, 52, 3, 2276-2278, March 1981.

8. J. M. Owens, C. V. Smith, Jr. and R. L. Carter, "The Status of Magnetostatic Wave Devices," 35th Ann. Freq. Control Symposium USAERADCOM, Ft. Monmouth, N. J. 077030, 358-363 (1981).

9. R. L. Carter, J. M. Owens, W. R. Brinlee, Y. W. Sam and C. V. Smith, Jr. "Tunable Magnetostatic Surface Wave Oscillator at 4 GHz," 1981 IEEE MTT-S Symposium Proceedings, Cat No. 81 Ch 1592-5, pp. 383-385, June 1981.

10. C. V. Smith, Jr., J. M. Owens, N. D. Parikh and R. L. Carter, "Anisotropic Propagation of Magnetostatic Waves in Epitaxial YIG Films," IEEE Trans. Magn., Mag-17, 2967-2969 (1981).

11. R. L. Carter, J. M. Owens, C. V. Smith, Jr., and K. W. Reed, "Ion Implanted Magnetostatic Wave Reflective Array Filter," J. Appl. Phys. 53, 2655-2657 (1982).

12. R. L. Carter, J. M. Owens, C. V. Smith, Jr., and K. W. Reed, "Ion Implanted Oblique Incidence Magnetostatic Wave Reflective Array Filters," 1982 IEEE MTTs Microwave Symposium Digest #82 CH 1705-3, pp. 83-85, June, 1982.

13. G. F. Manes, and J. M. Owens, "Microwave Signal Processing Using Magnetostatic Wave Devices," Alta Frequenza No. 2 VLI, pp. 103-106, (1982).

14. J. M. Owens, C. V. Smith, Jr., and R. L. Carter, "MSW Reflecting Array Filters," Proceedings of the the 1981 RADC Microwave Magnetics Technology Workshop, RADC-TR-83-15, Rome Air Development Center, Griffis Air Force Base, NY 13441, pp. 106-116 (1983).

15. C. V. Smith, Jr., J. M. Owens, R. L. Carter, and K. W. Reed, "Microwave Pulse Compression Loops Using Magnetostatic Wave Delay Lines," Proceedings of the 1981 RADC Microwave Magnetics Technology Workshop, RADC-TR-83-15, Rome Air Development Center, Griffis Air Force Base. NY 13441, pp. 277-289 (1983).

16. J. M. Owens and R. L. Carter, "Magnetostatics Advance: The Shape of Things To Come," Microwave System News, V. 13 No. 3, pp. 103-111 (1983).

17. K. W. Reed, J. M. Owens, R. L. Carter, and C. V. Smith, Jr., "An Oblique Incidence Ion Implanted MSFVW RAF with Linear Group Delay," 1983 IEEE MTT-S International Microwave, IEEE Cat. No. 82CH1871-3 pp. 259-261.

18. J. M. Owens, R. L. Carter, and Y. Y. Sam, "A Hybrid GaAs MIC Oscillator Using a Magnetostatic Wave Resonator," 1983 IEEE MTT-S International Microwave Proceedings. IEEE Cat. No. 82CH1871-3 pp. 323-326.

19. J. M. Owens and R. L. Carter "The Status of Magnetostatic Wave Resonator Oscillators, 1983 Frequency Control Symposium Procceedings, pp. 477-480 IEEE Cat. No. CH1957-0/83/0000.

20. Kok Wai Chang, J. M. Owens, R. L. Carter, "Linearly Dispersive Time-Delay control of Magnetostatic Surface Wave by Variable Ground Plane Spacing" Electronics Letters V. 19 No. 14 (July 7th 1983) pp. 346-347.

21. Kok Wai Chang, L. R. Adkins, R. L. Carter, H. L. Glass, J. M. Owens and F. S. Sterns, "Electronically Variable Time Delays Using Cascaded Magnetostatic Delay Lines," accepted for publication in J. Appl. Phys.

APPENDIX 1

"FILTER SYNTHESIS THEORY"
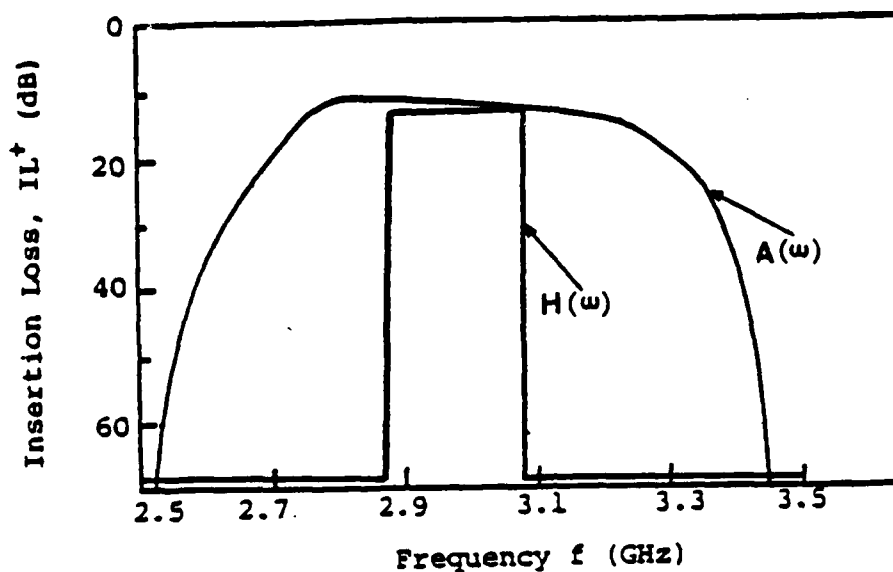
The frequency response for a zero path single bar I/O transducer, A(ω), and the desired response of a multibar bandpass filter, H(ω).

$$\tilde{G}(\omega) = \sum_{n=1}^{N} \tilde{\psi}_h(\omega) = \sum_{n=1}^{N} a_n \tilde{A}(\omega) e^{-\tilde{K}(\omega)\ell_n} \qquad (1)$$

$\tilde{G}(\omega)$ = array response

N = number of transducer elements.

$\tilde{\psi}_n(\omega)$ = nth element response.

a_n = weighting factor for the nth element.

$\tilde{A}(\omega)$ = transmission response of a single-bar/single-bar zero-path delay line.

$\tilde{K}(\omega)$ = α+jβ (α and β are loss factor and wave number, respectively).

ℓ_n = path length for the nth element.

$\tilde{H}(\omega)$ = desired frequency response.

114

$$\varepsilon = \frac{1}{\omega_2 - \omega_1} \int_{\omega_1}^{\omega_2} \{ \widetilde{H}(\omega) - \Sigma_{n=1}^{N} a_n \widetilde{A}(\omega) e^{-\widetilde{K}(\omega) l_n} \}$$

$$x \{ \widetilde{H}^{*}(\omega) - \Sigma_{n=1}^{N} a_n \widetilde{A}^{*}(\omega) e^{-\widetilde{K}^{*}(\omega) l_n} \} d\omega \quad (2)$$

$$\frac{\partial \varepsilon}{\partial a_m} = \frac{1}{\omega_2 - \omega_1} [\int_{\omega_1}^{\omega_2} \widetilde{A}(\omega) e^{-\widetilde{K}^{*}(\omega) l_n}$$

$$x \{ \widetilde{H}^{*}(\omega) - \Sigma_{n=1}^{N} a_n \widetilde{A}^{*}(\omega) e^{-\widetilde{K}^{*}(\omega) l_m} \} d\omega$$

$$+ \int_{\omega_1}^{\omega_2} \widetilde{A}^{*}(\omega) e^{-\widetilde{K}^{*}(\omega) l_n}$$

$$x \{ \widetilde{H}(\omega) - \Sigma_{n=1}^{N} a_n \widetilde{A}(\omega) e^{-\widetilde{K}^{*}(\omega) l_n} \} d\omega] \quad (3)$$

$$\frac{\partial \varepsilon}{\partial a_m} = \frac{-2}{\omega_2 - \omega_1} \{ Re \int_{\omega_1}^{\omega_2} \widetilde{A}(\omega) \widetilde{H}(\omega) e^{-\widetilde{K}^{*}(\omega) l_m} d\omega$$

$$- Re \Sigma_{n=1}^{N} a_n \int_{\omega_i}^{\omega_2} | \widetilde{A}(\omega) |^2$$

$$x \ e^{-[\widetilde{K}^{*}(\omega) l_m + \widetilde{K}(\omega) l_m]} d\omega = 0 \quad (4)$$

$$\begin{vmatrix} M_{11} M_{12} M_{13} & . & . & . & M_{1N} \\ M_{21} & . & . & . & . & . \\ . & . & . & . & . & . \\ M_{1} & . & . & . & . & M_{NN} \end{vmatrix} X \begin{vmatrix} a_1 \\ a_2 \\ . \\ a_N \end{vmatrix} = \begin{vmatrix} Q_1 \\ Q_2 \\ . \\ Q_N \end{vmatrix}$$

$$M_{ij} = Real \int_{\omega_1}^{\omega_2} | \widetilde{A}(\omega) |^2 e^{-[\widetilde{K}^{*}(\omega) l_i + \widetilde{K}(\omega) l_j]} \, dw$$

$$Q_i = Real \int_{\omega_1}^{\omega_2} \widetilde{A}^{*}(\omega) \widetilde{H} \ e^{-\widetilde{K}^{*}(\omega) l_i} \, d\omega$$

APPENDIX 2

"LIST OF THE PROGRAMS FOR SYNTHESIZING BANDPASS FILTER"

PROGRAM #1

```
C     MSSW  DISPERSION RELATION CALCULATES 152 W-K POINTS AND 305 W-K
C     POINTS FOR HILBERT TRANSFORM INTEGRATION
C     MSSW DISPERSION RELATION, GROUP VELOCITY AND TIME DELAY,PHASE VEL.
C     DESIGNED FOR STRUCTURE A/ B, REVERSE (+/-) DIRECTION
C*********************************************************************
C  EDITTED AND MODEFIED ON 7/24/84.          Y.J. ATAIIYAN
      DIMENSION FRQ(152),RK1(152),RK2(152),TM1(152),TM2(152),QF(305),QK1
     1(305),QK2(305)
      DIMENSION RI1(152),RI2(152),RIC(152),XI1(152),XI2(152),
     1XIL(152),TO1(20)
      DIMENSION R1(152),R2(152),RMX1(152),RMX2(152),XMX1(152),
     1XMX2(152),QRM(305),QRN(305),FQN(152),WAVL(152),ILMA(152),ILMB(152)
      DIMENSION FQ(152),TD1(152),TD2(152),XILMA(152)
      REAL ILMA,ILMB
      REAL*8 VP1,VP2,RKF,RKR,TM1,TM2
      REAL*8 FRQ,R1,R2,QF,QK1,QK2,FRQ3,FRQ4,FRQ1,FRQ2,DF,RFRQ,QRM,F,ZF,R
     1K1,RK2,QRN,RMX1,RMX2,ARGUE,H1,H2,H3,SUM1,SUM2,SUM,SIMP2,RM,RM1,RM2
     1,RND,OH,RN,RML2,XML2,GM,XMX1,XMX2
      REAL*8 FQ,R22,TD2,XM1,XM2,XM,EK,
     1ZC,BETA,AC,AR,AR1,AR2,AX,AX1,AX2,CZC,CBT,CAC,CAR,
     2CXM,ALPH,AL,BL,RIN,XIN,RI1,RI2,RIC,XI1,XI2,XIL,PT1,PT2,CL1,CL2
     3,XL1,XL2,X,CST
      REAL*8 T,OW,RNMAX,PN,U1,U2,AU1,AU2,
     1RK,RKS,RD,RT,BT,FT,DELT,EXT,A,B,C,D,PC,P1,P3,P21,P22,P2,P,
     ,DET1,DET2,E,G,RTT,RTU,TT,R11
      REAL*8 SSECH
      REAL*8 DELTF,A1,A2,RTL,RT1,TL,
     ,T1,DL,D1,FL,F1,TX,DX,FX,V0,V1,V2,V3,VG1,VG2,TDD,TDT
      COMMON F,RKF,RKR,RM1,RM2
      COMMON DO,TO,BO,RLGH,TU,SO,UO
      COMMON HI,GA,JCONF,NMAX,FPM
      DSECH(X)=DSQRT(1.-DTANH(X)*DTANH(X))
C ***** DEFINITION OF THE TERMS ****************************
C DO=YIG THICKNESS   (METERS)
C TO= AL2O3 THICKNESS (")
C BO= TRANSDUCER WIDTH (")
C RLGH= TRANSDUCER LENGTH (")
C TU= YIG/TRANSDUCER AIR GAP (")
C SO= SEPARATION BETWEEN TRANSDUCERS (")
C UO=  ?!!!
C HI= BIAS FIELD (OE)
C GA= GYROMAGNETIC RATIO (HZ/OE)
C ZO= CHARACTRISTIC IMP. OF THE TRANSDUCER.
C SO=WAVELENGTH AT CENTER FREQ.  IT DOES NOT HAVE ANY EFFECT
C    ON SINGLE BAR, FOR LOOP TRANSD. SPACINGS ARE SO/2, FOR
C    PARALLELL IT IS EQUAL TO SO.
C    CONDITION JUMP ON TRANSDUCER CONFIGURATIONS ( 1 FOR SINGLE BAR, 2
C    FOR PARALLEL ODD BARS, 3 FOR PARALLEL EVEN BARS, 4 FOR MEANDER
C    STRIPS, 5 FOR PI 0.5 CENTER SPACING, 6 FOR PI 1.5 CENTER SPACING)
C    NMAX IS THE STRIP NUMBER FOR MSW TRANSDUCERS
C INPUT THE FILE NAME FOR STORING THE DATA
```

117

```
        OPEN(UNIT=23,DEVICE='DSK',DIALOG)
         TYPE 1200
1200     FORMAT(1X,'ENTER YIG AND ALUMINA THICK IN MICRON')
         ACCEPT 1201,DO,TO
1201     FORMAT (2F)
         DO=DO*1.0E-6
         TO=TO*1.0E-6
        FPM=1750.
         TYPE 1202
1202     FORMAT(1X,'ENTER EXT H FIELD')
         ACCEPT 1203,HI
1203     FORMAT(1F)
        GA=2.8E6
        GM=GA*FPM
         TYPE 1204
1204     FORMAT(1X,'TYPE WIDTH AND LENGTH OF TRANSD. IN MICRON')
         ACCEPT 1201,BO,RLGH
         TYPE 1210
1210     FORMAT(1X,'ENTER I/O TRANSD. SPACINGS IN CM')
         ACCEPT 1203,PATH
         PATH=PATH*1.0E-2
         TYPE 1205
1205     FORMAT(1X,'ENTER AIR GAP(MICRON), AND LAMBDA AT CENTER'
     *,'FREQ. (MICRON)')
         ACCEPT 1201,TU,SO
         BO=BO*1.0E-6
         RLGH=RLGH*1.0E-6
         TU=TU*1.0E-6
         SO=SO*1.0E-6
        UO=1.256637E-6
         TYPE 1206
1206     FORMAT(1X,' ENTER CHARAC. IMP. OF TRANSD (ZC)')
         ACCEPT 1203,ZC
         TYPE 1207
1207     FORMAT(1X,'ENTER COND CODE AND # OF TRANSDS (I I)')
         TYPE 1208
1208     FORMAT(1X,' CC FOR SINGLE=1, PARAL ODD=2, PARAL EVEN=3
     *,MEAND=4, .5 SPACING PI=5, 1.5 SPACING PI=6')
         ACCEPT 1209,JCONF,NMAX
1209     FORMAT(2I)
         TYPE 1213
1213     FORMAT(1X,'IL IN DB (TYPE 1) OR LINEAR IL (TYPE 0)?')
         ACCEPT 1214,NYJA
1214     FORMAT(I)
        OH=HI/FPM
        FRQ3=DSQRT(OH*(OH+1.))*GM
        FRQ4=(OH+0.5)*GM
        FRQ1=FRQ3*1.01
        FRQ2=FRQ4*0.99
C       FREQUENCY SAMPLING 305 POINTS FOR HILBERT TRANSFORM
        QF(1)=FRQ3
        QF(3)=FRQ1
        QF(2)=0.5*(FRQ3+FRQ1)
        QF(103)=0.5*(FRQ2+FRQ1)
        QF(305)=FRQ4
```

```fortran
      QF(303)=FRQ2
      QF(304)=0.5*(FRQ2+FRQ4)
      DF=(QF(103)-QF(3))/100.0
      DO 100 I=1,99
      RI=I
      J=I+3
  100 QF(J)=QF(3)+RI*DF
      DO 101 I=1,199
      RI=I
      J=I+103
  101 QF(J)=QF(103)+RI*DF*0.5
C     FREQUENCY SAMPLING 152 POINTS FOR DISPERSION RELATION
      FRQ(1)=FRQ3+0.75*(FRQ1-FRQ3)
      FRQ(2)=FRQ1+0.5*DF
      DO 102 I=1,49
      RI=I
      J=I+2
  102 FRQ(J)=FRQ(2)+RI*DF*2.0
      FRQ(52)=QF(103)+DF*0.25
      DO 103 I=1,99
      RI=I
      J=52+I
  103 FRQ(J)=FRQ(52)+RI*DF
      FRQ(152)=FRQ2+0.25*(FRQ4-FRQ2)
C     DISPERSION RELATION
      DO 130 M=1,152
      F=FRQ(M)
       OW=F/GM
      U1=1.0-OH/(OW*OW-OH*OH)
      U2=OW/(OW*OW-OH*OH)
C     S=+1
      A1=U1+U2+1.
      A2=U1-U2-1.
C     REGI FALSI ITERATION TO FIND INITIAL GUESS FOR NEWTON ITERATION
      RTL=0.1*TO
      RT1=1.0E5*TO
      DO 20 I=1,500
      IF((I-500).EQ.0) WRITE(23,13)
      TL=DTANH(RTL)
      T1=DTANH(RT1)
      DL=DEXP(-2.*DO*RTL/TO)
      D1=DEXP(-2.*DO*RT1/TO)
         FL=(U1-U2+TL)*A1-(U1+U2-TL)*A2*DL
         F1=(U1-U2+T1)*A1-(U1+U2-T1)*A2*D1
      X=(RTL*F1-RT1*FL)/(F1-FL)
      TX=DTANH(X)
      DX=DEXP(-2.*DO*X/TO)
         FX=(U1-U2+TX)*A1-(U1+U2-TX)*A2*DX
      IF(DABS(FX)-1.0E-7) 51,51,31
   31 CLX=FX*FL
      CUX=FX*F1
      IF(CUX.GT.0.) RT1=X
      IF(CLX.GT.0.) RTL=X
   20 CONTINUE
C     NEWTON ITERATION
```

```fortran
   51 DO 90 L=1,500
      IF((L-500).EQ.0) WRITE(23,19)
      TX=DTANH(X)
      DX=DEXP(-2.*DO*X/TO)
  -      FX=(U1-U2+TX)*A1-(U1+U2-TX)*A2*DX
      DF=DX*A2*(+2.*DO*(U1+U2-TX)/TO+DSECH(X)**2)+A1*DSECH(X)**2
      IF(DABS(FX)-1.0E-10) 92,92,91
   91 X=X-FX/DF
   90 CONTINUE
   92 R11=X/TO
C     PHASE VELOCITY, GROUP VELOCITY AND DELAY TIME CALCULATION
      RK1(M)=R11
      FN1=FX
      TX=DTANH(X)
      DX=DEXP(+2.*DO*X/TO)
      VO=3.078760801D10*TO
      V1=DX*A1*(+2.*DO*(U1-U2+TX)/TO+DSECH(X)**2)+A2*DSECH(X)**2
      V2=((U1+U2-TX)-A1*DX)/((OW-OH)**2)
      V3=(A2-(U1-U2+TX)*DX)/((OW+OH)**2)
      VG1=VO*V1/(V2-V3)
        TDD=PATH/VG1
      TM1(M)=TDD
      VP1=6.283185307*F/R11
C     S=-1
      A1=U1+U2-1.
      A2=U1-U2+1.
C     REGI FALSI ITERATION TO FIND INITIAL GUESS FOR NEWTON ITERATION
      RTL=0.1*TO
      RT1=1.0E5*TO
      DO 209 I=1,500
      IF((I-500).EQ.0) WRITE(23,139)
      TL=DTANH(RTL)
      T1=DTANH(RT1)
      DL=DEXP(-2.*DO*RTL/TO)
      D1=DEXP(-2.*DO*RT1/TO)
      FL=DL*(U1-U2-TL)*A1-(U1+U2+TL)*A2
      F1=D1*(U1-U2-T1)*A1-(U1+U2+T1)*A2
      X=(RTL*F1-RT1*FL)/(F1-FL)
      TX=DTANH(X)
      DX=DEXP(-2.*DO*X/TO)
      FX=DX*(U1-U2-TX)*A1-(U1+U2+TX)*A2
      IF(DABS(FX)-1.0E-7) 519,519,319
  319 CLX=FX*FL
      CUX=FX*F1
      IF(CUX.GT.0.) RT1=X
      IF(CLX.GT.0.) RTL=X
  209 CONTINUE
C     NEWTON ITERATION
  519 DO 909 L=1,500
      IF((L-500).EQ.0) WRITE(23,199)
      TX=DTANH(X)
      DX=DEXP(-2.*DO*X/TO)
      FX=DX*(U1-U2-TX)*A1-(U1+U2+TX)*A2
      DF=DX*A1*(-2.*DO*(U1-U2-TX)/TO-DSECH(X)**2)-A2*DSECH(X)**2
      IF(DABS(FX)-1.0E-10) 929,929,919
```

120

```
   919 X=X-FX/DF
   909 CONTINUE
   929 R22=X/TO
C      PHASE VELOCITY, GROUP VELOCITY AND DELAY TIME CALCULATION
       RK2(M)=R22
       FN2=FX
       TX=DTANH(X)
       DX=DEXP(-2.*DO*X/TO)
       VO=3.078760801D10*TO
       V1=DX*A1*(-2.*DO*(U1-U2-TX)/TO-DSECH(X)**2)-A2*DSECH(X)**2
       V2=((U1+U2+TX)-A1*DX)/((OW-OH)**2)
       V3=(A2-(U1-U2-TX)*DX)/((OW+OH)**2)
       VG2=VO*V1/(V2-V3)
       TDT=1.0E-2/VG2
       TM2(M)=TDT
       VP2=6.283185307*F/R22
   130 CONTINUE
C      HILBERT TRANSFORM W-K POINTS
       DO 5130 M=2,304
       F=QF(M)
        OW=F/GM
       U1=1.0-OH/(OW*OW-OH*OH)
       U2=OW/(OW*OW-OH*OH)
C      S=+1
       A1=U1+U2+1.
       A2=U1-U2-1.
C      REGI FALSI ITERATION TO FIND INITIAL GUESS FOR NEWTON ITERATION
       RTL=0.1*TO
       RT1=1.0E5*TO
       DO 520 I=1,500
       IF((I-500).EQ.0) WRITE(23,13)
       TL=DTANH(RTL)
       T1=DTANH(RT1)
       DL=DEXP(-2.*DO*RTL/TO)
       D1=DEXP(-2.*DO*RT1/TO)
          FL=(U1-U2+TL)*A1-(U1+U2-TL)*A2*DL
          F1=(U1-U2+T1)*A1-(U1+U2-T1)*A2*D1
       X=(RTL*F1-RT1*FL)/(F1-FL)
       TX=DTANH(X)
       DX=DEXP(-2.*DO*X/TO)
          FX=(U1-U2+TX)*A1-(U1+U2-TX)*A2*DX
       IF(DABS(FX)-1.0E-7) 551,551,531
   531 CLX=FX*FL
       CUX=FX*F1
       IF(CUX.GT.0.) RT1=X
       IF(CLX.GT.0.) RTL=X
   520 CONTINUE
C      NEWTON ITERATION
   551 DO 590 L=1,500
       IF((L-500).EQ.0) WRITE(23,19)
       TX=DTANH(X)
       DX=DEXP(-2.*DO*X/TO)
          FX=(U1-U2+TX)*A1-(U1+U2-TX)*A2*DX
       DF=DX*A2*(+2.*DO*(U1+U2-TX)/TO+DSECH(X)**2)+A1*DSECH(X)**2
       IF(DABS(FX)-1.0E-10) 592,592,591
```

```
  591 X=X-FX/DF
  590 CONTINUE
  592 R11=X/TO
      QK1(M)=R11
      FN1=FX
C     S=-1
      A1=U1+U2-1.
      A2=U1-U2+1.
C     REGI FALSI ITERATION TO FIND INITIAL GUESS FOR NEWTON ITERATION
      RTL=0.1*TO
      RT1=1.0E5*TO
      DO 5209 I=1,500
      IF((I-500).EQ.0) WRITE(23,139)
      TL=DTANH(RTL)
      T1=DTANH(RT1)
      DL=DEXP(-2.*DO*RTL/TO)
      D1=DEXP(-2.*DO*RT1/TO)
      FL=DL*(U1-U2-TL)*A1-(U1+U2+TL)*A2
      F1=D1*(U1-U2-T1)*A1-(U1+U2+T1)*A2
      X=(RTL*F1-RT1*FL)/(F1-FL)
      TX=DTANH(X)
      DX=DEXP(-2.*DO*X/TO)
      FX=DX*(U1-U2-TX)*A1-(U1+U2+TX)*A2
      IF(DABS(FX)-1.0E-7) 5519,5519,5319
 5319 CLX=FX*FL
      CUX=FX*F1
      IF(CUX.GT.0.) RT1=X
      IF(CLX.GT.0.) RTL=X
 5209 CONTINUE
C     NEWTON ITERATION
 5519 DO 5909 L=1,500
      IF((L-500).EQ.0) WRITE(23,199)
      TX=DTANH(X)
      DX=DEXP(-2.*DO*X/TO)
      FX=DX*(U1-U2-TX)*A1-(U1+U2+TX)*A2
      DF=DX*A1*(-2.*DO*(U1-U2-TX)/TO-DSECH(X)**2)-A2*DSECH(X)**2
      IF(DABS(FX)-1.0E-10) 5929,5929,5919
 5919 X=X-FX/DF
 5909 CONTINUE
 5929 R22=X/TO
      QK2(M)=R22
      FN2=FX
 5130 CONTINUE
C     MSSW  RADIATION IMPEDANCE RM AND XM/ RM AS A SUBPROGRAM, XM
C     CALCULATED FROM HILBERT TRANSFORM OF XM BY USING 2ND ORDER CLOSED
C     FORM SIMPSON RULE FOR INTEGRATION
      GM=GA*FPM
      OH=HI/FPM
      FRQ3=DSQRT(OH*(OH+1.))*GM
      FRQ4=(OH+0.5)*GM
      FRQ1=FRQ3*1.01
      FRQ2=FRQ4*0.99
      DF=(FRQ2-FRQ1)/200.0
      RFRQ=FRQ4/FRQ3
      QF(1)=1.0
```

122

```
      QF(305)=RFRQ
      QRM(1)=0.
      QRM(305)=0.
      QRN(1)=0.
      QRN(305)=0.
      DO 200 I=2,304
      F=QF(I)
      RKF=QK1(I)
      RKR=QK2(I)
      CALL PGRM
      QRM(I)=RM1
      QRN(I)=RM2
      QF(I)=QF(I)/FRQ3
  200 CONTINUE
      DO 400 I=1,152
      F=FRQ(I)
      ZF=F/FRQ3
      RKF=RK1(I)
      RKR=RK2(I)
      CALL PGRM
      RMX1(I)=RM1
      RMX2(I)=RM2
      ARGUE=(ZF+1.)*(RFRQ-ZF)/((ZF-1.)*(RFRQ+ZF))
      RM=RM1
      RN=RM2
C     2ND ORDER CLOSED FORM OF SIMPSON RULE FOR INTEGRATION
      H1=(QRM(1)-RM)/(QF(1)*QF(1)-ZF*ZF)
      H2=(QRM(2)-RM)/(QF(2)*QF(2)-ZF*ZF)
      H3=(QRM(3)-RM)/(QF(3)*QF(3)-ZF*ZF)
      SUM1=(FRQ1-FRQ3)*(H1+4.*H2+H3)/(6.*FRQ3)
      H1=(QRM(303)-RM)/(QF(303)*QF(303)-ZF*ZF)
      H2=(QRM(304)-RM)/(QF(3C4)*QF(304)-ZF*ZF)
      H3=(QRM(305)-RM)/(QF(305)*QF(305)-ZF*ZF)
      SUM2=(FRQ4-FRQ2)*(H1+4.*H2+H3)/(6.*FRQ3)
      SUM=SUM1+SUM2
      DO 401 K=1,50
      JK=2*(K+1)
      J1=JK-1
      J2=JK+1
      H1=(QRM(J1)-RM)/(QF(J1)*QF(J1)-ZF*ZF)
      H2=(QRM(JK)-RM)/(QF(JK)*QF(JK)-ZF*ZF)
      H3=(QRM(J2)-RM)/(QF(J2)*QF(J2)-ZF*ZF)
      SIMP2=DF*(H1+4.*H2+H3)/(3.*FRQ3)
  401 SUM=SUM+SIMP2
      DO 402 K=51,150
      JK=2*(K+1)
      J1=JK-1
      J2=JK+1
      H1=(QRM(J1)-RM)/(QF(J1)*QF(J1)-ZF*ZF)
      H2=(QRM(JK)-RM)/(QF(JK)*QF(JK)-ZF*ZF)
      H3=(QRM(J2)-RM)/(QF(J2)*QF(J2)-ZF*ZF)
      SIMP2=DF*(H1+4.*H2+H3)*0.5/(3.*FRQ3)
  402 SUM=SUM+SIMP2
      XMX1(I)=0.318098862*(RM*DLOG(ARGUE)+2.*ZF*SUM)
C     2ND ORDER CLOSED FORM OF SIMPSON RULE FOR INTEGRATION
```

```
      H1=(QRN(1)-RN)/(QF(1)*QF(1)-ZF*ZF)
      H2=(QRN(2)-RN)/(QF(2)*QF(2)-ZF*ZF)
      H3=(QRN(3)-RN)/(QF(3)*QF(3)-ZF*ZF)
      SUM1=(FRQ1-FRQ3)*(H1+4.*H2+H3)/(6.*FRQ3)
      H1=(QRN(303)-RN)/(QF(303)*QF(303)-ZF*ZF)
      H2=(QRN(304)-RN)/(QF(304)*QF(304)-ZF*ZF)
      H3=(QRN(305)-RN)/(QF(305)*QF(305)-ZF*ZF)
      SUM2=(FRQ4-FRQ2)*(H1+4.*H2+H3)/(6.*FRQ3)
      SUM=SUM1+SUM2
      DO 550 K=1,50
      JK=2*(K+1)
      J1=JK-1
      J2=JK+1
      H1=(QRN(J1)-RN)/(QF(J1)*QF(J1)-ZF*ZF)
      H2=(QRN(JK)-RN)/(QF(JK)*QF(JK)-ZF*ZF)
      H3=(QRN(J2)-RN)/(QF(J2)*QF(J2)-ZF*ZF)
      SIMP2=DF*(H1+4.*H2+H3)/(3.*FRQ3)
  550 SUM=SUM+SIMP2
      DO 555 K=51,150
      JK=2*(K+1)
      J1=JK-1
      J2=JK+1
      H1=(QRN(J1)-RN)/(QF(J1)*QF(J1)-ZF*ZF)
      H2=(QRN(JK)-RN)/(QF(JK)*QF(JK)-ZF*ZF)
      H3=(QRN(J2)-RN)/(QF(J2)*QF(J2)-ZF*ZF)
      SIMP2=DF*(H1+4.*H2+H3)*0.5/(3.*FRQ3)
  555 SUM=SUM+SIMP2
      XMX2(I)=0.318098862*(RN*DLOG(ARGUE)+2.*ZF*SUM)
  400 CONTINUE
C     MSSW         FREQUENCY RESPONSE PROGRAM TO CALCULATE TRANSMISSION
C     LINE PARAMETERS, CIRCUIT ELEMENTS, INPUT IMPEDANCE, AND INSERTION
C     LOSS
      RN=NMAX
      ND=NMAX/2
      RND=ND
      CST=1.
      DO 105 J=1,152
      F=FRQ(J)
      TM9=TM1(J)
      TM8=TM2(J)
      RM1=RMX1(J)
      RM2=RMX2(J)
      XM1=XMX1(J)
      XM2=XMX2(J)
      RM=RM1+RM2
      XM=XM1+XM2
      BETA=3.636102608D-8*F
      AC=6.32D-7*DSQRT(F)/(BO*ZC)
      RML2=RM*RLGH*0.5
      XML2=XM*RLGH*0.5
      AR=0.5*RM/ZC
      AR1=0.5*RM1/ZC
      AR2=0.5*RM2/ZC
      AX=0.5*XM/ZC
      AX1=0.5*XM1/ZC
```

124

```
      AX2=0.5*XM2/ZC
      GO TO (81,82,82,93,94,94),JCONF
   81 CZC=1.
      CBT=1.
      CAC=1.
      CAR=1.
      CXM=1.
      GO TO 99
   82 CZC=1./RN
      CBT=1.
      CAC=1.
      CAR=1./RN
      CXM=1./RN
      GO TO 99
   93 CZC=1.
      CBT=RN
      CAC=RN
      CAR=1./RN
      CXM=1./RN
      GO TO 99
   94 CZC=1./RND
      CBT=2.
      CAC=2.
      CAR=1./RN
      CXM=1./RN
C     TRANSMISSION LINE PARAMETER MODIFICATIONS FOR TRANSDUCER ARRAYS
   99 ZC=CZC*ZC
      BETA=CBT*BETA
      AC=CAC*AC
      AR=CAR*AR
      AR1=CAR*AR1
      AR2=CAR*AR2
      AX=CXM*AX
      AX1=CXM*AX1
      AX2=CXM*AX2
      ALPH=AR+AC
      BET=BETA+AX
      AL=2.*ALPH*RLGH
      BL=2.0*BET*RLGH
C     INPUT IMPEDANCE AND CIRCUIT ELEMENTS
      RIN=ZC*DTANH(AL)/(1.+DCOS(BL)*DSECH(AL))
      XIN=ZC*DSIN(BL)*DSECH(AL)/(1.+DCOS(BL)*DSECH(AL))
      RI1(J)=RIN*AR1/ALPH
      RI2(J)=RIN*AR2/ALPH
      RIC(J)=RIN*AC/ALPH
      XI1(J)=XIN*AX1/BET
      XI2(J)=XIN*AX2/BET
      XIL(J)=XIN*BETA/BET
C     POWER RATIO, CONVERSION LOSS AND INSERTION LOSS
      PT1=200.0*RI1(J)/((RIN+50.0)**2.+XIN**2)
      PT2=200.0*RI2(J)/((RIN+50.0)**2.+XIN**2)
      CL1=10.*DLOG10(PT1)
      CL2=10.*DLOG10(PT2)
      XL1=2.*CL1-76.4E+6*TM9*CST*1.5
      XL2=2.*CL2-76.4E+6*TM8*CST*1.5
```

```
        IF(NYJA.EQ.1) GO TO 1215
      YOUNES=10.**(XL1/20.)
        GO TO 1216
1215    YOUNES=XL1
1216  ILMA(J)=YOUNES
      ILMB(J)=-2.*CL1
      FQN(J)=F/1.E9
      WAVL(J)=2.*3.14159/RK1(J)
      TOTRM=RMX1(J)+RMX2(J)
       TOTRK=RK1(J)+RK2(J)
      TOTRX=XMX1(J)+XMX2(J)
  105 CONTINUE
   13 FORMAT (1X,' NO CONVERGENCE OF 1ST ITERATION + WAVE')
   19 FORMAT (1X,' NO CONVERGENCE OF 2ND ITERATION + WAVE')
  139 FORMAT (1X,' NO CONVERGENCE OF 1ST ITERATION - WAVE')
  199 FORMAT (1X,' NO CONVERGENCE OF 2ND ITERATION - WAVE')
      DO 4567 II=1,152
4567  WRITE(23,3456)FRQ(II),ILMA(II)
3456  FORMAT(1X,E12.5,2X,E12.5)
      STOP
      END
      SUBROUTINE PGRM
C     RM SUBPROGRAM TO CALCULATE RADIATION RESISTANCE
      REAL*8 OH,T,F,RKF,RKR,OW,RNMAX,RN,PN,U1,U2,AU1,AU2,
     1RK,RKS,RD,RT,BT,FT,DELT,EXT,A,B,C,D,PC,P1,P3,P21,P22,P2,P,RM1,RM2,
     ,RM,X,DET1,DET2,E,G,RTT,RTU,TT,GM,SSECH
      COMMON F,RKF,RKR,RM1,RM2
      COMMON DO,TO,BO,RLGH,TU,SO,UO
      COMMON HI,GA,JCONF,NMAX,FPM
      SSECH(X)=1.-DTANH(X)*DTANH(X)
      DSECH(X)=DSQRT(1.-DTANH(X)*DTANH(X))
      TT=TO+TU
       GM=GA*FPM
      RN=NMAX
      ND=NMAX/2
      RND=ND
      OH=HI/FPM
       OW=F/GM
       U1=1.-OH/(OW*OW-OH*OH)
       U2=OW/(OW*OW-OH*OH)
C      S=+1
      AU1=U1+U2+1.
      AU2=U1-U2-1.
      RK=RKF
      RKS=RK*SO
       RD=RK*DO
      RT=TO*RK
      RTT=TT*RK
      RTU=TU*RK
      BT=DSIN(0.5*RK*BO)/(0.5*RK*BO)
      DET1=AU1*TT*DSECH(RTT)*DSECH(RTT)+AU2*DEXP(-2.*RD)*(2.*DO*(U1+U2-D
     1TANH(RTT))+TT*DSECH(RTT)*DSECH(RTT))
       DET2=AU1*(U1-U2+DTANH(RTT))-AU2*DEXP(-2.*RD)*(U1+U2-DTANH(RTT))
       DELT=(TO*DSECH(RT)*DSECH(RT)*DTANH(RTU)+TU*DSECH(RTU)*DSECH(RTU)*D
     1TANH(RT))*DET2+(1.+DTANH(RT)*DTANH(RTU))*DET1
```

```
      EXT=(-1.)*BT/(DELT*RK)
      A=EXT*(AU2*(U1+U2-DTANH(RTU))*DEXP(-2.*RD)+AU1*(U2-U1-DTANH(RTU)))
      B=EXT*DTANH(RT)*AU1*DSECH(RTU)
      C=EXT*DTANH(RT)*AU2*DEXP(-2.*RD)*DSECH(RTU)
      D=EXT*DTANH(RT)*2.*U1*DSECH(RTU)
      E=EXT*(AU2*(U1+U2)*DEXP(-2.*RD)+AU1*(U2-U1))*DTANH(RT)*(-1.)
      G=EXT*(AU1+DEXP(-2.*RD)*AU2)*DTANH(RT)
      PC=3.141592654*F*UO*RK
         P1=+0.5*D*D*DEXP(-2.*RD)/RK
         P3=0.5*A*A*(DTANH(RT)/RK-TO*DSECH(RT)*DSECH(RT))
        P21=U1*(B*B*(1.-DEXP(-2.*RD))/RK+C*C*(DEXP(+2.*RD)-1.)/RK-4.*B*C*
     ,DO)
        P22=U2*(B*B*(1.-DEXP(-2.*RD))/RK-C*C*(DEXP(+2.*RD)-1.)/RK)
      P2=0.5*(P21-P22)
      P4=0.5*TU*(E*E-G*G)*SSECH(RTU)+0.5*(E*E+G*G)*DTANH(RTU)/RK+E*G*DTA
     1NH(RTU)*DTANH(RTU)/RK
      P=PC*(P1+P2+P3+P4)
      GO TO (71,72,93,94,95,96),JCONF
   71 FT=1.
      GO TO 99
   72 FT=1.
      DO 920 N=1,ND
      PN=N
  920 FT=FT+2.*DCOS(PN*RKS)
      GO TO 99
   93 FT=0.
      DO 930 N=1,ND
      PN=N
  930 FT=FT+2.*DCOS((PN-0.5)*RKS)
      GO TO 99
   94 FT=0.
      DO 940 N=1,ND
      PN=N
  940 FT=FT+2.*((-1.)**N)*DSIN((PN-0.5)*0.5*RKS)
      GO TO 99
   95 FT=0.
      DO 950 N=1,ND
      PN=N
  950 FT=FT+2.*DSIN((PN-0.75)*RKS)
      GO TO 99
   96 FT=0.
      DO 960 N=1,ND
      PN=N
  960 FT=FT+2.*DSIN((PN-0.25)*RKS)
   99 P=P*FT*FT
      RM1=2.*P
C     S=-1.
      AU1=U1-U2+1.
      AU2=U1+U2-1.
      RK=-RKR
      RKS=RK*SO
       RD=RK*DO
      RT=TO*RK
      RTT=TT*RK
      RTU=TU*RK
```

127

```
      BT=DSIN(0.5*RK*BO)/(0.5*RK*BO)
      DET1=AU1*TT*DSECH(RTT)*DSECH(RTT)+AU2*DEXP(+2.*RD)*(2.*DO*(U1-U2+D
     1TANH(RTT))+TT*DSECH(RTT)*DSECH(RTT))
      DET2=DEXP(2.*RD)*AU2*(U1-U2+DTANH(RTT))-AU1*(U1+U2-DTANH(RTT))
      DELT=(TO*DSECH(RT)*DSECH(RT)*DTANH(RTU)+TU*DSECH(RTU)*DSECH(RTU)*D
     1TANH(RT))*DET2+(1.+DTANH(RT)*DTANH(RTU))*DET1
      EXT=BT/(DELT*RK)
      A=EXT*(AU2*(U2-U1-DTANH(RTU))*DEXP(+2.*RD)+AU1*(U2+U1-DTANH(RTU)))
      B=EXT*DTANH(RT)*AU2*DEXP(+2.*RD)*DSECH(RTU)
      C=EXT*DTANH(RT)*AU1*DSECH(RTU)
      D=EXT*DTANH(RT)*2.*U1*DSECH(RTU)
      E=EXT*(AU2*(U2-U1)*DEXP(+2.*RD)+AU1*(U2+U1))*DTANH(RT)*(-1.)
      G=EXT*(DEXP(2.0*RD)*AU2+AU1)*DTANH(RT)
      PC=3.141592654*F*UO*RK*(-1.)
          P1=-0.5*D*D*DEXP(+2.*RD)/RK
          P3=0.5*A*A*(DTANH(RT)/RK-TO*DSECH(RT)*DSECH(RT))
        P21=U1*(B*B*(1.-DEXP(-2.*RD))/RK+C*C*(DEXP(+2.*RD)-1.)/RK-4.*B*C*
     ,DO)
          P22=U2*(B*B*(1.-DEXP(-2.*RD))/RK-C*C*(DEXP(+2.*RD)-1.)/RK)
      P2=0.5*(P21-P22)
      P4=0.5*TU*(E*E-G*G)*SSECH(RTU)+0.5*(E*E+G*G)*DTANH(RTU)/RK+E*G*DTA
     1NH(RTU)*DTANH(RTU)/RK
      P=PC*(P1+P2+P3+P4)
      GO TO (81,82,83,84,85,86),JCONF
   81 FT=1.
      GO TO 89
   82 FT=1.
      DO 820 N=1,ND
      PN=N
  820 FT=FT+2.*DCOS(PN*RKS)
      GO TO 89
   83 FT=0.
      DO 830 N=1,ND
      PN=N
  830 FT=FT+2.*DCOS((PN-0.5)*RKS)
      GO TO 89
   84 FT=0.
      DO 840 N=1,ND
      PN=N
  840 FT=FT+2.*((-1.)**N)*DSIN((PN-0.5)*0.5*RKS)
      GO TO 89
   85 FT=0.
      DO 850 N=1,ND
      PN=N
  850 FT=FT+2.*DSIN((PN-0.75)*RKS)
      GO TO 89
   86 FT=0.
      DO 860 N=1,ND
      PN=N
  860 FT=FT+2.*DSIN((PN-0.25)*RKS)
   89 P=P*FT*FT
      RM2=2.*P
      RETURN
      END
```

```
C-----------------------------------------------------------------------
C  PROGRAM DESCRIPTION:
C
C         THIS PROGRAM CALCULATES THE COMPLEX DISPERSION RELATION FOR
C
C              1) ION IMPLANTED MSSW,
C
C              2) UNIMPLANTED MSSW.
C
C  THE ASSUMED FORM IS,
C
C              EXP(J(WT-KY)),
C
C  CORRESPONDING TO A DISPERSION FACTOR OF THE FORM,
C
C              K = BETA - J*ALPHA.
C
C-----------------------------------------------------------------------
C
C  SET UP CONSTANTS AND DECLARE COMPLEX AND REAL-------------------
       COMPLEX J,CHO,GAMFO,K3,K4,GK,
      1GAMMA,E2KU,E2KD,FOFKFO,COSHKV,SINHKV
       REAL MO
       OPEN(UNIT=23,DEVICE='DSK',DIALOG)
       PI=3.1415927
       J=CMPLX(0.0,1.0)
       GYRO=17.6E+06
       MO=1750.0
       ZERO=1.0E-04
       FRACT=1.0E-04
       TYIGIM=0.0
C
C-----------------------------------------------------------------------
C  USER SUPPLIED INPUTS
C-----------------------------------------------------------------------
       TYPE 1200
1200   FORMAT(1X,'ENTER YIG AND SUBST. THICKNESS (MICRON)')
       ACCEPT 1201,TYIG,TAL203
1201   FORMAT(2F)
C  YIG THICKNESS (MICRONS)-----------------------------------------
C
C  ALUMINA SUBSTRATE THICKNESS (MICRONS)---------------------------
       TYPE 1202
1202   FORMAT(1X,'ENTER H FIELD')
       ACCEPT 1203,HO
1203   FORMAT(F)
C  INTERNAL BIAS FIELD (OERSTEDS)----------------------------------
C
C  GILBERT LOSS PARAMETERS (FO IN HERTZ AND DELTA-H MIN IN OERSTEDS)-
       FO=3.0E+09
```

```
          DHMIN=0.5
C
C  DESIRED FREQUENCY INCREMENT IN OUTPUT DATA (MHZ)————————————
          TYPE 1204
1204      FORMAT(1X,'ENTER FREQ. INCR. (MHZ)')
          ACCEPT 1203,DELF
       DELFH=DELF*1.0E6
C
C  DESIRED START AND STOP FREQUENCY IN OUTPUT (GHZ)————————————
C  *** IMPORTANT *** : THE FSTART SHOULD BE BIGGER THAN F(1) FROM
C  WU'S PROGRAM, AND FSTOP SHOULD BE SMALLER THAN F(152) FROM WU'S
C  PROGRAM.
          TYPE 1205
1205      FORMAT(1X,'ENTER FSTART FSTOP (GHZ). '/
     *,' NOTE THAT FSTART SHOULD BE BIGGER THAN FSTART IN MSSW'
     *,' PROGRAM AND FSTOP SHOULD BE SMALLER THAN ITS FSTOP')
          ACCEPT 1201,FSTART,FSTOP
       FSTSTH=FSTART*1.0E9
       NUMBER=INT((FSTOP-FSTART)*1000./DELF)
       WRITE(23,111) FSTSTH,DELFH,NUMBER
111    FORMAT(1X,E12.5,2X,E12.5,4X,I5)
C
C——————————————————————————————————————————————————————————————————
C
       TYIGIM=TYIGIM*1.0E-06
       TYIGPU=(TYIG*1.0E-06)-TYIGIM
       TAL203=TAL203*1.0E-06
       WSTART=FSTART*2.0E+09*PI
       WSTOP=FSTOP*2.0E+09*PI
       DELW=DELF*2.0E+06*PI
       W=WSTART-DELW
C
C  MAKE AN INITIAL GUESS ON GAMMA——————————————————————————————
       GAMFO=CMPLX(0.0,0.0)
11111  W=W+DELW
       F=W/(2.0*PI)
C
C  CALCULATE GILBERT LOSS TERMS————————————————————————————————
       DELH=DHMIN*(FO/F+F/FO)/2.0
       CHO=CMPLX(HO,DELH/2.0)
C
C  CALCULATE PERMITIVITY RELATED CONSTANTS FOR FORWARD PROPAGATION———
       K3=1.0 + MO/(CHO - W/GYRO)
       K4=1.0 + MO/(CHO + W/GYRO)
C
C  INCREMENT NEWTON RAPHSON ON FORWARD UNIMPLANTED GAMMA——————————
       DO2 IK2=1,200,1
       SINHKV=-J*CSIN(J*GAMFO*TAL203)
       COSHKV=CCOS(J*GAMFO*TAL203)
       E2KU=CEXP(2.0*GAMFO*TYIGIM)
       E2KD=CEXP(2.0*GAMFO*TYIGPU)
       FOFKFO=(K4+1.0)*(K3*COSHKV+SINHKV)*E2KU*E2KD
     1        -(K3-1.0)*(K4*COSHKV-SINHKV)
       IF(CABS(FOFKFO).LE.ZERO) GO TO 1000
       GAMFO=CLOG((K3-1.0)*(K4*COSHKV-SINHKV)
```

130

```
      1       /((K4+1.0)*(K3*COSHKV+SINHKV)))/(2.0*(TYIGPU+TYIGIM))
       CHRE=ABS(REAL(GAMMA-GAMFO))
       CHIM=ABS(AIMAG(GAMMA-GAMFO))
       OLDRE=ABS(REAL(GAMMA))
       OLDIM=ABS(AIMAG(GAMMA))
       IF(CHRE.GT.FRACT*OLDRE) GO TO 77
       IF(CHIM.LT.FRACT*OLDIM) GO TO 1000
   77 GAMMA=GAMFO
    2 CONTINUE
       WRITE(23,31) F,GAMFO,CHRE,CHIM
   31 FORMAT(1X,'FREQ = ',1E10.3,5X,'GAMFO = ',2(E10.3,1X),4X,
      1/,1X,'CHRE   = ',1E10.3,5X,'CHIM   = ',1E10.3)
       STOP
 1000 FREQ=F/1.0E+09
       GK=J*GAMFO
       WRITE(23,101) GK
  101 FORMAT(5X,E12.5,2X,E12.5)
       IF(W.LT.WSTOP) GO TO 11111
       STOP
       END
```

```
C  THIS PROGRAM IS GENERAL SYNT. OF TRANSDUCERS.
C       ************************************************************
C       ****       IMPORTANT       ********************************
C       ************************************************************
C       BE SURE TO CHANGE THE DIMENSIONS OF L,YY,XX TO THE
C       NUMBER OF TRANSDUCERS.
C  TO SOLVE THE MATRIX, THIS PROGRAM NEEDS A SUBROUTINE. IN
C  THIS PROGRAM IT USES THE SUBROUTINE CALLED "SIMQ" WHICH IS
C  STORED IN THE MAIN COMPUETR. IF THIS PROGRAM IS USED ANYWHERE
C  BUT "UTA-DEC20 SYSTEM", YOU NEED TO ADD MATRIX SOLVING
C  PROGRAM.
        DIMENSION FREQ(152),AAW(152),FRQ(1500),AW(1500),
     1K(1500),L(16),YY(16),XX(16,16),H1(1500),H2(1500)
        DIMENSION H(1500)
        COMPLEX K,H,Y1,Y2,Y3,Y4,Y5,X1,X2,X3,X4,X5,Z1,Z2,Z3,K2
        REAL ISP,L0,LOSSDB,L,PII,KHAR,LOC
        PII=3.1415927
        TYPE 1000
C FOUR FILE NAME IS NEEDED:
C ONE FOR READING F VS IL (LINEAR) DATA,
C ONE FOR READING COMPLEX K VALUES,
C ONE TO STORE THE F-IL DATA,
C AND ONE TO STORE XDUCER AND FILTER DATA.
        OPEN(UNIT=23,DEVICE='DSK',DIALOG)
        OPEN(UNIT=24,DEVICE='DSK',DIALOG)
        OPEN(UNIT=25,DEVICE='DSK',DIALOG)
        OPEN(UNIT=26,DEVICE='DSK',DIALOG)
C       READ 152 DATA OF F VS I.L(LINEAR)
        READ(23,3)(FREQ(I),AAW(I),I=1,152)
C       READ START FREQ. ,F INCREAMENT, AND TOTAL # OF DATA.
        READ(24,333) F0,DF,NUMBER
        TYPE 1
C       ACCEPT # OF TRANSDUCERS.
        ACCEPT 2,NUM
        F0=F0-DF
C       READ COMPLEX K VALUES.
        READ(24,3)(K(I),I=1,NUMBER)
C       EXPAND THE 152 F VS I.L. DATA TO THE NUMBER OF DATA FROM
C       COMPLEX K FILE. THIS IS TO MATCH F AND I.L. TO THE K VAL
        DO 82 J=1,NUMBER
        F0=F0+DF
        DO 80 I=1,152
        IF(FREQ(I).LE.F0) GO TO 81
        DDF1=FREQ(I)-FREQ(I-1)
        DDAW=AAW(I)-AAW(I-1)
        DDF2=FREQ(I)-F0
        RATIO1=DDAW/DDF1
        RESULT=AAW(I)-RATIO1*DDF2
        FRQ(J)=F0
        AW(J)=RESULT
```

132

```
              GO TO 82
81            IF(I.EQ.152) GO TO 88
               GO TO 80
88             FRQ(J)=FO
              AW(J)=0.0
              GO TO 82
80            CONTINUE
82            CONTINUE
              TYPE 13
C             ACCEPT CEN. F IN HRZ.
              ACCEPT 34,FCENT
C             FIND DATA # CORRESPONDING TO C.F
              DO 90 I=1,NUMBER
              IF(FRQ(I).LE.FCENT) GO TO 90
              IFO=I
              GO TO 91
90            CONTINUE
91            CONTINUE
              TYPE 22
C             ACCEPT THE INTEGER # (N) TO FIND TRANS. SPACING OF N*LAMBDA
              ACCEPT 34,FSP
C             CALCULATE THE W.L. OF C.F.
              XKXK=AIMAG(K(IFO))
              XXX=2.0*PII*1.0E6/XKXK
              XLAM=INT(XXX)
              SO1=XLAM*FSP
C             CALCULATES TRANSD. SPACING (METERS)
              SO=SO1*1.0E-6
              TYPE 1200
1200          FORMAT(1X,' ENTER I/O SPACING (CM)')
C             ACCEPT CENT/CENT SPACING OF I/O TRANSDUCERS (CM)
              ACCEPT 34,LO
.             LO=LO*1.0E-2
C             FIND I/O SPASING FOR EACH TRANSDUCERS.
              DO 6 I=1,NUM
6             L(I)=LO+(I-1)*SO
              TYPE 5
C             ACCEPT B.W OF DESIRED FILTER (MHZ)
357           ACCEPT 34,BW
C             FIND FREQ. CORRESP. TO THE B.W AND CALCULATING THE
C             DATA # CORRESP. TO THESE FREQS.
              BWW1=(BW*1.0E6)/(2.0*DF)
              BW1=INT(BWW1)
              IF1=IFO-BW1
              IF2=IFO+BW1
              IF(IF1.LT.1) GO TO 648
              IF(IF2.GT.NUMBER) GO TO 648
              GO TO 234
648           TYPE 432
432           FORMAT(1X,'B.W. IS TOO BIG, TRY SMALLER B.W.')
              GO TO 357
234           CONTINUE
              KHAR=XKXK*2.0
C             FIND W.L. OF THE FIRST HARMONIC OF THE BAND-PATH FILTER
              XLAMH=2.0*PII*1.0E6/KHAR
```

```
          DO 123 I=1,NUMBER
          XKXK=AIMAG(K(I))
          IF(XKXK.LE.KHAR) GO TO 123
          IHAR=I
          GO TO 321
123       CONTINUE
321       IF12=IHAR
          IF(IHAR.LE.IF2) IF12=IF2+10
C         EQUATION FOR CALCULATING THE DESIRED PHASE(PH=C*F)
          DO 7 I=1,NUMBER
          K2=K(I)
          HHH2=-AIMAG(K2)
          LOC=((NUM-1)/2.)*SO+LO
          H21=HHH2*LOC
          H22=INT(H21/(2.*PII))
          H2(I)=H21+H22*2.*PII
7         CONTINUE
C         CALCULATE UPPER AND LOWER VALUES OF THE BAND-PATH FILTER
C         IN THE LINEAR SCALE. (E.G. IF H1 IS 1.0 AND .001, IT MEANS
C         WE WANT THE FILTER TO HAVE 0-DB IN THE PASS-BAND, AND
C         -60DB OUTSIDE THE PASSBAND.
          DO 20 I=1,NUMBER
          IF(I.GE.IF1) GO TO 21
          H1(I)=0.0001
          GO TO 20
21        IF(I.LE.IF2) H1(I)=1.0
          IF(I.GT.IF2) H1(I)=0.0001
20        CONTINUE
          DO 25 I=1,NUMBER
          HH1=H1(I)
          HH2=H2(I)
          H(I)=HH1*CMPLX(COS(HH2),SIN(HH2))
25        CONTINUE
          TYPE 567
567       FORMAT(1X,'DO YOU WANT SYNT. ONLY FOR THE FIRST FUND.
      AHARMONIC (YES=CR, NO=1)')
          ACCEPT 2,ICHO
          ISYN=NUMBER
          IF(ICHO.EQ.0) ISYN=IF12
          DO 30 I1=1,NUM
          Y5=(0.0,0.0)
          DO 31 J1=1,ISYN
          Y1=K(J1)
          Y2=CONJG(Y1)
          Y3=Y2*L(I1)
          Y4=CEXP(-Y3)
31        Y5=H(J1)*Y4*AW(J1)*DF+Y5
          YY(I1)=REAL(Y5)
30        CONTINUE
          DO 50 I1=1,NUM
          DO 50 I2=1,NUM
          X5=(0.0,0.0)
          DO 40 J1=1,ISYN
          X1=K(J1)
          X2=CONJG(X1)
```

134

```
          X3=X2*L(I1)+K(J1)*L(I2)
          X4=CEXP(-X3)
40        X5=(AW(J1)**2.)*X4*DF+X5
          XX(I1,I2)=REAL(X5)
50        CONTINUE
          KS=0
          CALL SIMQ(XX,YY,NUM,KS)
          YO=0.0
          DO 100 I=1,NUM
          IF(ABS(YY(I)).GT.YO) GO TO 111
          GO TO 100
111       YO=ABS(YY(I))
100       CONTINUE
          DO 101 I=1,NUM
          YY(I)=YY(I)/YO
101       CONTINUE
          WRITE(26,92)FRQ(1),FRQ(NUMBER),FCENT,XLAM,NUM,SO1,
      ABW,FRQ(IF1),FRQ(IF2),XLAMH,FRQ(IHAR),FRQ(1),FRQ(ISYN),
      B(YY(I),I=1,NUM)
  92   FORMAT(1X,'NATURAL CUT-OFF FRQ.S ARE: ',E12.5,' & ',E12.5
      A,/' CENTER FRQ. IS:',E12.5,' WITH THE W.L(MIC) OF '
      B,F6.1/,' # OF XDUCERS = ',I3, '    WITH SEPARATION (MIC) OF '
      C,F6.1/,' FILTER B.W (MHZ)=',F5.1,/' (START F='
      D,E12.5,' AND STOP F=',E12.5,' )'/
      E' W.L (MIC) OF THE FIRST HARM=',F6.1,'  AND FRQ='
      F,E12.5,/' SYNTH. START AT :',E12.5,' AND ENDS AT: '
      G,E12.5/' THE WEIGHTING FACTORS ARE:'/,5(1X,E12.5))
          DO 200 I1=1,NUMBER
          ZYY=0
          Z3=(0.0,0.0)
          DO 201 I2=1,NUM
          Z1=-K(I1)*L(I2)
          Z2=CEXP(Z1)
          ZYY=ZYY+(YY(I2)**2.)
201       Z3=Z2*AW(I1)*YY(I2)+Z3
          Z4=CABS(Z3/ZYY)
          LOSSDB=20.*ALOG10(Z4)
          A1=AIMAG(Z3)
          A2=REAL(Z3)
          A3=A1/A2
          A4=ATAN(A3)
          TETA=A4*180./PII
          WRITE(25,33)FRQ(I1),LOSSDB
200       CONTINUE
1         FORMAT(1X,'ENTER # OF TRANSDUERS ')
2         FORMAT(I)
3          FORMAT(2E)
13        FORMAT(1X,'ENTER CENTER FREQUENCY (HZ)' )
5         FORMAT(1X,'ENTER B.W (MHZ) ')
22        FORMAT(1X,'ENTER XDUCER SPACING IN TERMS OF LAMBDA')
26        FORMAT(1X,5(1X,E11.4))
33        FORMAT(1X,2E)
34        FORMAT(E)
333       FORMAT(2E,I)
1000      FORMAT(1X,'THIS PROGRAM ASKS FOR FOUR    FILE NAMES. THE
```

135

```
1 FIRST ONE IS FREQ. VS I.L. (152 DATA) , THE   SECOND FILE
2 IS THE COMPLEX VALUES OF K., THIRD FILE STORES THE  F
3 VS I.L.(DB),  AND THE LAST FILE STORES PARAMETERS.')
  STOP
  END
```

```
C     THIS PROGRAM COMBINES THE I.L. DATA FROM SINGLE BAR(ZERO
C     PATH) AND LOOP (ZERO PATH).          1/15/85
      OPEN(UNIT=23,DEVICE='DSK',DIALOG)
      OPEN(UNIT=24,DEVICE='DSK',DIALOG)
      OPEN(UNIT=25,DEVICE='DSK',DIALOG)
      DO 1 I=1,152
      READ(23,2)F,X
      READ(24,2)F,Y
      RES1=SQRT(X)
      RES2=SQRT(Y)
      RES=RES1*RES2
1     WRITE(25,3)F,RES
2     FORMAT(2E)
3     FORMAT(1X,2(2X,E12.5))
      STOP
      END
```

APPENDIX 3

"PROGRAM FOR CALCULATING F-I.L RESPONSE WITH EXTERNAL ATTENUATORS"

```
C  THIS PROGRAM IS FOR MULTIBAR TRANSDUCER WITH EXTERNAL ATTENUATORES.
C  OR THIS PROGRAM CAN BE USED TO CHECK THE RESULTS OF SYNTH.VALUES
C  BE SURE TO CHANGE THE DIMENSION OF L,YY AND Yl TO THE # OF XDUCER
        DIMENSION FREQ(152),AAW(152),FRQ(1500),AW(1500),
     1K(1500),L(16),YY(16),Y1(16)
        COMPLEX K,Z1,Z2,Z3
        REAL L0,LOSSDB,L,PII
        PII=3.1415927
        TYPE 1000
C PROGRAM ASKS FOR 4 FILE NAME:
C  FIRST IS TO READ F VS LINEAR IL DAT
C  SECOND TO READ COMPLEX K VALUES
C  THIRD TO STORE THE F VS IL(DB) OF FILTER RESPONSE
C  AND THE LAST TO STORE XDUCER AND FILTER DATA.
        OPEN(UNIT=23,DEVICE='DSK',DIALOG)
        OPEN(UNIT=24,DEVICE='DSK',DIALOG)
        OPEN(UNIT=25,DEVICE='DSK',DIALOG)
        OPEN(UNIT=26,DEVICE='DSK',DIALOG)
        READ(23,3)(FREQ(I),AAW(I),I=1,152)
        READ(24,333) FO,DF,NUMBER
        TYPE 1
        ACCEPT 2,NUM
        FO=FO-DF
        READ(24,3)(K(I),I=1,NUMBER)
        DO 82 J=1,NUMBER
        FO=FO+DF
        DO 80 I=1,152
        IF(FREQ(I).LE.FO) GO TO 81
        DDF1=FREQ(I)-FREQ(I-1)
        DDAW=AAW(I)-AAW(I-1)
        DDF2=FREQ(I)-FO
        RATIO1=DDAW/DDF1
        RESULT=AAW(I)-RATIO1*DDF2
        FRQ(J)=FO
        AW(J)=RESULT
        GO TO 82
81      IF(I.EQ.152) GO TO 88
         GO TO 80
88       FRQ(J)=FO
        AW(J)=0.0
        GO TO 82
80      CONTINUE
82      CONTINUE
        TYPE 22
        ACCEPT 34,SO1
        SO=SO1*1.0E-6
        TYPE 2000
2000    FORMAT(1X,'ENTER I/O CENTER/CENTER SPACING (CM)')
        ACCEPT 2001,LO
2001    FORMAT(E)
```

139

```
        LO=LO*1.0E-2
        DO 6 I=1,NUM
6       L(I)=LO+(I-1)*SO
        TYPE 1200
1200    FORMAT(1X,'LINEAR (TYPE 0) OR DB (TYPE 1) COEF. ?')
        ACCEPT 1201,NYJA
1201    FORMAT(I)
        TYPE 13
13      FORMAT(1X,'ENTER THE VALUES OF THE ATTENUATORES '
     1'  STARTING WITH THE '/,' TRANSDUCER CLOSE TO INPUT'
     2,' (F FORMAT). ONE DATA PER LINE')
        DO 90 I=1,NUM
        ACCEPT 34, Y1(I)
        IF(NYJA.EQ.0) GO TO 1203
        Y11=ABS(Y1(I))
        Y2=Y11/20.
        Y3=10.0**Y2
        IF(Y1(I).LT.0) GO TO 234
        YY(I)=1/Y3
        GO TO 90
234      YY(I)=-1./Y3
        GO TO 90
1203    YY(I)=Y1(I)
        IF(Y1(I).LT.0) GO TO 1205
        Y1(I)=20.*ALOG10(Y1(I))
        GO TO 90
1205    Y1(I)=ABS(Y1(I))
        Y1(I)=-20.*ALOG10(Y1(I))
90      CONTINUE
34      FORMAT(F)
        WRITE(26,92) FRQ(1),FRQ(NUMBER),NUM,SO1,(Y1(I),I=1,NUM)
        WRITE(26,29) (YY(I),I=1,NUM)
92      FORMAT(1X,'NATURAL CUT-OFF FRQ.S ARE: ',E12.5,' & ',E12.5/
     1,' NUMBER OF XDUCERS = ',I3,' WITH SEPARATION (MIC) OF ',F8.2/
     2,' VALUES OF THE ATTENUATORES (IN DB) ARE:'/,5(1X,E12.5))
29      FORMAT(1X,' OR THEIR NORMALIZED (0 TO 1) VALUES ARE: '/
     1,5(1X,E12.5))
        DO 200 I1=1,NUMBER
        ZYY=0.0
        Z3=(0.0,0.0)
        DO 201 I2=1,NUM
        Z1=-K(I1)*L(I2)
        Z2=CEXP(Z1)
        ZYY=ZYY+(YY(I2)**2.0)
201     Z3=Z2*AW(I1)*YY(I2)+Z3
        Z4=CABS(Z3/ZYY)
        LOSSDB=20.*ALOG10(Z4)
        A1=AIMAG(Z3)
        A2=REAL(Z3)
        A3=A1/A2
        A4=ATAN(A3)
        TETA=A4*180./PII
        WRITE(25,33)FRQ(I1),LOSSDB
200     CONTINUE
1       FORMAT(1X,'ENTER # OF TRANSDUERS ')
```

```
2          FORMAT(I)
3           FORMAT(2E)
22         FORMAT(1X,'ENTER XDUCER SPACING IN MICRON ')
26         FORMAT(1X,5(1X,E11.4))
33         FORMAT(1X,2E)
333        FORMAT(2E,I)
1000       FORMAT(1X,'THIS PROGRAM ASKS FOR FOUR FILE NAMES. THE
      1 FIRST ONE IS FREQ. VS I.L.',/,' (152 DATA) , THE SECOND FILE
      2 IS THE COMPLEX VALUES OF K,',/,' THIRD FILE IS FOR STORING
      3 PROGRAM INFORMATION AND DATA, AND THE ',/,' LAST FILE IS TO STORE
      4 THE RESULTED F VS I.L. DATA')
           STOP
           END
```

MSSW TRANSVERSAL FILTERS BASED ON CURRENT WEIGHTING IN NARROW (10 μm) TRANSDUCERS

Y.J. Ataiiyan, J.M. Owens, K.W. Reed, R.L. Carter, W.A Davis

The Center for Advanced Electron Devices and Systems (CAEDS)
The University of Texas at Arlington, Arlington, Tx. 76019

ABSTRACT

A Magnetostatic Surface Wave, tunable bandpass filter using current weighted transducer arrays based on transversal filtering techniques has been built. A 100 MHz bandpass filter was realized with a minimum insertion loss of 15 dB and sidelobe suppression of 20 dB. The usable tunability range of the device was from 2 to 3.5 GHz.

INTRODUCTION

Magnetostatic Wave (MSW) devices have opened a new door to high frequency signal processing above 1 GHz, where Surface Acoustic Wave (SAW) devices have high insertion loss and are difficult to fabricate. One area that has eluded researchers has been the development of tunable MSW transversal filters. This paper presents results on the realization of the first synthesized MSW transversal filters. Progress in this area has been slow, primarily as a result of the dispersive nature of MSW's, strong coupling of radiating current elements, interaction between neighboring elements, and reflections from the elements in the array. To overcome the first problem, a computer program was developed to synthesize the desired bandpass filter. This was based on theoretically calculated insertion loss and frequency data for a zero-path length delay line with single bar transducers on both the input and the output. The program generated the normalized current distribution for each transducer element. A bandpass filter utilizing nondispersive waves (e.g. SAW), would require a current distribution of the form SIN(X)/X. Conversely, for MSW's the current distribution must be distorted to compensate for the dispersion of the wave. In order to reduce element interaction and reflections from the array, transducer elements were made as narrow as possible (10 um for operation with a 300 um center-band wavelength), and in order to limit coupling short open circuited transducers

were used.

THEORY

Magnetostatic Waves (MSW) are basically magnetically coupled dispersive waves that propagate in a magnetically biased ferrite material such as Yttrium Iron Garnet (YIG). The theoretical and experimental characteristics of the MSW technology are well documented elsewhere [1,2,3,4].

Regardless of the type of the wave in the propagating medium (SAW or MSW) and independent of the weighting technique, the procedure for synthesizing a filter is fundamentally the same [5,6]. For a non-interacting N element transducer array with a weighting factor of a_n for each element and path-length ℓ_n, the array response can be written in the form:

$$\bar{G}(\omega) = \sum_{n=1}^{N} a_n \bar{A}(\omega) e^{-\bar{K}(\omega)\ell_n} = \sum_{n=1}^{N} \bar{Y}_n(\omega)$$

(1)

where,

$\bar{G}(\omega)$ = array response

$\bar{K}(\omega)$ = $\alpha + j\beta$ (α and β are loss factor and wave number, respectively)

$\bar{Y}_n(\omega)$ = nth element response.

The quantity $\bar{A}(\omega)$ denotes the complex value of the transmission response for a single-bar/single-bar transducer pair with zero path. This transducer characteristic is obtained by modeling the transducer filaments as a simple lossless microstrip in a manner discribed by Wu [7]. A pointing vector calculation is used to define a radiation resistance representative of the coupling to the ferrite.

The linearized array response given in equation (1) can be made to fit the desired frequency response of the array,

$\bar{H}(\omega)$. The R.M.S error, ε, can be calculated from equation (2).

$$\varepsilon = \frac{1}{\omega_2-\omega_1}\int_{\omega_1}^{\omega_2}\{\bar{H}(\omega)-\sum_{n=1}^{N}a_n\bar{A}(\omega)e^{-\bar{K}(\omega)\ell_n}\}$$

$$\times\{\bar{H}^*(\omega)-\sum_{n=1}^{N}a_n\bar{A}^*(\omega)e^{-\bar{K}^*(\omega)\ell_n}\}\,d\omega \quad (2)$$

which should be minimized with respect to the weighting factors a_m:

$$\frac{\partial\varepsilon}{\partial a_m}=\frac{1}{\omega_2-\omega_1}[\int_{\omega_1}^{\omega_2}\bar{A}(\omega)e^{-\bar{K}(\omega)\ell_m}$$

$$\times\{\bar{H}^*(\omega)-\sum_{n=1}^{N}a_n\bar{A}^*(\omega)e^{-\bar{K}^*(\omega)\ell_m}\}d\omega$$

$$+\int_{\omega_1}^{\omega_2}\bar{A}^*(\omega)e^{-\bar{K}^*(\omega)\ell_m}$$

$$\times\{\bar{H}(\omega)-\sum_{n=1}^{N}a_n\bar{A}(\omega)e^{-\bar{K}^*(\omega)\ell_n}\}d\omega] \quad (3)$$

The integrals in equation (3) are conjugate of each other, so the sum can be expressed as twice the real part. Some manipulation yields,

$$\frac{\partial\varepsilon}{\partial a_m}=\frac{-2}{\omega_2-\omega_1}\{Re\int_{\omega_1}^{\omega_2}\bar{A}(\omega)\bar{H}(\omega)e^{-\bar{K}^*(\omega)\ell_m}d\omega$$

$$-Re\sum_{n=1}^{N}a_n\int_{\omega_1}^{\omega_2}|\bar{A}(\omega)|^2$$

$$\times e^{-[\bar{K}^*(\omega)\ell_m+\bar{K}(\omega)\ell_n]}d\omega=0 \quad (4)$$

Setting the partial derivatives of the error function with respect to each of the N parameters to zero yields a matrix of N linear, linearly independent equations. For simplicity, parameters M_{ij} and Q_i are defined as:

$$M_{ij}=Real\int_{\omega_1}^{\omega_2}|\bar{A}(\omega)|^2 e^{-[\bar{K}^*(\omega)\ell_i+\bar{K}(\omega)\ell_j]}d\omega$$

$$Q_i=Real\int_{\omega_1}^{\omega_2}\bar{A}^*(\omega)\bar{H}(\omega)e^{-\bar{K}^*(\omega)\ell_i}d\omega$$

The set of equations in (4) can be expressed as.

$$\begin{vmatrix}M_{11} & M_{12} & M_{13} & \cdots & M_{1N}\\ M_{21} & \cdot & \cdot & \cdots & \cdot\\ \cdot & \cdot & \cdot & \cdots & \cdot\\ M_{1} & \cdot & \cdot & \cdots & M_{NN}\end{vmatrix}\times\begin{vmatrix}a_1\\a_2\\ \cdot\\a_N\end{vmatrix}=\begin{vmatrix}Q_1\\Q_2\\ \cdot\\Q_N\end{vmatrix}$$

This set of equations can be algebratically inverted to obtain the unnormalized element weighting coefficients. once the numerical integration has been carried out on the matrix elements. The weighting coefficients were then constrained to be real and normalized to unity (-1 to +1).

EXPERIMENTAL PROCEDURE

The 16 element filter in this experiment was designed to have a passband of 100 MHz at the center frequency, $f_o=2.7$ GHz. and as much sidelobe suppression as theoretically possible using a 25 μm thick YIG film. The current is distributed among the elements via a simplified 16 way power-divider. which provide phase equalization for each open circuited finger. Individual

transducers within the array are all 10 μm wide and 4mm long. with only 3mm under the YIG (see figure 1). Transducers are fed from both ends with the current weighting in each transducer determined by the placement of an open circuited gap. positioned relative to the longitudinal array axis. As an example. a gap at the center of a transducer would result in a zero net current contribution for that element. It was assumed that in the case of an open-circuited microstrip of length $\ell \ll \lambda/4$. with fringe effects neglected. the current exhibits linear variation along the length. Therefore. the gap in each element was positioned so that the average current on opposing elements had the required sign and value dictated by the synthesis program. In order to reduce the harmonic responses of the array. a shorted $\lambda/2$ spaced loop transducer is used on the output.

The transducers are fabricated from up-plated gold on 10 mil thick. 1"x1" alumina substrates. The 3mm wide. 25 μm thick YIG film is angle-lapped at the ends to minimize reflections there.

EXPERIMENTAL RESULTS

Figure 2 shows the theoretical prediction of the insertion loss versus frequency for a typical filter with the desired characteristics described earlier. The minimum insertion loss of the fabricated device was observed to be -25dB. which is mainly due to the power-divider mismatch and associated 20:1 VSWR in the passband of the filter. Figure 3 is the transmission response for the device in the frequency range of 1.5 GHz to 3.0 GHz. In this picture the output of the device is amplified to show the sidelobe suppression. otherwise not clearly distinguishable from direct breakthrough.
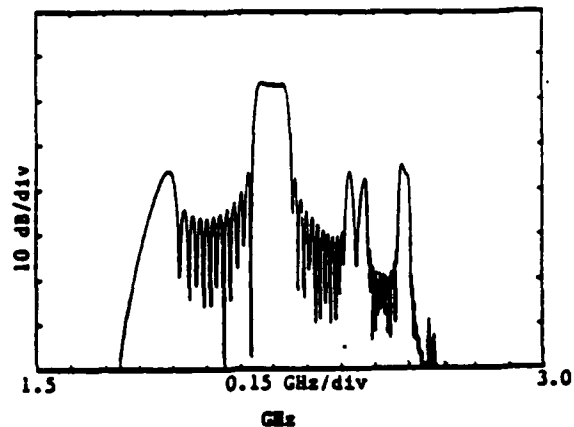
Figure 2: Theoretical prediction of S_{12}.

Figure 1: Circuit pattern of the 100 MHz tunable bandpass filter. The position of the gap is marked with "." at the left side for each transducer. Actual dimension: 1"X1".
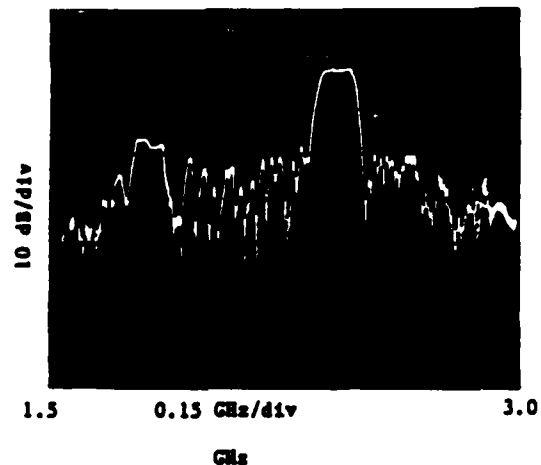
Figure 3: The experimental S_{12} of the device.

144

The theoretical simulation of the tunability of the filter is shown in figure 4. This was done by superimposing the calculated transmission responses of the filter at four different bias fields. Figure 5 shows the experimental results obtained by varying the magnetic bias field. Figures 4 and 5 clearly demonstrate a decrease in the passband for higher center frequencies. This is due to the band limiting characteristics of MSSW delay line dictated by the applied bias field.
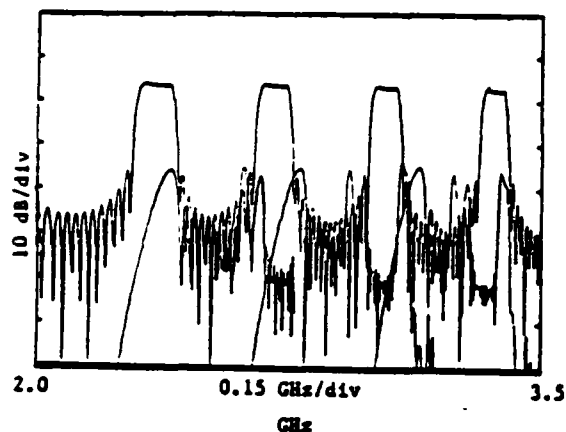
CONCLUSION

The current weighting technique using open gap transducers to realize MSSW filters, demonstrates a good correlation between the theoretical predictions and obtained performance. With this technique, it is possible to construct a tunable bandpass filter with sidelobe suppression as high as 20 dB, with less than 3 dB amplitude ripple . . The vriation of the minimum insertion loss in the tunable range of the device can be as low as 2 dB. An improvement of about 10 dB on the minimum insertion loss was achieved by a narrow band matching of the existing power-divider. Therefore, we believe further improvement in delivering the maximum power to each finger via construction of a better matched broad band power-divider can bring the minimum insertion loss close to -10 dB.

ACKNOWLEDGMENT

Figure 4: Theoretical prediction for tunability of S_{12}.
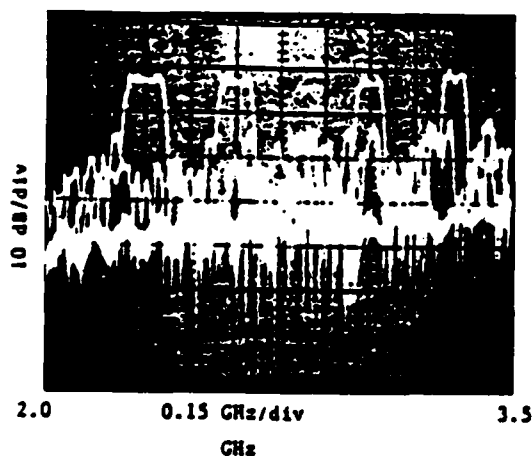
Figure 5: Tunability of S_{12} (200 - 450 Oe).

REFERENCES

[1] J.M. Owens and C.V. Smith Jr., "Beyound SAW Filters: Magnetostatics Show Promise", MSN, P.44, June 1979.

[2] M.R. Stiglitz and J.C. Sathares, "Magnetostatic Eaves Take Over Where SAWs Leave Off", Microwave Journal, P.18, February 1982.

[3] J.M. Owens and R.L. Carter, "Magnetostatics Advance: The Shape of Waves to Come", MSN, P .103, March 1983.

[4] H.L. Glass and M.T. Elliot, paper 08.3-8, 10th International Conference Crystallography, Amsterdam, August 1975.

[5] D.S. Humpherys, "The Analysis, Design, and Synthesis of Electrical Filters", Prentice-Hall, Inc., N.J., Chapter 6, 1970.

[6] K.W. Reed, "Magnetostatic Ion Implanted Reflective Array Filters",Dissertation, Univ Texas Arlington, Dec. 1985.

[7] H.J. Wu, "Magnetostatic Wave Transducers", Dissertation, Univ Texas Arlington, Dec. 1978.

Electronically Variable Time Delays Using Magnetostatic Wave Technology

L.R. Adkins, H.L. Glass, K.K Jin, F.S. Stearns
Rockwell International;
Y.T. Ataiiyn, R.L. Carter, J.M. Owens
The University of Texas at Arlington;
D.D. Stancil
North Carolina State University

Variable time delays are necessary in phased array systems to prevent phase squinting and pulse stretching. Methods for providing these time delays include an assortment of fixed cables, ferrite loaded cables, surface acoustic wave (SAW) devices and magnetostatic wave (MSW) devices. Fixed cables are bulky, limiting the number that can be employed per system. Ferrite loaded cables and SAW devices are applicable primarily at frequencies below 1 GHz and provide relatively small delay differentials. MSW wave technology is capable of operating at frequencies up to 20 GHz and providing differential time delays on the order of tens of nanoseconds. An MSW device has recently been demonstrated with a bandwidth greater than 200 MHz centered at 3 GHz. This device has a phase error across the band as low as 8° and is capable of providing nearly 50 nS differential delay. Thus, MSW technology appears to be the most promising technique for the next generation of phased array systems.

Introduction

The need for enhanced performance and miniaturization in phased array system components has fueled the exploration of new techniques for providing time delays. Ideally, a time delay component should be small and rapidly tunable over a delay range of a few tens of nanoseconds, should have excellent phase linearity characterisitics, and should be inexpensive. In this paper, we describe recent advances in the state of the art for one new tunable time delay technique, the magnetostatic wave (MSW) delay line.

True time delays perform two principal functions in phased array systems: they eliminate "phase squinting" in broadband beams and they allow the undistorted transmission and reception of narrow pulses. Consider the first problem. In a phased array antenna the beam is steered by adjusting the phase of the electromagnetic signals from each of a large number of radiating elements so that the radiated waves add coherently only in a specified direction. If frequency independent phase shifters such as diode phasers are used to provide the needed phase shift, then for a given steering angle the signal will be strictly coherent only at one frequency.

Consider an array of radiators with spacing d as shown in Figure 1. If the steering angles is i and D is the path difference between adjacent radiators, then the relation between θ and D is given by $d \cdot \sin(\theta) = D$. Thus, the required phase at each radiator for wavelength L will be $2\pi D/L$. Clearly, a frequency independent phase shifter can satisfy this requirement at only one frequency. Other frequency components will sum coherently in slightly different directions, and the net system result will be high sidelobes outside a relatively narrow passband. This is illustrated in Figure 2 by a simulated beam pattern from an array of radiators.

For this calculation, a uniform linear array with 10 isotropic elements was assumed (i.e. no attempt was made to modify the sin(x)/x response of the passband). The desired beam angle for the array was 45°, the element spacing was .5 wavelength and the phase error was simulated using a random number generator. Calculations were made for two center frequencies separated by 250 MHz (2.875 and 3.125 GHz), with the assumption that beamsteering was accom-

plished using ideal phase shifters. Figure 2 shows clearly that the common passband of these two frequencies has been narrowed by the
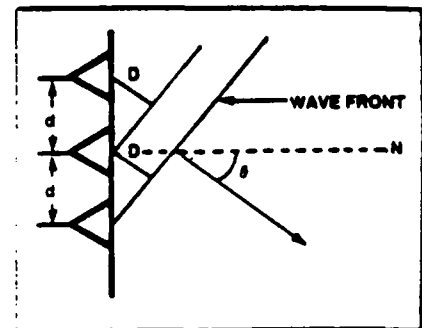

Fig. 1 Beam steered through angle θ

beamsteering. In effect, a broadband imaging system has been "squinted" into a narrower-band one.

The second problem, the pulse distortion of a narrow pulse, is independent of bandwidth and will arise whenever the steering angle is large. This is illustrated in Figure 3. Let T_A represent the time required for an electromagnetic signal to travel across an antenna array. If the beam is steered an angle i away from the array normal, then the lead-
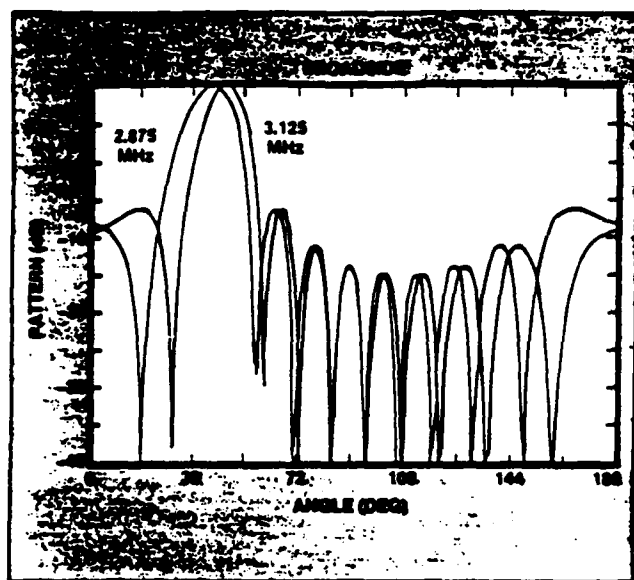
Fig. 2 Beam shape for an ideal phase shifter at two frequencies separated by 250 MHz.
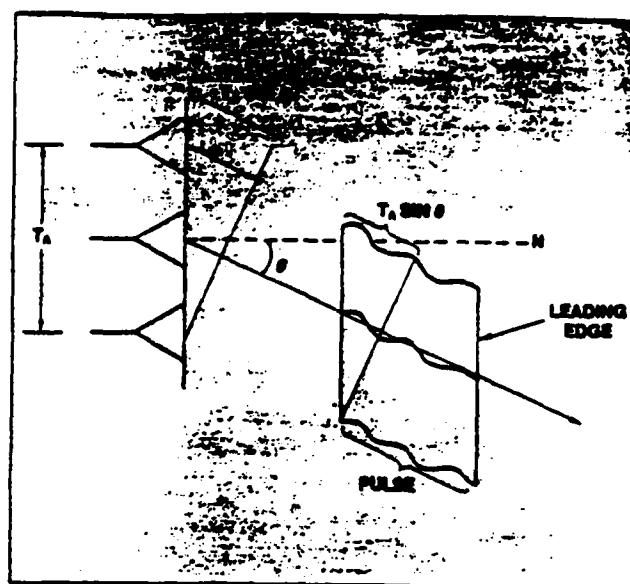

Fig. 3 Pulse distortion due to uncompensated time delay across the array.

ing edge of a transmitted pulse from the near side of the array will arrive at a target T_A*sin(θ) earlier than the leading edge of the pulse transmitted from the far side of the array. In effect, the pulse width will be stretched by an amount T_A*sin(θ). Since T_A is usually on the order of a few tens of nanoseconds, the effect is important only for narrow pulses. However, narrow pulses are mandatory when high resolution imaging of a target is required, and thus the problem is highly significant.

Fixed Delay Elements

In most present day systems, time delays are provided by an assortment of fixed transmission lines, either stripline or cable. An excellent elementary review of this approach has been given by Brookner.[1] For large angle sweeping, a 3-bit phase shifter, consisting of three unequal length striplines, is provided at each radiating element. These lines have paths equivalent to 1/2, 1/4, and 1/8 wavelength and can be combined to give phase differences of 0° to 360° in steps of 45°. The three striplines together are less than one wavelength long, so that the total phase shift is never more than 360°. Thus, although broadband operation is realized, high resolution, narrow pulses a few tens of wavelengths wide cannot be reconstructed unambiguously using these elements alone.

For narrow pulse work, the array is commonly divided into subarrays, and each of these units is provided with a 3-bit phase shifter comprised of long cables. For a system such as the COBRA DANE radar, delays as long as 64 wavelengths can be obtained for each subarray. Although this technique is believed to be adequate for most current applications, there is necessarily some distortion of the pulse due to the finite delay across each subarray. However, it is clearly impractical to provide each element of the array with long delay lines, since something like 100 miles of cable would be required for a radar like COBRA DANE. Even using the subarray approach, about one mile of cable is necessary. It would clearly be desirable to replace these great lengths of cable with compact modules: therefore, considerable effort has been expended in recent years in exploring methods of varying delays electronically.

The principal approaches investigated to date include ferrite loaded helical transmission lines,[2] surface acoustic wave (SAW) delay lines[3-5] and magnetostatic wave (MSW) devices. The delay is changed in the ferrite loaded line by applying an external magnetic field. This changes the permeability of the ferrite, the impedance of the transmission line and, hence, the velocity of the electromagnetic wave. The velocity of the surface acoustic

wave is changed by applying a large voltage across the delay path. Both the ferrite loaded line and the SAW delay line operate at low frequencies (below 2 GHz) and provide relatively small differential delays (<20 nS). In contrast, magnetostatic wave (MSW) devices have the potential of operating at frequencies up to 20 GHz with differential delays greater than 50 nS. Thus, this paper is concerned with the current status of MSW technology.

Magnetostatic Delay Line

Considerable progress has been made recently toward the realization of an MSW variable time delay device that can operate in the microwave frequency range and provide electronically tunable delays of a few tens of nanoseconds. This device has been developed under the sponsorship of Rome Air Development Center through a joint effort of Rockwell International, The University of Texas at Arlington and North Carolina State University.
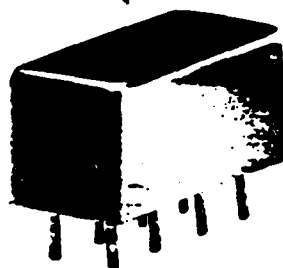
The propagating medium for magnetostatic wave (MSW) devices consists of an epitaxial ferrite film (usually yttrium iron garnet or YIG) on a garnet substrate. This structure is usually prepared in the form of a bar with input and output transducers at each end. The device is placed between the poles of a magnet, and an RF signal is fed into one transducer. An illustration of a
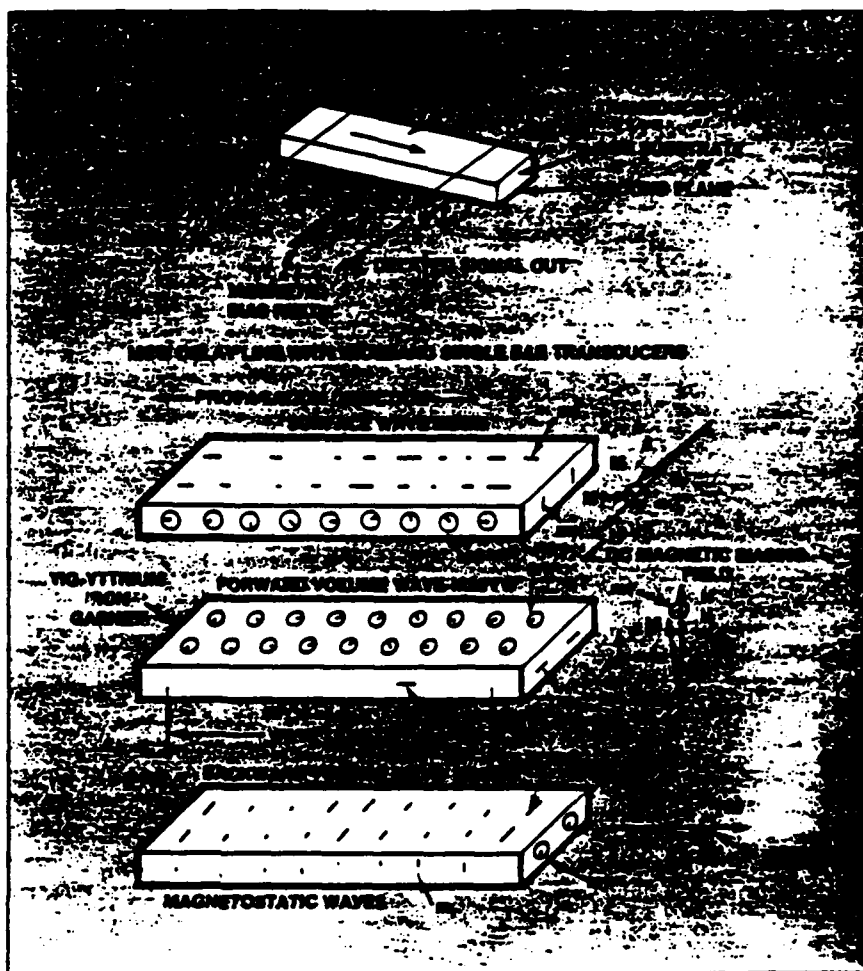
147

Fig. 4 Excitation of MSSW. MSBVW and MSFVW on a YIG delay line using a shorted electrode transducer. (from Stiglitz and Setnares[6]).

standard MSW delay line is shown in Figure 4.[6] At a specific combination of signal frequency and magnetic field strength, magnetic spin waves will be launched from the input transducer down the bar. These waves are reconverted into electromagnetic energy at the output transducer. Since the velocity of magnetostatic waves in the YIG is some three orders of magnitude smaller than electromagnetic waves in free space. a substantial delay is realized with a delay path of about 1 cm. Magnetostatic waves are somewhat analogous to surface acoustic waves. but they have two advantages for phased array systems applications: they operate from 1 to 20 GHz. and their frequency of operation can be electronically tuned by changing the value of the magnetic bias field.

MSW delay lines are inherently dispersive, i.e. the group velocity does not in general equal the phase velocity. The specific dispersive characteristics of an MSW delay line are dependent on a number of variables. but one useful feature is that the slope of the dispersion can be either positive or negative. depending on the orientation of the magnetic bias field. This aspect has been applied in the design of a variable delay line that operates at the center frequency near 3 GHz and exhibits a delay differential of more than 40 nS.

A schematic diagram of the approach is shown in Figure 5. Two MSW delay lines having dispersive characteristics with slopes of opposite signs are cascaded together. If the dispersions are linear and the slopes are equal in absolute magnitude. then the net dispersion will be zero across the passband. If one delay line is provided with a constant bias while the bias on the other is varied. the net delay will change
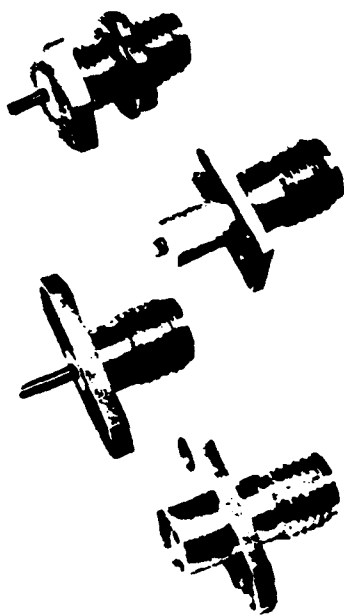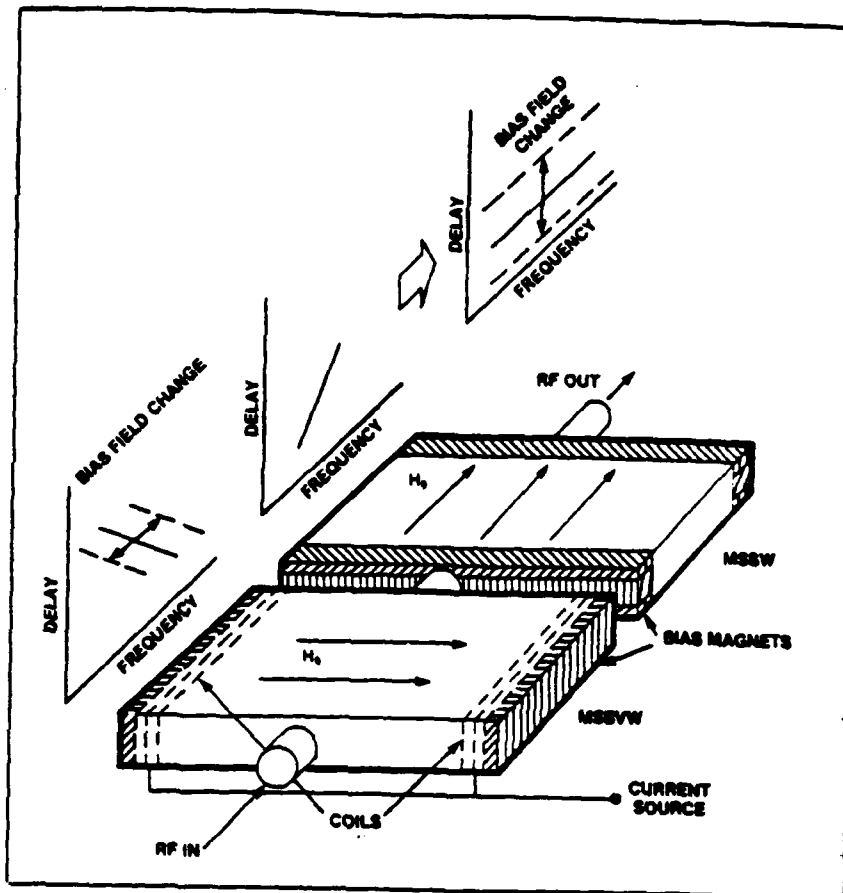
Fig. 5 Electronically tunable time delay using a magnetostatic wave cascaded delay line (CDL)

but remain flat as a function of frequency over the passband. We will refer to a device of this type as a MSW cascaded delay line (CDL). A laboratory version of the approach was first reported by Sethares and Owens, and an improved laboratory version was reported by the authors of this article in 1984. This device has now been packaged and is shown in Figure 6.

The negatively sloped dispersion is provided by a backward volume wave (MSBVW) delay line while a surface wave (MSSW) delay line gives the positive slope characteristic. The MSBVW mode is obtained when the bias field is parallel to the direction of propagation. The MSSW mode is produced when the field is applied in the plane of the film and is perpendicular to the direction of propagation. One problem inherent in MSW dispersion is that it is in general non-linear. Thus, some method for linearizing these characteristics must be used. For the MSBVW delay line, the dispersion was linearized by adjusting the
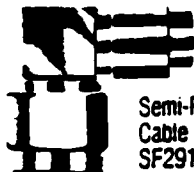
spacing between the film and the ground plane. For the MSSW delay line a variable ground plane was provided. These techniques are described in more detail by Chang et al. and in reference 3.

The packaging deserves some comment. It is important that the fields seen by the delay lines be uniform to prevent additional unwanted frequency dispersion. Such uniformity is readily achieved with large laboratory magnets, but small packaged components usually produce non-uniform magnetic fields. Our approach was to place the biasing magnets at opposite ends of the packages and focus their fields along the central axis by means of a series of smaller magnets with opposing fields suitably spaced along the remaining sides, top and bottom. As the fields required were relatively small (600 oe), ferrite magnets were used throughout. In the photograph the magnets are the dark colored rectangles, while the light rectangles are aluminum spac-
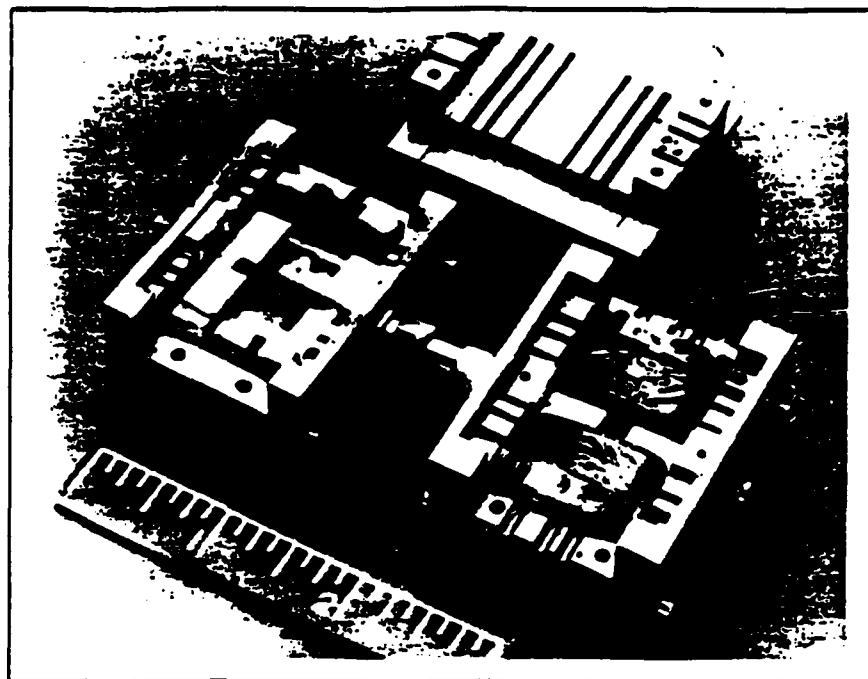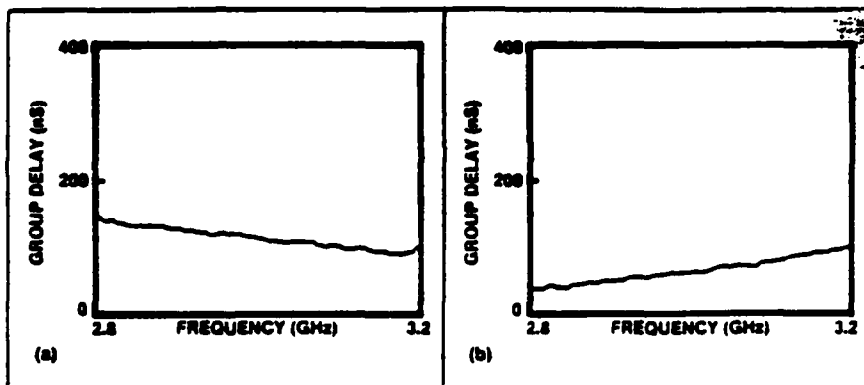
149

Fig. 6 Packaged CDL.

Fig. 7 Linear dispersions with MSBVW and MSSW delay lines:
(a) MSBVW; (b) MSSW.

ers. The uniformity of the biasing fields was excellent using this technique. The variable field was provided by means of coils in the MSBVW package, and the outer shell of both components was stainless steel.

The frequency dispersive characteristics of the packaged MSSW and MSBVW delay lines are shown in Figure 7, and the net frequency dispersion from the complete CDL is given in Figure 8. The figure shows a delay differential of 34 nS (approximately 100 wavelengths at center frequency) when the current through the coil is changed from 0 to .6 amps. The maximum delay change that has been demonstrated with this configuration is 47 nS.

From a visual inspection of these illustrations, the linearity of the individual delay lines and the flatness of the cascaded device appear to be excellent. For a more quantitative measure of these characteristics, the root mean square (RMS) of the phase deviation from linearity across the band was computed. This calculation was based on the fact that the phase is linear across a non-dispersive passband. Phase data as a function of frequency were obtained from the automatic network analyzer and were fitted to a linear curve. The deviation of the measured phase from the calculated curve was taken to be the phase error, and the RMS value was computed from these data using stan-

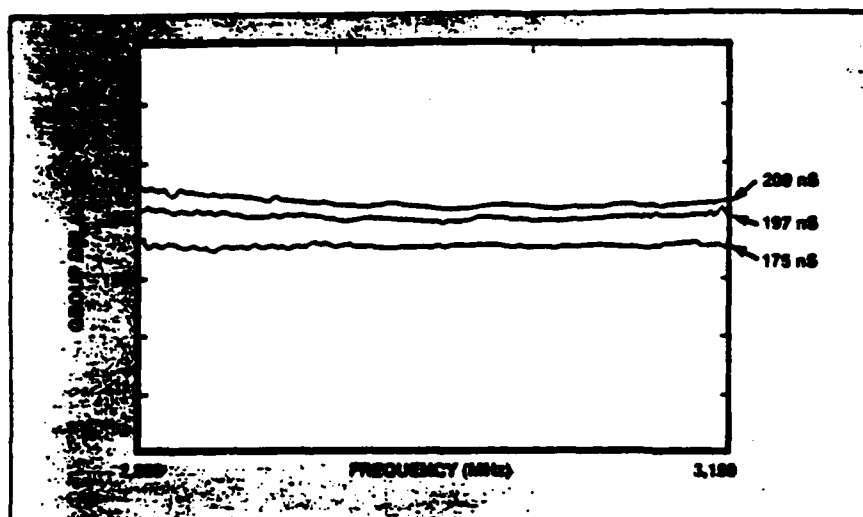Fig. 8 Dispersion curves for the packaged CDL at three current settings.

CRITICAL DEVICE CHARACTERISTICS

Characteristic	Measured Value
Center frequency	2.989-3.011 GHz
Bandwidth	7.1 - 4.6%
Group delay	34 - 47 nS
Phase error (RMS)	8.05° (best) 17.9° (worst)
Insertion loss	30 dB (center)
Switching time	< 100 μS
Power handling	100 mW

dard statistical techniques. The critical characteristics of the device are given in the Table 1.

The characteristics listed above come very close to meeting system needs. Referring back to the discussion on fixed delay lines, CDLs with these characteristics could replace the assortment of long cables at the subarray, reducing a mile of cable to a set of compact (<120 cm³) components. However, it still will be necessary to provide the radiators with 3-bit 0° to 360° phase shifters. Since the MSW delay lines are frequency dispersive, the group velocity linearized by the CDL is not equal to the phase velocity. Thus, the CDL cannot simultaneously provide a given absolute phase and the required group delay. To provide phase coherence across the array, 0° to 360°

phase shifters will be necessary. This should not be a serious drawback, however, since these phase shifters are reasonably small and can be integrated on a semiconductor chip.

Simulated beam shapes using CDLs plus phase shifters are shown in Figures 9 and 10. Except for the addition of MSW delay lines to the beamsteering mechanism, the assumptions here are identical to those used in calculating Figure 2. As before, the beam shape is calculated for two center frequencies: 2.875 and 3.125 GHz. For the two figures here, the delay lines have RMS phase errors of 8° and 12°, repsectively. It is clear that beam squinting has been dramatically reduced using components with these characteristics.

Conclusion

As a variable time delay component, the MSW CDL has two clear advantages over competing technologies such as ferrite loaded cables and surface acoustic wave delay lines: the frequency of operation is well into the microwave region (3 GHz for the present device), and delay differentials on the order of tens of nanoseconds (47 nS for the present device) are obtainable. With respect to the first feature, note that although the present device has a center frequency of 3 GHz. MSW technology is capable of performing at frequencies up to 20 GHz. This is in contrast to surface acoustic wave devices that are essentially confined to a frequency regime of 1 GHz or less and the ferrite loaded helix that operates at or below the VHF region (300 MHz). The differential delay obtainable with the MSW device also is impressive. A delay change of 47 nS has been obtained with the MSW CDL while a maximum variation of 4 nS has been reported for the helix and about 10 nS for the SAW delay line. In the SAW case, a voltage on the order of kilovolts was required to realize the reported change.

The main drawbacks to the MSW device are sensitivity to temperature change, moderate insertion loss and low power handling capability. The power handling capability is intrinsic to the magnetostatic interaction process, but the insertion loss characteristic and temperature stability can be improved with further research. Thus, the results reported here indicate that MSW devices will be capable of meeting many of the time delay requirements of future generation phased array systems.

References

1 Brookner. Eli. "Phased Array Radars. Scientific American. 252. pp. 94-102. 1985.

2 Clark. Donald E.. "HF Low-Loss Nanosecond Variable Delay Line." IEEE Southeastcon 1981 Conference Proceedings. CH1650. pp. 135-139. 1981.
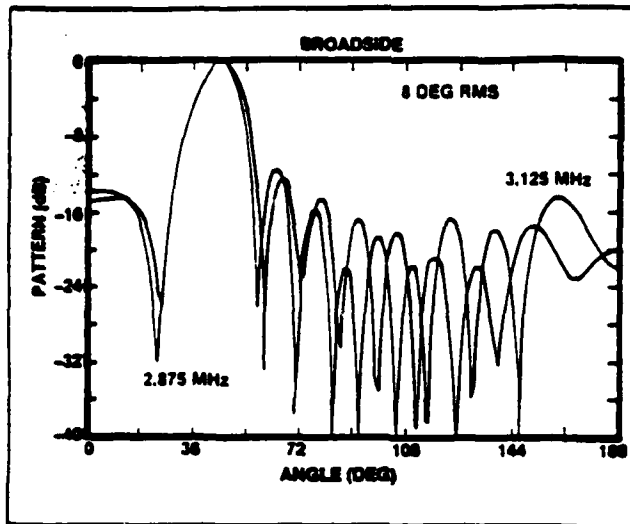
3. Joshi. S.G.. "Electronically Variable Time

151

Fig. 9 Beam snape for an array using an MSW delay line plus a
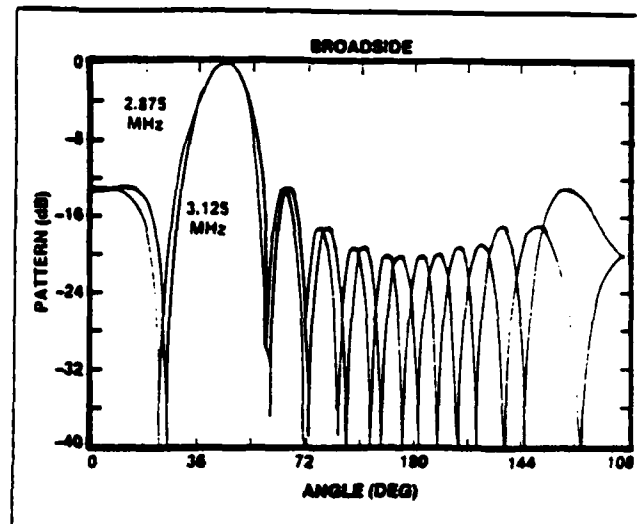phase shifter. The RMS phase error is assumed to be 8°.

Fig. 10. Beam snape for an array using an MSW delay line plus a
phase snifter. The RMS pnase error is assumed to be 12°

Delay in a LiNbO₃ SAW Delay Line." Proceedings of the IEEE. 70. pp. 95-96. 1982.

4. Budreau. Alan J.. Gary J. Scalzi. Paul H. Carr. Henry L Bertoni. "Electrostatically Vanable SAW Delay Lines — Theory and Experiment." IEEE Trans. Sonics and Ultrasonics. SU-31. pp. 646-461. 1984.

5. Ganguly. A.K.. K.L Davis. D.C. Webb. C. Vittoria. "Magnetic Control of Surface Elastic Waves in a Novel Layered Structure." Magnetism and Magnetic Materi-als-1976. AIP Conf. Proc. No. 34. Joint MMM-INTERMAG Conference. June 15-18. 1976. pp. 259-261

6. Stiglitz. Martin R.. James C. Sethares. "Magnetostatic Waves Take Over Where SAWs Leave Off." Microwave Journal. 25. pp. 18-38. February 1982.

7 Sethares. J.C.. J.M. Owens. C.V Smith. "An Electronically Vanable Magnetostatic Wave Time Delay Device." Electronics Letters. 16. p. 825. 1980.

8. Adkins. L.R. H L Glass. F S Stearns K.W Chang. R L Carter. J M Owens "Electronically Variable Time Delays using Cascaded Magnetostatic Delay Lines. Journal of Applied Physics. 55 pp. 2518-2520. 1984

9. Chang. K.W.. J.M. Owens R L Carter "Linearly Dispersive Time-Delay Control of Magnetostatic Surface Wave by Variable Ground-Plane Spacing." 19. pp 546-547 1983.

152

MISSION
of
Rome Air Development Center

RADC plans and executes research, development, test and selected acquisition programs in support of Command, Control, Communications and Intelligence (C^3I) activities. Technical and engineering support within areas of competence is provided to ESD Program Offices (POs) and other ESD elements to perform effective acquisition of C^3I systems. The areas of technical competence include communications, command and control, battle management information processing, surveillance sensors, intelligence data collection and handling, solid state sciences, electromagnetics, and propagation, and electronic reliability/maintainability and compatibility.